LATVIJAS UNIVERSITĀTE
ĶĪMIJAS
FAKULTĀTE

Kaspars Leduskrasts

STARPMOLEKULĀRĀS MIJIEDARBĪBAS CIETVIELU LUMINOFORU IZSTRĀDĒ

Promocijas darba kopsavilkums

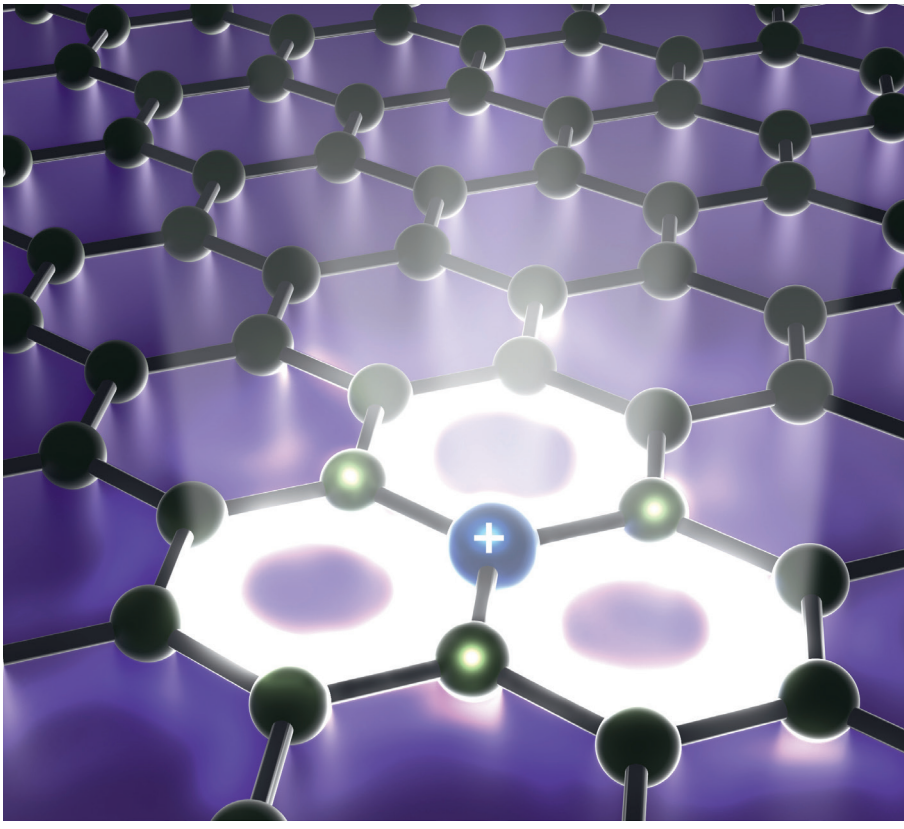

Rīga, 2022

LATVIJAS
UNIVERSITĀTE

ĶĪMIJAS FAKULTĀTE

Kaspars Leduskrasts

STARPMOLEKULĀRĀS MIJIEDARBĪBAS CIETVIELU LUMINOFORU IZSTRĀDĒ

PROMOCIJAS DARBA KOPSAVILKUMS

Doktora grāda iegūšanai ķīmijas nozarē

Apakšnozare: organiskā ķīmija

Darba vadītājs

profesors *Dr. chem.* **Edgars Sūna**

Rīga, 2022

Promocijas darbs tika izstrādāts Latvijas Organiskās Sintēzes institūtā laika posmā no 2014. līdz 2022. gadam.

LATVIJAS UNIVERSITĀTE

Darbs sastāv no kopsavilkuma, ievada, 4 nodaļām, 45 literatūras avotiem, 5 pielikumiem.

Darba vadītājs: profesors *Dr. chem.* **Edgars Sūna**

Darba recenzenti:

1) *Dr. chem.,* vadošais pētnieks **Pāvels Arsenjans** (Latvijas Organiskās sintēzes institūts);
2) *Dr. chem.*, asoc. prof. **Kaspars Traskovskis** (Rīgas Tehniskā Universitāte);
3) *Dr. chem.*, prof. **Arri Priimägi** (Tamperes Universitāte, Somija).

Promocijas darba aizstāvēšana notiks 2022. gada 5. jūlijā plkst. 15:00, Latvijas Universitātes Ķīmijas nozares promocijas padomes atklātā sēdē, Latvijas Universitātes Dabaszinātņu akadēmiskajā centrā, Rīgā, Jelgavas ielā 1.

Ar promocijas darba kopsavilkumu var iepazīties Latvijas Universitātes Bibliotēkā Rīgā, Kalpaka bulvārī 4.

Promocijas padomes priekšsēdētājs _____ /Edgars Sūna/
(paraksts)

Promocijas padomes sekretāre _____ /Vita Rudoviča /
(paraksts)

ISBN 978-9934-18-847-3
ISBN 978-9934-18-848-0 (PDF)

PATEICĪBAS

Esmu pateicīgs Latvijas Zinātņu akadēmijai (Taivānas–Lietuvas–Latvijas projekts "Jauni materiāli un tehnoloģijas augstai krāsu atveidei un saules gaismas spektra līdzībai OLED apgaismojuma avotos") un Eiropas Reģionālās attīstības fondam (Projekts "Nākošās paaudzes agregācijas inducētās emisijas luminogēni kā mākslīgās gaismas avoti") par finansiālo atbalstu.

Visnozīmīgākā pateicība šī darba izstrādē pienākas vadītājam prof. Edgaram Sūnam, kura iniciatīva, neatlaidība un atvērtā pieeja dažādām ķīmijas nozarēm ļāva uzplaukt šī darba tēmām. Esmu pateicīgs par darba vadītāja viedo atbalstu, kad maldījos lielajā organiskās sintēzes un publikāciju rakstīšanas mežā.

Vēlos pateikties Dr. Sergejam Beļakovam, Dr. Anatolijam Mišņevam un Dr. Dmitrijam Stepanovam par viņu ieguldījumu monokristālu rentgendifrakcijas analīzē, kā arī Latvijas Organiskās Sintēzes institūta KMR grupai par atbalstu spektroskopijas jautājumos un Pāvelam Dimitrijevam par dinamiskās gaismas izkliedes mērījumiem.

Vēlos izteikt pateicību Dr. Artim Kinēnam par kvantu ķīmisko aprēķinu veikšanu un Artūram Mazarēvičam par savienojumu sintēzi.

KOPSAVILKUMS

Starpmolekulārās mijiedarbības cietvielu luminoforu izstrādē. Leduskrasts K., zinātniskais vadītājs Dr. chem., prof. Sūna E. Promocijas darbs, 80 lapas, 20 attēli, 45 literatūras avoti. Latviešu un angļu valodā.

Promocijas darba izstrādes gaitā tika pētīti organisko luminoforu cietvielu emisijas mehānismi un izstrādāta jauna pieeja augstas emisijas intensitātes un izteikti ilga (>100 ms) emisijas dzīves laika sasniegšanai cietvielā. Augsta emisijas intensitāte gan šķīdumā, gan cietā stāvoklī tika skaidrota ar lādiņa pārneses emisijas mehānismu, ko nodrošina starpmolekulāras π–π^+ mijiedarbības. Izstrādātā metodoloģija tika izmantota augsti emisīvu organisku izstarotāju izstrādē gan cietā stāvoklī, gan šķīdumā. Jauns fosforescējošo materiālu dizains ar izteikti ilgu emisijas dzīves laiku balstās uz pieeju, kas nomāc ātru $T_1 \rightarrow S_0$ relaksācijas ceļu. Izmantojot jauno dizainu, tika izveidota virkne tiofēna fosforescējošo materiālu ar izteikti ilgiem emisijas dzīves laikiem.

Atslēgvārdi: CIETVIELU LUMINISCENCE, AGREGĀCIJAS INDUCĒTĀ EMISIJA, FOSFORESCENCE, STARPMOLEKULĀRĀS MIJIEDARBĪBAS, LĀDIŅA PĀRNESE

SATURS

SAĪSINĀJUMI

ACQ	agregācijas izraisītā dzēšana
AIE	agregācijas inducētā emisija
AIEgēni	AIE luminogēni
CT	lādiņa pārnese
DFT	blīvuma funkcionālā teorija
DMF	dimetilformamīds
DMSO	dimetilsulfoksīds
Et_2O	dietilēteris
EtOAc	etilacetāts
HOMO	augstākā aizpildītā molekulārā orbitāle
HT	Hikeļa teorija
IF	ietekmes faktors
ISC	starpsistēmu pāreja
KMR	kodolmagnētiskā rezonanse
LEEC	gaismu izstarojošās elektroķīmiskās šūnas
LUMO	zemākā neaizpildītā molekulārā orbitāle
MeCN	acetonitrils
MeI	jodmetāns
NOE	kodolu Overhauzera efekts
OFET	organiski lauka efekta tranzistori
OLED	organiskā gaismas izstarojošā diode
OPV	organiskie fotoelementi
PDI	perilēn-3,4-dikarboksimīds
RIR	iekšmolekulāro rotāciju nomākšana
RIV	iekšmolekulāro vibrāciju nomākšana
SOC	spinu orbitāļu sadarbība
THF	tetrahidrofurāns
Φ	kvantu iznākums

IEVADS

Gaismu izstarojošas molekulas (luminofori) tiek plaši pielietotas optoelektroniskajās ierīcēs, piemēram, gaismu izstarojošās elektroķīmiskajās šūnās (LEEC),[1] organiskajās gaismu izstarojošās ierīcēs (OLED),[2] organiskajos fotoelementos (OPVs),[3] organiskajos lauka efektu tranzistoros (OFETs),[4] kā arī telesakaru datu apstrādē,[5] glabāšanā[6] un šifrēšanā,[7,8] bioloģisko paraugu iezīmēšanā[9] un diagnostikā,[10] molekulārajos sensoros[11] un citās jomās. Vairumā gadījumu, piemēram, LEEC, OLED, OFET, OPVs un sensoros nepieciešama luminoforu darbība cietvielā. Šis nosacījums sarežģī efektīvu izstarotāju izveidi, jo cietvielās starp luminoforiem veidojas dažādas mijiedarbības, kas var negatīvi ietekmēt to emisiju. Piemēram, plaša π sistēma ir galvenais struktūrelements lielākajā daļā luminoforu, kas ir efektīvi šķīdumos. Turpretim plašu π-sistēmu saturošie cietvielu izstarotāji veido starpmolekulāras π–π mijiedarbības, kas izraisa strauju emisijas zudumu.

Promocijas darbā ir izstrādāta jauna luminoforu dizaina metode. Tās pamatā ir nevēlamu π–π mijiedarbību aizstāšana ar labvēlīgākām $\pi–\pi^+$ un $\pi^+–\pi^+$ mijiedarbībām, kas uzlabo emisiju. Šīs mijiedarbības notiek saskaņā ar lādiņa pārneses emisijas mehānismu, pastiprinot luminoforu cietvielu izstarojošās spējas. Vēlamās $\pi–\pi^+$ un $\pi^+–\pi^+$ mijiedarbības var izveidot, luminofora molekulas arēna struktūrelementu aizvietojot ar piridīnija fragmentu, kam ir katjonā π^+-sistēma. Šajā molekulārajā dizainā ne tikai saglabāta relatīvi vienkārša planāra struktūra, bet vienlaikus arī nodrošināta augsta cietvielu emisija (sk. 3.1. – 3.4. nodaļas).

Fosforescentie materiāli pēc ierosināšanas izrāda relatīvi ilgu emisijas dzīves laiku (līdz sekundēm),[12] un tos plaši lieto optoelektronikā un šūnu vizualizēšanā.[13] Visbiežāk organiskajos fosforescējošos materiālos ievada heteroatomus, piemēram, slāpekli vai sēru kā nedalītā elektronu pāra avotu.[14] Fosforescences intensitātes pieaugums cietvielās parasti samazina fosforescences dzīves laiku.[15] Saikne starp fosforescences intensitāti un dzīves laiku ir būtiska problēma, kas apgrūtina cietvielu fosforescento materiālu mērķtiecīgu modificēšanu. Promocijas darbā izstrādāta jauna organisko fosforescento materiālu dizaina stratēģija, kurā nav korelācijas starp fosforescences intensitāti un dzīves laiku. Šī pieeja balstās uz tiofēnu saturoša luminofora atvasināšanu, tajā ievadot telpisku aizvietotāju n-tipa orbitāli saturošā sēra atoma tuvumā. Telpiskā aizvietotāja izmērs kristāliskajā režģī nodrošina lielāku attālumu starp luminoforiem, kas savukārt nodrošina ilgāku fosforescences dzīves laiku, saglabājot fosforescences Φ praktiski nemainīgu (sk. 4. nodaļu).

Darba publikāciju saraksts

Promocijas darbs ir balstīts uz 5 zinātniskajām publikācijām:

1) **Leduskrasts**, **K.**; Suna, E. Aggregation induced emission by pyridinium–pyridinium interactions. *RSC Adv.* **2019**, *9*, 460–465. DOI:10.1039/C8RA08771G. IF_{2020} = 3,36.
2) **Leduskrasts**, **K.**; Kinens, A.; Suna, E. Cation–π interactions secure aggregation induced emission of Planar Organic Luminophores. *Chem. Commun.* **2019**, *55*, 12663–12666. DOI:10.1039/C9CC06829E. IF_{2020} = 6,22.

3) **Leduskrasts**, **K**.; Suna, E. Aggregation Induced Emission in One Easy Step: Pyridinium AIEgens and Counter Ion Effect. *RSC Adv.* **2020**, *10*, 38107–38113. DOI:10.1039/D0RA07137D. IF_{2020} = 3,36.
4) **Leduskrasts**, **K**.; Suna, E. Intermolecular Charge-Transfer Luminescence by Self-Assembly of Pyridinium Luminophores in Solutions. *ChemistryOpen*, **2021**, *10*, 1081–1086. DOI:10.1002/open.202100191. IF_{2020} = 2,91.
5) Mazarevics, A.; Kinens, A.; **Leduskrasts**, **K**.; Suna, E. Ultra-long Room Temperature Phosphorescence: Decoupling Lifetimes and Quantum Yields in Purely Organic Emitters. *Manuskripts iesniegts.*

Konferenču tēzes

1) **Leduskrasts**, **K**. Overcoming aggregation caused quenching by cation-π interaction. Latvijas Universitātes 77. konference. Organiskās ķīmijas sekcija, **2019**. g. 15. februārī: Rīga, Latvija; 47.
2) **Leduskrasts**, **K**. Cation–π Interactions for high Emission Intensity. *Materials of the 12th Paul Walden Symposium on Organic Chemistry*, October 28–29, **2021**: D-9, Riga, Latvia; 33.

1. NODAĻA. LITERATŪRAS APSKATS

1.1. Luminiscence

Luminiscence ir spontāna gaismas emisija no ierosināta luminofora. Tā ir auksta ķermeņa starojums, kas dokumentēts jau 16. gadsimtā un kuru šādi sauc kopš 1888. gada.[16] Luminiscenci klasificē pēc ierosmes enerģijas avota (hemi-, kristalo-, elektro-, mehano-, foto-, radio- un termoluminiscence).[17] Organisko luminoforu fotofizikālās īpašības visbiežāk raksturo ar fotoluminiscenci. Luminofora fotoluminiscences procesus var attēlot ar vienkāršotu Jablonska diagrammu (1.1. att.).[18]

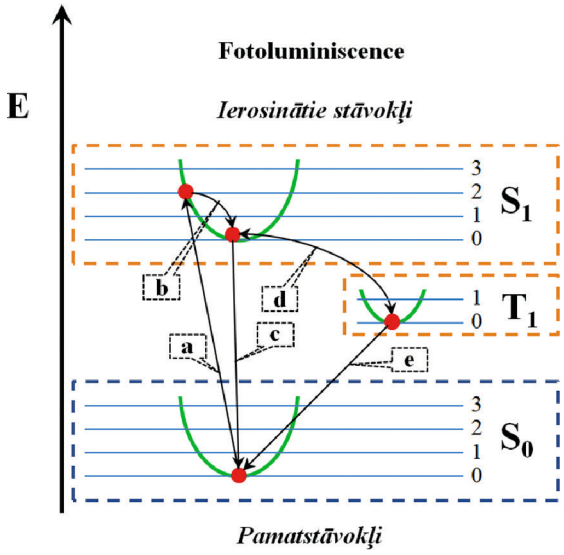

1.1. att. **Jablonska diagramma**

Burti **a**–**e** (1.1. att.) ataino enerģijas pārejas procesus laika skalā:

a absorbcija (10^{-15} s);
b vibrāciju relaksācija (10^{-14} – 10^{-11} s);
c fluorescence (10^{-9} –10^{-7} s);
d starpsistēmu pāreja (10^{-8}–10^{-3} s);
e fosforescence (10^{-6}–10^{3} s).

Pēc enerģijas absorbcijas luminofors tiek ierosināts no singleta pamatstāvokļa (S_0) uz ierosinātu singleta stāvokli (S_1; **a** process) ar secīgu vibrāciju relaksāciju (**b** process) un **fluorescenci** (**c** process). Fluorescence ir emisija no ierosinātiem S_n stāvokļiem (1.1. att.). Tās norisei nepieciešami trīs secīgi procesi: **a** → **b** → **c**. Procesi **a** un **b** ir ātri, bet process **c** – lēnāks, tāpēc **a** un **b** procesi neietekmē luminiscences ātrumu, un tā notiek procesa **c** laika skalā.

Cits fluorescences veids ir tā sauktā **aizkavētā fluorescence**. Lai notiktu aizkavētā fluorescence, pamatstāvokļa luminoforam ir jāveic piecas secīgas pārejas: **a** → **b** → **d** → $\mathbf{d}_{(atgiezenisks)}$ → **c**. Tā kā process $\mathbf{d}_{(atgriezenisks)}$ parasti ir vislēnākais, tas arī nosaka aizkavētās emisijas laika skalu. Process $\mathbf{d}_{(atgriezenisks)}$ (t.i., atgriezeniska starpsistēmu pāreja jeb ISC) notiks, ja zemākā ierosinātā S_1 stāvokļa un zemākā ierosinātā tripleta (T_n) stāvokļa enerģijas līmeņu starpība būs mazāka kā ~ 0,1 *eV*.[19]

Fosforescence ir plaši pētīts fotoluminiscences paveids. Fosforescence ir emisija no ierosinātiem T_n stāvokļiem, un tā ietver četrus secīgus procesus: **a** → **b** → **d** → **e**. Fosforescence parasti notiek laika skalā, kas ir ilgāka par 10^{-6} s. Jāatzīmē, ka relatīvi ilgais fosforescences dzīves laiks var izraisīt ierosinātā T_1 stāvokļa dzēšanu neradiatīvās relaksācijas ceļā.[20]

Absorbciju, fluorescenci un fosforescenci var novērot ar UV-Vis spektroskopiju (1.2. att.). Absorbcija parasti tiek iniciēta no zemākā pamatstāvokļa (S_0). Tajā ir vairākas joslas, kas atbilst ierosinātas molekulas dažādiem S_n stāvokļiem (1.2. att., kur n = 1, 2, 3). Pēc tam notiek ātra neizstarojoša relaksācija līdz zemākajam ierosinātajam S_1 (vai T_1) stāvoklim (**b** process, 1.1. att.). Šī iemesla dēļ izstarojošie procesi vairumā gadījumu notiek no zemākās enerģijas S_1 vai T_1 stāvokļiem,[21] un fluorescences un fosforescences spektri parasti nav atkarīgi no ierosmes viļņa garuma.

Izstarojošie relaksācijas procesi no S_1 (fluorescence) vai T_1 (fosforescence) stāvokļiem spēj nokļūt augstākos S_0 enerģijas vibrāciju līmeņos, kā rezultātā veidojas strukturēti fluorescences un fosforescences spektri ar emisijas joslām, kas atbilst pieejamajiem vibrāciju līmeņiem (1.2. att.). Daži fluorescences veidi, piemēram, lādiņa pārneses (CT) tipa emisija, neizrāda strukturētu emisiju.[22]

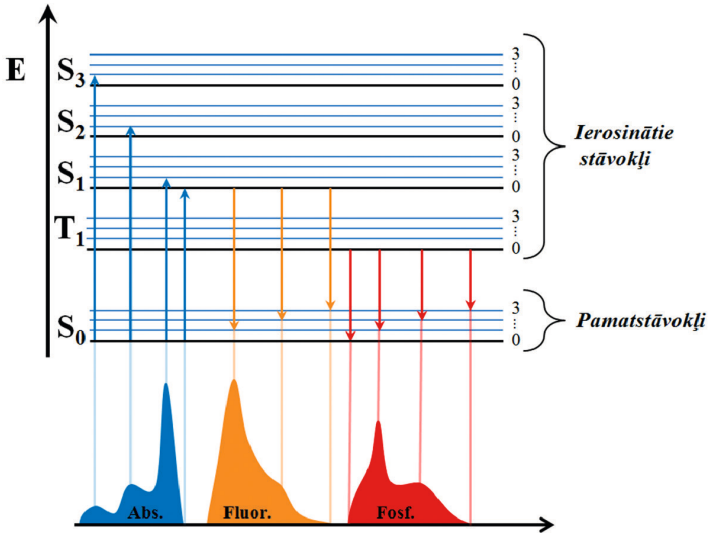

1.2. att. **Jablonska diagrammas un UV-VIS spektru korelācija**

Viens no svarīgākajiem efektīva luminofora kritērijiem ir fotoluminiscences kvantu iznākums (Φ). To definē kā emitēto fotonu daļu no absorbēto fotonu skaita, un to aprēķina ar vienādojumu 1:

(1) $\Phi_{\%} = \frac{\sum PE}{\sum PA} \times 100$, kur

$\Phi_{\%}$ – kvantu iznākums, %;
$\sum PE$ – visu izstaroto fotonu summa;
$\sum PA$ – visu absorbēto fotonu summa.

Fluorescence ir salīdzinoši ātrs spinu saglabājošs process, kam raksturīgi augsti Φ. Turpretim fosforescences pamatā ir enerģētiski neizdevīgas S uz T un T uz S spinu pārejas, kas parasti noved pie zemiem Φ. Turklāt salīdzinoši garais ierosinātā tripleta stāvokļa dzīves laiks bieži ir saistīts ar konkurējošu neizstarojošu relaksāciju un emisijas slāpēšanu ārēju faktoru, piemēram, ūdens vai skābekļa rezultātā. Šie efekti noved pie Φ samazināšanās.

Iepriekš minētie emisijas procesi ir raksturīgi luminoforiem izolētā stāvoklī (parasti šķīdumā ar koncentrāciju zem 10^{-5} M vai polimēru matricās), kur izstarotājs nesaskaras ar nozīmīgām starpmolekulārām mijiedarbībām. Arī cietvielu luminiscence tiek plaši izmantota. Cietā stāvoklī starpmolekulārās mijiedarbības starp luminoforiem būtiski ietekmē to emisīvās īpašības.

1.2. Organiskie izstarotāji

Organiskas gaismu izstarojošas molekulas (luminoforus) var iedalīt divās lielās grupās: metālorganiskie un organiskie luminofori (1.3. att.). Lielākā daļa metālorganisko luminoforu sastāv no pārejas metāla (piemēram, Ir, Pt) un bidentātiem ligandiem oktaedriskā (**1**) vai planārā kvadrātveida (**2**) ģeometrijā.[23] Savukārt organiskie luminofori parasti ir policikliski aromātiski karbo- vai heterociklu, piemēram, antracēna (**3**), karbazola (**4**) vai pirēna (**5**) atvasinājumi.[24] Metālorganisko luminoforu galvenie trūkumi ir to augstās izmaksas un toksicitāte, kā arī zemā noturība pret mitrumu un skābekli, turpretim organiskajos izstarotājos šie ierobežojumi ir mazāk izteikti (1.3. att.).

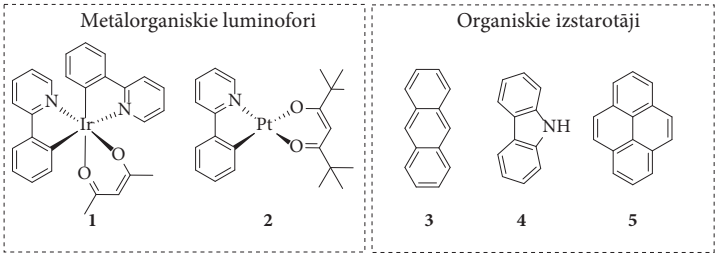

1.3. att. **Arhetipiskie luminofori**

Organisko izstarotāju luminiscences īpašības ir saistītas ar elektronu pārejām konjugētās π-sistēmās. Vienkāršākā π-sistēma ir etēns **6**, kam ir viena saiti veidojoša (π) un viena saiti irdinoša (π*) molekulārā orbitāle. Pēc etēna ierosināšanas (izmantojot 180 nm elektromagnētisko starojumu) elektrons veic π → π* pāreju, veidojot ierosinātu stāvokli **6*** (1.4. att.). Tātad π → π* pāreja atbilst 1.1 nodaļā apskatītajai $S_0 \rightarrow S_1$ pārejai. Secīgi izstarojoši $S_1 \rightarrow S_0$ relaksācijas procesi izraisa fluorescenci. Konjugēto π-sistēmu skaita palielināšana izraisa enerģijas starpības samazināšanos starp augstāko aizpildīto

(HOMO) un zemāko neaizpildīto molekulāro orbitāli (LUMO) jeb S_0 un S_1 stāvokļiem, kas ļauj absorbēt elektromagnētisko starojumu ar zemāku enerģiju. Lai izprastu S_0 un S_1 enerģijas starpības samazināšanās iemeslu paplašinātās π-sistēmās, jāapspriež vienkāršā Hikeļa (*Hückel*) teorija (HT), kas apskata molekulāro orbitāļu enerģijas līmeņus.

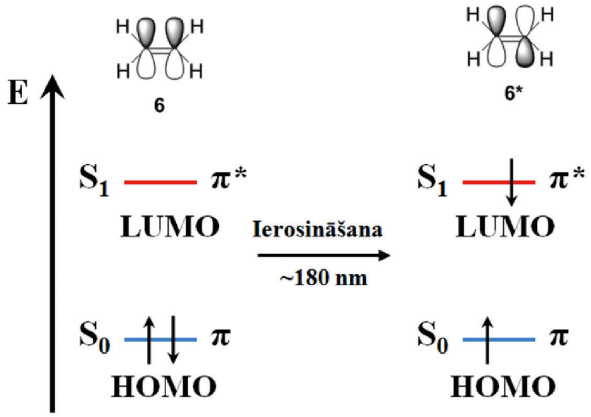

1.4. att. **Etēna (6) ierosināšana**

Saskaņā ar vienkāršo HT enerģijas atskaites punkts molekulārajām orbitālēm, piemēram, HOMO un LUMO ir vienas sp^2 orbitāles enerģija (α, 1.5. att.). HOMO veidošanās etēnā **6** rezultējas no elektroniskās sadarbības (norādīta kā β) starp divām sp^2 orbitālēm, kas izraisa stabilizējošu efektu (parādīts zilā krāsā, 1.5. att.). Elektroniskā sadarbība β starp divām sp^2 orbitālēm var izraisīt arī destabilizāciju (parādīts sarkanā krāsā, 1.5. att.), tādējādi veidojot LUMO. Enerģijas (E) vērtības HOMO un LUMO etēnā ir attiecīgi $E^{HOMO} = \alpha + \beta$ un $E^{LUMO} = \alpha - \beta$.[a] Atšķirībā no vienas π-sistēmas etēnā konjugētais 1,3-butadiēns (**7**) veido divas saiti veidojošas un divas saiti irdinošas molekulārās orbitāles. 3-butadiēna (**7**) stabilizējošā elektroniskā sadarbība β starp visām četrām sp^2 orbitālēm veido $HOMO_{-1}$, kam raksturīga zemāka enerģija kā etēna HOMO. Vienlaikus stabilizējošā elektroniskā sadarbība β starp abām sp^2 orbitālēm kopā ar destabilizējošo elektronisko sadarbību β starp divu sp^2 orbitāļu pāriem nodrošina, ka diēna **7** HOMO enerģija ir ***augstāka*** par etēna (**6**) HOMO. Turpretim LUMO un $LUMO_{+1}$ gadījumā 1,3-butadiēnā (**7**) dominē destabilizējošas elektroniskās sadarbības β. Destabilizējošas sadarbības β starp divām sp^2 orbitālēm apvienojumā ar stabilizējošo elektronisko sadarbību β starp diviem sp^2 orbitāļu pāriem dēļ rodas diēna **7** LUMO enerģijas vērtība, kas ir ***zemāka*** par etēna (**6**) LUMO. Pilnīga destabilizēšana savienojumā **7** starp visām četrām sp^2 orbitālēm noved pie $LUMO_{+1}$, kas ir ar augstāku enerģiju kā LUMO etēnā (**6**). Tādējādi daļēji stabilizējošas un destabilizējošas elektroniskās sadarbības β rezultātā savienojumiem ar paplašinātām konjugētām sistēmām būs samazināta HOMO un LUMO (attiecīgi S_0 un S_1 stāvokļu) enerģijas starpība. Vienkāršā HT dod ieskatu HOMO un LUMO līmeņu enerģiju vērtībās nelielās organiskās molekulās. Tomēr vienkāršā HT veic daudzus pieņēmumus enerģijas līmeņu aprēķinos, tāpēc, lai novērtētu HOMO un

[a] Gan α, gan β ir negatīvas vērtības, tāpēc negatīvo vērtību summa dod zemāku E^{HOMO} enerģiju.

LUMO enerģijas līmeņu enerģijas lielākām molekulām, piemēram, organiskajiem luminoforiem, ir jāizmanto blīvuma funkcionālā teorija (DFT).

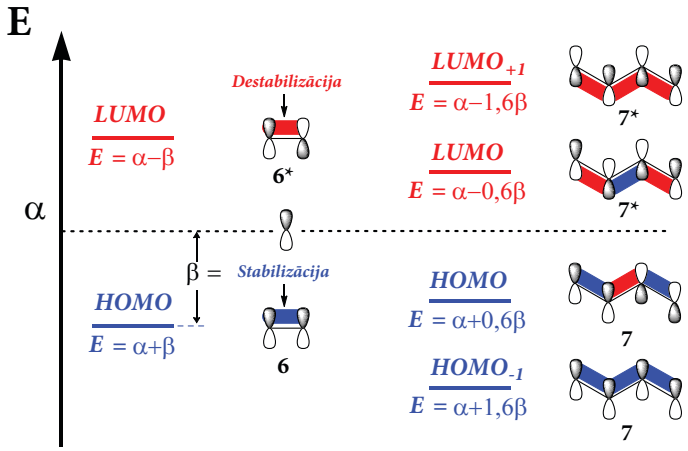

1.5. att. **Savienojumu 6 and 7 MO enerģijas līmeņi**

Paplašinātas aromātiskās π-sistēmas nodrošina relatīvi nelielu S_0 un S_1 enerģijas starpību lielākajā daļā organisko luminoforu. Piemēram, π-sistēmas paplašināšana samazina enerģijas starpību starp S_0 un S_1 stāvokļiem un izraisa absorbcijas maksimuma (λ_{Abs}) batohromo nobīdi no 255 nm benzolā (**8**) līdz 477 nm tetracēnā **10** (1.1. tabula). Liels konjugētas π-sistēmas izmērs uzlabo spēju absorbēt gaismu, kas tiek raksturota ar atenuācijas koeficientu (k_A). Tādējādi kondensētas π-sistēmas paplašināšana izraisa nelineāru k_A pieaugumu no 180 $cm^{-1}M^{-1}$ benzolā (**8**) līdz 360 $cm^{-1}M^{-1}$ naftalīnā (**9**), 7100 $cm^{-1}M^{-1}$ antracēnā (**3**) un 110000 $cm^{-1}M^{-1}$ tetracēnā (**10**) (1.1. tabula).

1.1. tabula. **Arēnu 3, 8–10 absorbcijas maksimumi (λ_{Abs}) un atenuācijas koeficienti (k_A)**

Luminofors	Struktūra	λ_{Abs}, nm	k_A, $cm^{-1}M^{-1}$
8		255	180
9		286	360
3		375	7100
10	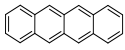	477	110000

Arī heteroatomiem ir liela ietekme uz organisko izstarotāju fotofizikālājām īpašībām, jo to nedalīto elektronu pāru orbitāles piedalās elektroniskajās HOMO un LUMO pārejās. Benzola (**8**) absorbcijas spektrā ir joslas, kas saistītas tikai ar π → π* pārejām (***a***, 1.6. A att.). Savukārt aizvietojot vienu oglekļa atomu ar heteroatomu (slāpekli), molekulā tiek ieviests nedalīts elektronu pāris jeb saiti neveidojoša (n) orbitāle. Piemēram, piridīna (**11**) absorbcijas spektrā būs novērojamas gan π → π*, gan n → π* pārejas un

attiecīgi divas absorbcijas joslas ***a*** un ***b***. Nedalītajam elektronu pārim n-orbitālē parasti piemīt zemāka stabilitāte un augstāka enerģija kā π molekulārās orbitāles pamatstāvoklī. Tāpēc n → π* pārejai būs raksturīga mazāka enerģijas starpība kā π → π* pārejai, un salīdzinājumā ar joslu ***a*** absorbcijas joslai ***b*** būs novērojama batohromā nobīde (1.6. A att.).

Heteroatomu n-orbitāļu iekļaušana luminoforu molekulā, izmantojot ISC, ļauj ne tikai ģenerēt T_n stāvokļus, bet arī palielināt ISC ātrumu. Organiskajos heteroatomu nesaturošos savienojumos ISC ir izteikti lēns vājas spinu-orbitāļu sadarbības (SOC)[25] starp singleta S_1 ($^1\pi\pi^*$) un tripleta T_n ($^3\pi\pi^*$) ierosinātajiem stāvokļiem dēļ, jo elektronu ($^1\pi\pi^* \rightarrow {}^3\pi\pi^*$) kvantu stāvokļa maiņa ir spinu nesaglabājoša un aizliegta pāreja (1.6. B att.). ISC ātruma palielināšana ir iespējama, ja pāreja no singleta uz tripletu ir saistīta ar orbitāles tipa maiņu. Šo efektu dēvē par *El-Sayed* likumu (1.6. B att.). Orbitāles tipu var mainīt, molekulā ievadot nedalītā pāra n-orbitāli. Tā kā n-orbitāles enerģija samazinās, sadarbojoties ar σ-orbitālēm, $^1n\pi^*$ stāvokļa enerģija tuvojas $^3\pi\pi^*$ tripleta enerģijas stāvoklim.[26] Mazā enerģijas atšķirība starp $^1n\pi^*$ un $^3\pi\pi^*$ stāvokļiem palielina SOC un paātrina ISC.

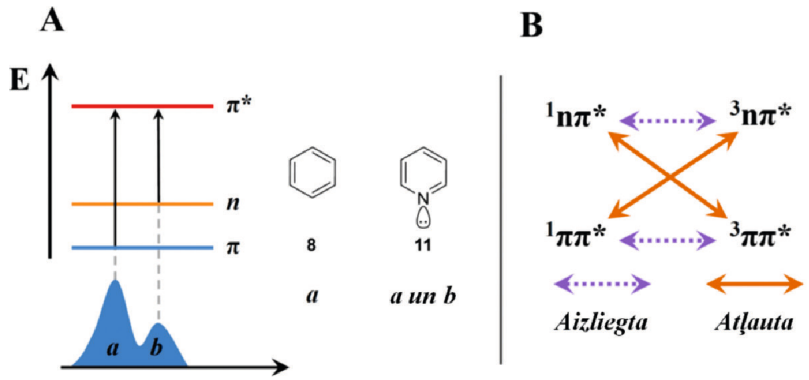

1.6. att. **A: Heteroatoma ietekme un fotoluminiscentajām īpašībām; B: *El-Sayed* likums**

Salīdzinot ar singleta S_1 stāvokļiem, tripleta ierosināto stāvokļu T_n relaksācija ir lēnāka, kā rezultātā tiem ir ilgāks dzīves laiks. Efektīva ISC no S_1 uz T_n stāvokļiem var samazināt fluorescences emisijas intensitāti, turklāt T_n stāvokļi spēj relaksēties, izmantojot arī neradiatīvus ceļus. Neradiatīvā relaksācija ir īpaši izteikta vidē, kur luminofora molekula iekšmolekulāri var brīvi vibrēt un rotēt, tāpēc efektīva T_1 stāvokļu ģenerēšana šķīdumos spēj pilnībā dzēst luminofora emisiju.

Vāji izstarojoša luminofora emisiju ir iespējams palielināt, izmantojot iekšmolekulāras mijiedarbības. Lai gan Brauna (*Brownian*) kustību rezultātā starpmolekulārās mijiedarbības ir ļoti dinamiskas un salīdzinoši vājas, tomēr dažas, piemēram, π–π$^+$ mijiedarbības ir pietiekami enerģētiski izdevīgas,[27] lai tās veidotos arī šķīdumā, piemērotos apstākļos. Piemēram, vāji emisīvā piridīna (**12**) kvatenizēšana ar MeI deva piridīnija sāli **13**, kas CH_2Cl_2/benzola šķīdumā izrādīja vāju emisiju (1.7. att.). Savukārt tīrā CH_2Cl_2 savienojumam **13** tika novērots 114 reižu lielāks emisijas pieaugums. Tas tika saistīts ar iekšmolekulārās π–π$^+$ mijiedarbības veidošanos, ko varēja novērot ^{1}H NOE kodolmagnētiskās rezonanses (KMR) eksperimentos. Tādēļ starpmolekulārās π–π$^+$ mijiedarbības veidošanu var izmantot šķīduma emisijas pieauguma nodrošināšanai.

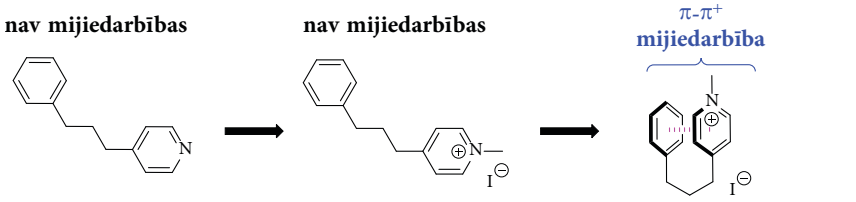

1.7. att. **Iekšmolekulāru π–π⁺ mijiedarbību efekts šķīdumā**

1.3. Luminoforu emisija cietvielās

Emisijas intensitātes kritums, palielinot luminofora koncentrāciju šķīdumā, pirmoreiz tika publicēts 1954. gadā.[28] Pētījumi šajā virzienā parādīja, ka, luminoforiem agregējoties, emisija samazinās, šo fenomenu dēvē par agregācijas izraisīto dzēšanu (ACQ). ACQ efektu novēro vairumam organisko luminoforu, to labi ilustrē THF-ūdens maisījumu eksperiments (1.8. att.). Attiecīgi ūdens pievienošana luminofora THF šķīdumam izraisa pakāpenisku emisijas samazināšanos, līdz tiek novērota pilnīga emisijas dzēšana. Pievienotais ūdens samazina organiskā emitētāja šķīdību, izraisot luminofora molekulu agregāciju. Tādējādi emisijas zudums ir saistīts ar starpmolekulārajām mijiedarbībām luminoforu starpā.[29]

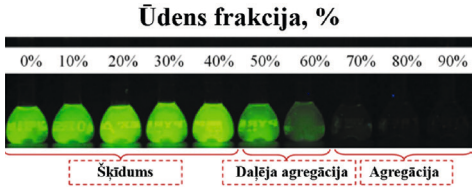

1.8. att. **ACQ efekts**

Cietvielu luminoforos starpmolekulāro mijiedarbību prognozēšana ir ļoti sarežģīts uzdevums, jo vairāki parametri, piemēram, kristalizācijas šķīdinātājs, temperatūra, higroskopiskums, kristalizācijas ātrums un kristalizācijas pakāpe var ietekmēt kristāliskās struktūras pakojumu. Vienkāršākais emisijas zuduma noteikšanas veids ir mērķtiecīgs luminofora molekulas dizains, kurā būtu pētāmā mijiedarbība. Piemēram, lai pārbaudītu starpmolekulāro π–π mijiedarbību ietekmi uz ACQ efektu, tika iegūta virkne kovalenti saistītu dimērisko perilēn-3,4-dikarboksimīda (PDI) atvasinājumu **14**–**16** (1.2. tabula).[30]

PDI savienojumu sērijā spēcīgākā iekšmolekulārā π–π mijiedarbība novērojama luminoforā **14**, savienojumā **15** tā bija vājāka, savukārt luminoforā **16** – nenozīmīga. Šķīdumā savienojumiem **14**, **15** un **16** tika novērota batohroma absorbcijas maksimuma (λ^{abs}_{max}) nobīde no 476 līdz 483 un pat 511 nm (1.2. tabula). Savienojumiem **14**–**16** tika novērota arī hipsohromiska emisijas maksimuma (λ^{em}_{max}) maiņa no 740 uz 543 nm,

attiecīgi. Līdz ar to π–π mijiedarbības šķīdumā mēreni ietekmē λ^{abs}_{max}, bet spēcīgi λ^{em}_{max}. Jāatzīmē, ka viskrasākās izmaiņas tika noteiktas kristāliskā stāvokļa Φ (Φ_c). Tādējādi savienojumā **16** ar nenozīmīgu iekšmolekulāru π–π mijiedarbību Φ_c vērtība bija 92 %. π–π mijiedarbības spēka pieaugums izraisīja strauju Φ_c vērtības samazināšanos no 61 % savienojumā **15** līdz tikai 2 % izstarotājā **14**. Šie dati skaidri parāda, ka π–π mijiedarbība ir atbildīga par novēroto ACQ efektu.

1.2. tabula. **Savienojumu 14, 15 un 16 fotofizikālās īpašības**

Luminofors	Struktūra	λ^{abs}_{max}, nm	λ^{em}_{max}, nm	Φ_c, %
14	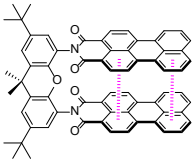	476	740	2
15	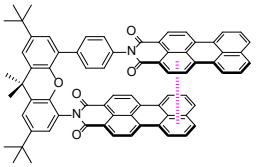	483	603	61
16	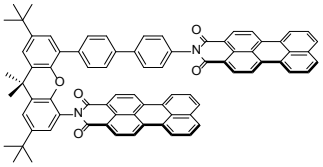	511	543	92

Tā kā spēcīgām π–π mijiedarbībām ir tendence samazināt luminoforu Φ vērtības, viena no stratēģijām augsta Φ sasniegšanai cietvielās ir izstarotāju dizains, kuros nebūtu nevēlamās π–π mijiedarbības. 2001. gadā Tangs ziņoja par poliaizvietotu silolu **17**,[31] kam nebija izteiktas enerģiskas π–π mijiedarbības fenilaizvietotāju ārpusplaknes novietojuma dēļ. Savienojumu **17** izteikti emisīvu padara π–π mijiedarbību trūkums cietvielā un agregātos. To arī ilustrē eksperiments, kurā pēc ūdens pievienošanas neizstarojošs savienojuma **17** THF šķīdums kļūst augsti izstarojošs (1.9. att.). Savītās telpiskās struktūras dēļ savienojums **17** šķīdumā spēj rotēt un vibrēt, kā rezultātā tiek panākta efektīva neizstarojoša relaksācija. Vājas starpmolekulāras mijiedarbības, piemēram, H–π saites nomāc savienojuma **17** vibrāciju un rotāciju agregātos, radot augstu emisiju. Iepriekšminēto parādību sauc par agregācijas izraisīto emisiju (AIE), un tā ir pretēja ACQ.

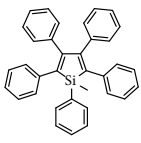

17

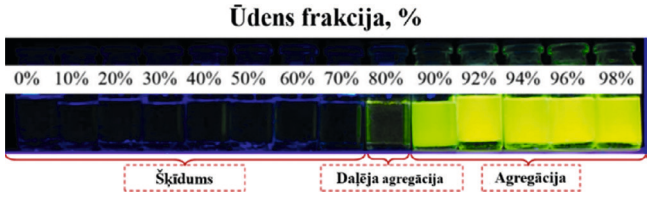

1.9. att. **AIE efekts**

Lielākā daļa no AIE luminogēniem (AIEgēniem) ir izstrādāti, pamatojoties uz tādu pašu dizainu kā luminoforā **17**, un tiem ir līdzīgi emisijas mehānismi. Šīs stēriski traucētās molekulas izstaro gaismu cietā stāvoklī to ierobežotās iekšmolekulārās vibrācijas (RIV) un rotācijas (RIR) dēļ. Gan RIV, gan RIR nomāc ierosināto stāvokļu kustību izraisītos neizstarojošos relaksācijas ceļus. Piemēram, AIE īpašības attēlo izstarotājs **18**, tam ir vāja emisija MeCN šķīdumā, bet intensīva, dzeltena emisija agregātos (1.10. att.).[32] Šķīdumā fenilgredzenu rotācija, kā arī CN saites vibrācija dzēš ierosinātos stāvokļus. Savukārt apgrūtinātās rotācijas un vibrācijas dēļ agregācija nomāc ierosināto stāvokļu relaksācijas kanālus, padarot savienojumu **18** emisīvu.

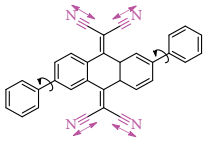

18

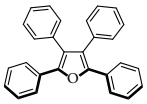

19

1.10. att. **AIE savienojums 18 and ACQ savienojums 19**

RIV un RIR mehānismi ir izprasti, un tie ir plaši izmantoti AIEgēnu dizainā. Daži mērķtiecīgi dizainētie luminofori tomēr neizrāda AIE īpašības. Piemēram, tetrafenilfurāns **19** (1.10. att.) izrāda augstu emisiju šķīdumā (40 % Φ), turpretim pēc agregācijas zaudē savas emisīvās spējas (1 % Φ).[33] DFT aprēķini parādīja, ka savienojumā **19** furāna gredzens ar 2. un 5. pozīcijas fenilaizvietotājiem veido gandrīz planāru konjugētu sistēmu, kas nodrošina augstu emisijas intensitāti šķīdumā. Tomēr kristāliskā stāvoklī luminofora **19** konjugētā sistēma starpmolekulāri mijiedarbojas ar blakus esošās molekulas skābekļa atoma n-orbitāli, kas secināts no rentgenstruktūras analīzes datiem. Acīmredzot n–π mijiedarbību rezultātā notiek cietvielas emisijas dzēšana. Tādējādi spēcīga orbitāļu (piemēram, n–π vai π–π) starpmolekulārā mijiedarbība lielā mērā ietekmē visu luminoforu emisijas intensitāti, ieskaitot tos, kas veidoti kā AIEgēni.

1.4. Cietvielu fosforescence

Luminoforu molekulu kustība kristālrežģī ir traucēta zemas enerģijas, piemēram, H–π saišu un augstas enerģijas, piemēram, π–π mijiedarbību dēļ. Šīs cietvielu mijiedarbības samazina ierosināto stāvokļu kustības izraisīto relaksāciju un no tripleta stāvokļiem palīdz veidoties emisijai jeb fosforesencei. Luminoforu savstarpējo mijiedarbību nozīme cietvielu fosforescencē ir parādīta turpmāk apskatītajā darbā: attiecīgi tika pētītas benzofenonu **20**–**23** fosforescentās īpašības MeCN šķīdumā un cietā stāvoklī (1.3. tabula).[34] Izstarotāji **20**–**23** izrādīja niecīgu emisiju MeCN šķīdumos ar Φ zem 0,5 %. Savukārt spēcīga emisija savienojumiem **20**–**23** tika novērota kristāliskajā stāvoklī ar fluorescences un fosforcences Φ_{kr} vērtību summu robežās no 8,3 līdz 39,7 %. Palielinātā cietvielu emisija tika saistīta ar neizstarojošās relaksācijas nomākšanu starpmolekulāro mijiedarbību rezultātā. Balstoties uz rentgena analīzes datiem savienojumu **20**–**23** kristālos tika identificēts starpmolekulāru ūdeņraža saišu tīkls (C–H ··· O un C–H ··· X (X = F, Cl, Br)), kā

arī halogēnu-halogēnu mijiedarbības (C–Br ··· Br–C), kas, ierobežojot konformacionālo brīvību, padarīja tos emisīvus.

1.3. tabula. **Savienojumu 20–23 fotofizikālās īpašības**

Luminofors	Struktūra	Φ_{MeCN}, %	Φ_{kr}, %	Novērotās starpmolekulārās mijiedarbības
20	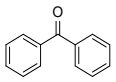	<0,1	15,9	C–H···O
21	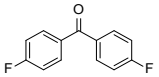	<0,1	39,7	C–H···O C–H···F
22	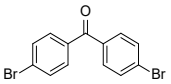	<0,1	8,30	C–H···O C–H···Cl
23	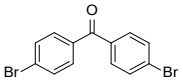	0,5	12,0	C–H···O C–H···Br C–Br···Br–C

Starpmolekulārās mijiedarbības kristāliskajā stāvoklī ierobežo luminofora molekulas kustību un ietekmē arī fosforescences dzīves laiku (τ_{phos}). Piemēram, karbazolu saturošajos luminoforos **24**–**26** tika novērota būtiska korelācija starp τ_{phos} un starpmolekulāro attālumu. Ilgākais cietvielas fosforescences τ_{phos} novērots izstarotājam **24** (748 ms), tam bija arī visblīvākais kristālu pakojums ar starpmolekulāro N-N attālumu 5,53 Å (1.4. tabula).[35] Savienojumos **25** un **26** starpmolekulārais N-N attālums bija 6,02 un 6,17 Å, un τ_{phos} samazinājās līdz 340 un 114 ms, attiecīgi. Izstarotāja **24** ilgais τ_{phos} skaidrojams ar labāku tripleta eksitonu stabilizāciju spēcīgas elektroniskās sadarbības dēļ starp blīvi pakotajām luminofora molekulām kristālrežģī.

1.4. tabula. **Savienojumu 24–26 emisīvās īpašības**

Nr	Struktūra	Luminofors	τ_{phos}, ms	N-N attālums, Å
1	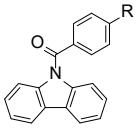	**24** (R = H)	748	5,53
2		**25** (R = Me)	340	6,02
3		**26** (R = OMe)	114	6,17

Starpmolekulārās mijiedarbības kristālrežģī būtiski ietekmē fosforescences intensitāti un dzīves laiku, tāpēc ir nepieciešama paredzama starpmolekulāro mijiedarbību novērtēšanas metode efektīvu cietvielu luminoforu izstrādei. Rentgenstaru kristalogrāfija ir visplašāk izmantotā metode luminoforu kristāla stāvokļa ģeometrijas noteikšanai un starpmolekulāro mijiedarbību stipruma novērtēšanai. Tās pamatā ir attālumu mērījumi starp atomiem vai blakus esošu izstarotāju molekulām. Attālums starp luminoforu

molekulām viens pats nedod pietiekamu informāciju par starpmolekulārajām mijiedarbībām molekulāro orbitāļu nevienmērīgas lokalizācijas dēļ. Starpmolekulārās LUMO-LUMO, HOMO-HOMO un HOMO-LUMO mijiedarbības stiprumu precīzāk raksturo attiecīgo viļņu funkciju pārklāšanās. Divu viļņu funkciju starptelpu mijiedarbības enerģiju sauc par elektronisko sadarbību.

Elektroniskā sadarbība (***V***) ir stabilizējošs spēks. Tas ir vienāds ar stabilizēšanas enerģiju β, kas rodas divu sp^2 orbitāļu pārklāšanās rezultātā (sk. 1.5. att.). Tā kā β ir vienāda ar ***V*** (HOMO), jebkura relatīvi tuva cietvielas starpmolekulāra mijiedarbība (piemēram, C–H···O, n–π, π–π utt.) nodrošinās stabilizējošu efektu, palielinot ***V***. Starpmolekulārā elektroniskā sadarbības (***V***) spēka pieaugums starp luminoforiem ir viens no galvenajiem faktoriem, kas nodrošina fosforescenci cietvielās.[36] Spēcīga starpmolekulāra ***V*** starp ππ* un nπ* stāvokļiem ir svarīga, lai iegūtu izteikti ilgu fosforescences dzīves laiku τ_{phos}.[37] Īpaši garus τ_{phos} var iegūt, stabilizējot lādiņu atdalītos tripleta stāvokļus.[38] Tripleta stāvokļu atdalīšanas un atkārtotas savienošanās ātrumus nosaka ***V***,[39] kas arī raksturo lādiņa pārneses (CT) ātrumu starp molekulām.[40]

Tā kā CT vai lādiņa kustība kristālrežģī lielā mērā ietekmē fosforescējošā materiāla τ_{phos}, un *El Sayed* likums izpildās iekšmolekulāri, fosforescences dzīves laikam un Φ būtu jāmainās neatkarīgi. Tomēr zinātniskās literatūras dati liecina, ka augsts fosforescences Φ nodrošina samazinātu fosforescences dzīves laiku cietvielā.[41] Organisku fosforescējošu cietvielu materiālu izstrāde ar augstu fosforescences Φ un ilgu dzīves laiku ir ļoti sarežģīts uzdevums.

2. NODAĻA. PROMOCIJAS DARBA MĒRĶI, UZDEVUMI, ZINĀTNISKĀ NOVITĀTE UN PRAKTISKĀ NOZĪME

2.1. Promocijas darba mērķi un uzdevumi

Balstoties uz publicēto pētījumu, kurā stāstīts par iekšmolekulāro π–π^+ mijiedarbību ievērojamo ietekmi uz emisiju šķīdumā (sk. 1.2. nodaļas 1.7. att.), tika izvirzīta hipotēze, ka starpmolekulāras π–π^+ un π^+–π^+ mijiedarbības varētu būt piemērotas arī augstas cietvielu emisijas un AIE efekta iegūšanai, izvairoties no ACQ efekta. Promocijas darba ***pirmais mērķis bija starpmolekulāru π–π^+ un π^+–π^+mijiedarbību izmantošana cietvielu AIE luminogēnu (AIEgēnu) izveidē.***

Pirmā mērķa sasniegšanai tika izvirzīti šādi uzdevumi:

1) pārbaudīt, vai slāpekļa heterociklus saturošu ACQ luminoforu kvaternizēšana izraisa AIE efektu, izmantojot π–π^+ un π^+–π^+ mijiedarbības;
2) pārbaudīt, vai ar protonēšanas palīdzību no slāpekli saturošiem ACQ luminoforiem iespējams iegūt AIEgēnus;
3) izpētīt pretjona efektu uz katjonisku AIEgēnu fotofizikālajām īpašībām;
4) mērķtiecīgi veidot luminofora struktūru, kas izrādītu augstu emisiju gan šķīdumā, gan cietvielā.

Tika izvirzīta arī otra hipotēze – starpmolekulārā mijiedarbība starp heteroatoma nedalīto elektrona pāri un blakus esošas izstarotāja molekulas π-sistēmu cietvielā varētu būt atbildīga par fosforescences dzīves laika samazināšanos (sk. 1.4. nodaļu). Ja šī hipotēze ir patiesa, tad telpisku aizvietotāju izmēra maiņa blakus nedalītajam elektronu pārim izmainīs tā mijiedarbību spēku, kā rezultātā būtu iespējams veidot fosforescējošus materiālus ar izteikti ilgu dzīves laiku (>100 milisekundes) un augstu fosforescences Φ. ***Otrais promocijas darba mērķis bija izpētīt starpmolekulāru mijiedarbību ietekmi uz cietvielu fosforescences dzīves laiku un izstrādāt jaunu, efektīvu fosforescējošu materiālu ieguves dizaina stratēģiju.***

Otrā mērķa sasniegšanai tika izvirzīti šādi uzdevumi:

5) dizainēt un sintezēt virkni tiofēnu saturošu cietvielu izstarotāju ar mainīgu telpisko aizvietotāju izmēru tuvu sēra nedalītajam elektronu pārim;
6) izveidot sakarību starp novērotajām mijiedarbībām un fosforescences īpašībām cietvielā.

2.2. Zinātniskā novitāte

Promocijas darbā tika izstrādāta jauna izstarotāju molekulārā dizaina pieeja gan cietvielā, gan šķīdumā. Izmantojot jaunu uz starpmolekulārām π–π^+ un π^+–π^+ mijiedarbībām balstītu dizainu, tika izstrādāti organiskie luminogēni ar augstu emisijas intensitāti gan šķīdumā, gan cietvielā. Vēlamās π–π^+ un π^+–π^+ mijiedarbības tika veidotas, luminoforu arēna fragmentu aizvietojot ar katjonu piridīnija gredzenu. No emisijas mehānisma

pētījumiem tika secināts, ka starpmolekulāra lādiņa pārnese ir atbildīga par augsto piridīnija sāļu emisiju gan šķīdumā, gan cietvielā.

Pētījumu gaitā tika izstrādāta jauna organisko fosforescento materiālu dizaina stratēģija, kurā novērsta korelācija starp fosforesences intensitāti un dzīves laiku. Izstrādātā pieeja balstās uz telpiski liela aizvietotāja ievadīšanu tiofēna luminoforā, blakus n-tipa sēra orbitālei. Telpiskais aizvietotājs nodrošina lielāku starpmolekulāru attālumu kristālrežģī un palīdz nomākt ātru $T_1 \rightarrow S_0$ relaksācijas kanālu, kā rezultātā pieaug fosforescences dzīves laiks, neietekmējot Φ.

2.3. Praktiskā nozīme

Nekovalentas $\pi–\pi^+$ un $\pi^+–\pi^+$ mijiedarbības izstarotājos paver to vairākas izmantošanas iespējas:

- racionālā cietvielu luminoforu dizainā;
- plaša klāsta vāji izstarojošu ACQ materiālu pārveidošanā par intensīvi izstarojošiem AIEgēniem;
- izstarotāju un sensoru dizainā ar daudziem praktiskiem pielietojumiem šķīdumā.

Izstrādātajā metodē novērsta korelācija starp fosforescences intensitāti un dzīves laiku, tādējādi iespējams precīzi kontrolēt fosforescējošās īpašības. Šī pieeja ļauj iegūt efektīvus organiskos izstarotājus ar izteikti ilgu emisijas dzīves laiku un augstu fosforescences kvantu iznākumu istabas temperatūrā, ko var plaši pielietot biomedicīnā un materiālzinātnē.

3. NODAĻA. π–π⁺ UN π⁺–π⁺ MIJIEDARBĪBU IZMANTOŠANA AIEGĒNU DIZAINĀ

3.1. Neplanārie kvaternāro piridīnija sāļu AIEgēni

Novērtējot izstarotāja **13** veiksmīgo iekšmolekulāro π–π⁺ mijiedarbību izmantošanu šķīdumā (sk. 1.2. nodaļu), tika nolemts sintezēt karbazolu (Cz) saturošus benzilpiridīnija sāļus **27**–**29** ar mērķi pārbaudīt, vai starpmolekulāras π–π⁺ un π⁺–π⁺ mijiedarbības var izmantot arī cietvielu luminoforu dizainā (3.1. att.).

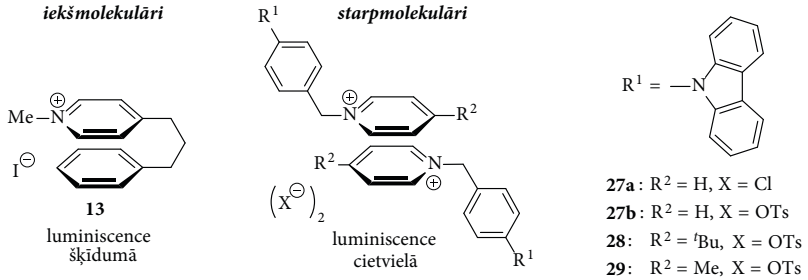

3.1. att. **π–π⁺ un π⁺–π⁺ mijiedarbību izmantošana AIEgēnu dizainā**

Benzilpiridīnija sāļiem piemīt samazinātas konformacionālās svārstības, salīdzinot ar publicēto savienojumu **13**. Piridīnija sāļu pretjona efekts pētīts hlorīdu (**27a**) un tozilātu (**27b**) saturošos savienojumos. Alkilaizvietotāju ievadīšana piridīnija gredzena 4. pozīcijā (-*t*Bu un –Me savienojumos **28** un **29** attiecīgi) deva ieskatu par stērisko traucējumu ietekmi uz mijiedarbībām starp luminoforiem.

3.1. tabula. **Piridīnija sāļu 26–29 emisijas īpašības**

Nr.	Izstarotājs	Cietv. λ_{Em}, nm	Šķīduma Φ (%)	Cietv. Φ (%)	α_{AIE}
1	**27a**	505	<0,1	17,3	>173
2	**27b**	432	<0,1	18,7	>187
3	**28**	465	<0,1	18,5	>185
4	**29**	442	<0,1	9,7	>97

Kā paredzēts, benzilpiridīnija fragmenta brīvā rotācija un luminoforu **27**–**29** nespēja iesaistīties starpmolekulārās π–π⁺ mijiedarbībās padarīja tos neizstarojošus MeCN šķīdumos ar Φ vērtībām zem 0,1 %. Turpretim cietvielā piridīnija sāļi **27**–**29** izrādīja plašu nestrukturētu emisiju ar maksimumiem diapazonā no 432–505 nm. To Φ ir robežās no 9,7 % (**29**) līdz 18,7 % (**27b**) (3.1. tabula). Līdz ar to luminofori **27**–**29** izrādīja izteiktas AIE īpašības. Lielākais emisijas pieaugums (α_{AIE}) cietvielā attiecībā pret šķīdumu

novērots savienojumam **27b** (187 reizes). Jāuzsver, ka sāļu **27a** un **27b** Φ bija ļoti līdzīgi, kas norādīja uz pretjonu nelielo ietekmi uz Φ.

Savienojumu **27**–**29** monokristālu rentgena analīzes dati palīdzēja noteikt galvenās mijiedarbības, kas atbildīgas par AIE efektu. Piridīnija sāļu **27a**, **27b**, **28** kristālrežģī bija novērojamas starpmolekulāras π^+–π^+ mijiedarbības starp lādētajiem piridīnija gredzeniem (3.2. tabula). Par mijiedarbībām liecināja tuvs nobīdīts un paralēls piridīnija gredzenu novietojums kristālrežģī (3,734 Å (**27a**) līdz 4,211 Å (**27b**) attālumā; 3.2. tabula). Savukārt piridīnija sāls **29** veidoja π–π^+ mijiedarbības starp piridīnija gredzenu un 1,4-diaizvietoto fenilēngrupu, ko apliecina relatīvi tuvais attālums (no 3,803 Å līdz 4,027 Å) starp divām neparalēli novietotām π-sistēmām (3.2. tabula).

3.2. tabula. **Piridīnijā sāļu 27–29 mijiedarbības kristālrežģī**

27a	**27b**	**28**	**29**
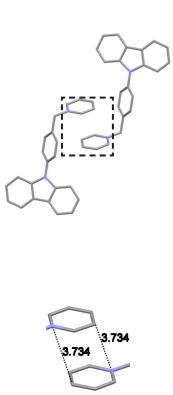	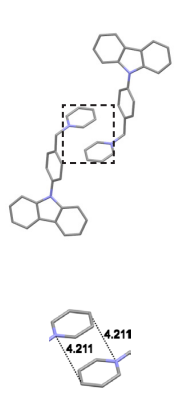	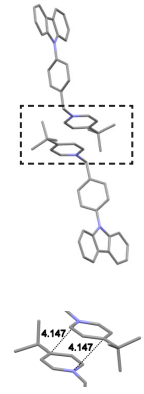	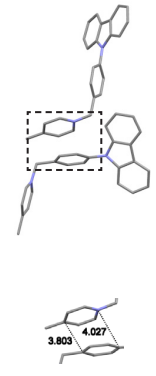

Piridīnija sāls **29** zemā Φ vērtība, salīdzinot ar **27a**, **27b** un **28** (3.1. tabula), liecina, ka π^+–π^+ piridīnija–piridīnija mijiedarbība nodrošina lielāku cietvielas emisijas intensitāti kā π–π^+ piridīnija–arēna mijiedarbība. Turklāt piridīnija **27a** (505 nm) un **27b** (432 nm, sk. 3.1. tabulu) emisijas maksimuma novirze ir saistīta ar π^+–π^+ mijiedarbības attāluma pieaugumu. Tas liecina, ka emisijas maksimums ir atkarīgs no attāluma starp piridīnija gredzeniem. Svarīgi, ka gan hlorīda, gan tozilāta pretjoni netraucēja veidoties π^+–π^+ un π–π^+ mijiedarbībām. Kopumā noteiktās cietvielu fotoluminiscences īpašības apvienojumā ar rentgenstaru kristalogrāfijas datiem sniedz pārliecinošus pierādījumus tam, ka π^+–π^+ un π–π^+ mijiedarbību veidošanās rada paaugstinātu cietvielu emisiju. Pilnīgs pētījuma pārskats ir apkopots publicētajā rakstā, sk. I pielikumu.

3.2. Planāro kvaternāro piridīnija sāļu AIEgēni

Pēc sekmīgas π^+–π^+ vai π–π^+ mijiedarbību izmantošanas AIEgēnu izstrādē pētījumus turpinājām ar AIEgēnu iegūšanu no ACQ izstarotājiem, tajos aizvietojot nevēlamās arēna-arēna π–π mijiedarbības ar arēna-katjona π–π^+ mijiedarbībām. Par pētījuma sākumpunktu tika izvēlēts arhetipisks neemisīvs ACQ izstarotājs **30** un tā izomēri **31**, **32** (sk. 3.3. tabulu), kam raksturīga planāra konjugēta π-sistēma (3.2. att.).

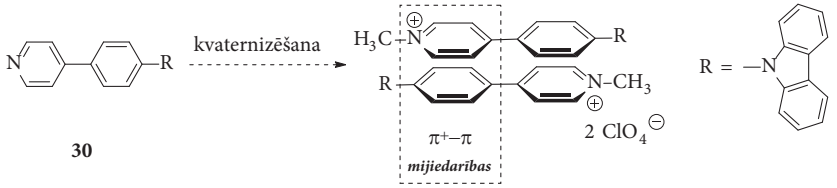

3.2. att. **Dizaina stratēģija ACQ izstarotāju pārvēršanai AIEgēnos**

Piridīnija jodīdi, ko ieguvām pēc piridīnu **30**–**32** alkilēšanas ar MeI, tika secīgi pakļauti jonu apmaiņai ar $AgClO_4$, iegūstot piridīnija perhlorātus **33**–**35** (3.3. tabula). MeCN šķīdumā piridīni **30**–**32** izrādīja izteiktu emisiju ar Φ vērtībām no 46,5 % līdz 74,6 % (1.–3. rinda). Savukārt piridīnija sāļiem **33**–**35** MeCN šķīdumā novērota niecīga emisija ar Φ vērtībām zem 0,1 % (4.–7. rinda). Konjugētie piridīni **30**–**32** izrādīja ACQ efektu ar α_{AIE} vērtībām zem 0,2. Interesanti, ka piridīnija sāls **33b** ar jodīda anjonu uzrādīja zemu cietvielu Φ (0,4 %; 5. rinda), turpretim piridīnija perhlorāti **33a**, **34** un **35** izrādīja intensīvu cietvielu emisiju ar Φ vērtībām 79,8, 72,2 un 46,9 %, attiecīgi (3.3. tabula, 4., 6., 7. rinda,). Piridīnija perhlorāts **33a** izrādīja vislielāko α_{AIE} vērtību – virs 800 (4. rinda). Luminiscences dati liecina, ka piridīnu saturošu luminoforu ar ACQ efektu var pārvērst par luminoforu ar AIE efektu, veicot piridīna slāpekļa atoma kvaternizēšanu ar secīgu jodīda-perhlorāta apmaiņu (3.3. tabula).

3.3. tabula. **Savienojumu 30–35 fotofizikālās īpašības**

Nr.	Izstarotājs	Cietv. λ_{Em}, nm	Šķīduma Φ, %	Cietv. Φ, %	α_{AIE}
1	**30** 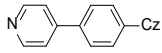	371, 387, 407	73,1	5,7	0,1
2	**31** 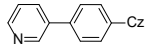	368	46,5	0,6	<0,1
3	**32** 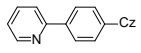	378, 436	74,6	16,8	0,2
4	**33a** 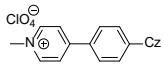	489	<0,1	79,8	>800
5	**33b** 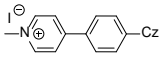	473	<0,1	0,40	>4
6	**34** 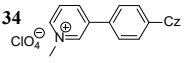	446	<0,1	72,2	>700
7	**35** 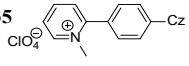	465	<0,1	46,9	>470

Cz = *N*-karbazolil

Monokristāla rentgenstruktūranalīze sniedza padziļinātu ieskatu piridīnija sāls **33a** mijiedarbībās, kam novērota augstākā emisijas intensitāte savienojumu **33**–**35** rindā. Abi katjoniskie luminoforu fragmenti iesaistījās simetriskās karbazola-piridīnija π–π^+

mijiedarbībās, kā arī mijiedarbībās ar īsu attālumu (3,53 Å) starp attiecīgajiem centroīdiem kristālrežģī (3.3. A att.). Jāatzīmē, ka līdzīgs pakojums ar π–π^+ mijiedarībām novērots arī piridīnija jodīdam **33b** (nav attēlots). Neraugoties uz acīmredzamo līdzību kristālrežģa pakojumā starp **33a** un **33b**, ievērojamā atšķirība cietvielu Φ (5. un 4. rinda, 3.3. tabula) liecina, ka jodīda jons savienojumā **33b** dzēš emisiju ar mehānismu, kas nav saistīts ar telpisku vai elektronisku ietekmi uz π–π^+ mijiedarbībām.

Lai izprastu cietvielu gaismas emisijas mehānismu katjonā **33a**, tika veikti no laika atkarīgie DFT (TD-DFT) aprēķini, izmantojot rentgenstruktūranalīzē iegūtās molekulu ģeometrijas. Aprēķini neapstiprināja iekšmolekulāru vienas molekulas HOMO-LUMO lādiņa pārnesi kā cietvielu emisiju avotu, jo aprēķinātā emisijas maksimuma intensitāte un novietojums neatbilda tam, kas eksperimentāli novērots katjonā **33a**. Turpretim aprēķinātais emisijas spektrs simetriskajā **33a** dimērā (emisijas maksimums ar λ_{max} = 495 nm un liels oscilatorais spēks f = 0,3784) atbilda eksperimentāli novērotajam cietvielu emisijas spektram (λ_{max} = 489 nm, 3.3. C att.). Līdz ar to TD-DFT aprēķini liecināja, ka emisija ir saistīta ar starpmolekulāru CT cauri telpai no LUMO, kas lokalizēta piridīnija un fenilēnsavienotājā, uz HOMO, kas lokalizēts karbazolā (3.3. B att.). Šāds CT emisijas mehānisms pilnībā atbilst samazinātai emisijai šķīdumos, kur CT caur telpu ir mazvarbūtīga.

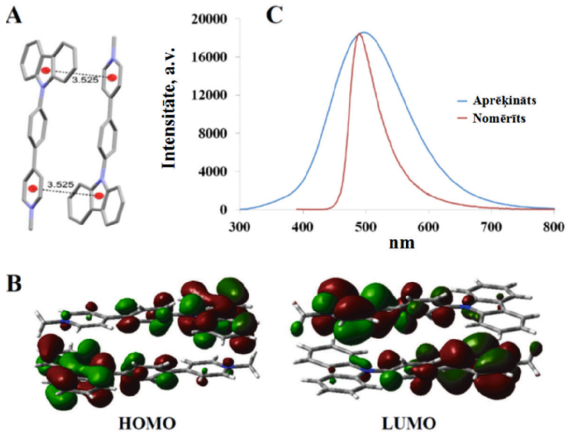

3.3. att. **A: Savienojuma 33a rentgenstaru struktūras attēlojums; B: TD-DFT aprēķinu rezultāti 33a dimērā; C: Aprēķinātais un nomērītais emisijas spektrs savienojumā 33a**

Mūsu pētījumi parāda, ka π–π^+ mijiedarbības var plaši pielietot efektīvu cietvielu izstarotāju iegūšanā. Pilns pētījuma pārskats ir apkopots publicētajā rakstā (sk. II pielikumu).

3.3. AIEgēnu veidošana, protonējot konjugētus piridīnus

Pēc veiksmīgā AIEgēnu dizaina, izmantojot kvaternizēšanas metodi, pētījumus turpinājām ar konjugētu piridīnu protonēšanu π–π^+ mijiedarbību iegūšanai. Šāda pieeja arī ļautu ACQ luminoforus pārvērst efektīvos cietvielu izstarotājos. Piridīnija luminoforos

papildus veicām arī sistemātisku pretjonu ietekmes izpēti novēroto cietvielu Φ atšķirību dēļ starp piridīnija perhlorātu **33a** (79,8 %) un jodīdu **33b** (0,4 %; sk. 3.3. tabulu). ACQ izstarotāju **30** protonējām ar $HClO_4$, HCl, HBr, HI, MsOH un HNO_3, iegūstot attiecīgos sāļus **36**–**41** (3.4. tabula). Perhlorātu **36** ieguvām kā vāji kristālisku cietvielu (**36A**) un kā divus dažādus polimorfus (**36B** un **36C**).

Atšķirībā no augsti emisīvā piridīna **30** MeCN šķīdumā piridīnija sāļiem **36**–**41** praktiski nebija novērojama emisija, to Φ vērtības bija zem 0,1 % (1. rinda pret 2. – 9. rindu, 3.4. tabula). Savukārt cietvielā piridīnija **36A**, **36B**, **36C**, **37**, **38**, **40** un **41** sāļiem novērota plaša, nestrukturēta emisijas josla ar maksimumiem diapazonā no 492 līdz 514 nm (2. – 6., 8. un 9. rinda). Jodīda anjonu saturošais piridīnija sāls **39** bija vienīgais neemisīvais materiāls (7. rinda), un tas pilnībā atbilst iepriekš novērotajam fluorescences kritumam piridīnija jodīdā **33b**. Vispiemērotākie piridīnija pretjoni ir perhlorāts (**36C**) un mezilāts (**40**). Jāatzīmē, ka savienojuma **36A** vāji kristāliskā forma uzrādīja zemāku Φ (5,5 %, 2. rinda) nekā polimorfi **36B** (24,1 %, 3. rinda) un **36C** (54,6 %, 4. rinda). Acīmredzot piridīnija sāļu emisijas efektivitāte cietā stāvoklī ir atkarīga gan no kristālizācijas pakāpes, gan no specifiskām mijiedarbībām kristālrežģī. Tajā pašā laikā protonēšana ir efektīva metode AIEgēnu izstrādei.

3.4. tabula. **Savienojumu 30, 36–41 fotofizikālās īpašības**

Nr.	Izstarotājs	Cietv. λ_{Em}, nm	Šķīduma Φ, %	Cietv. Φ, %
1	**30** 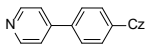	371, 387, 407	73,1	5,7
2	**36A** 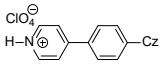	496	<0,1	5,5
3	**36B** 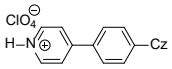	503	<0,1	24,1
4	**36C** 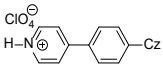	492	<0,1	54,6
5	**37** 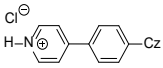	496	<0,1	42,4
6	**38** 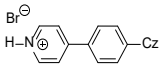	514	<0,1	18,2
7	**39** 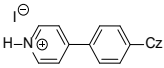	–	<0,1	<0,1
8	**40** 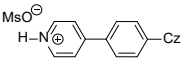	484	<0,1	45,8
9	**41** 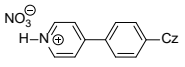	468	<0,1	33,4

Cz = N-karbazolil

No 4-fenilpiridīnija perhlorāta (**42**) un attiecīgā hlorīda (**43**) rentgenstruktūras kristalogrāfisko analīžu datiem tika iegūta nozīmīga informāciju par perhlorāta pretjona ietekmi uz emisijas īpašībām. Abiem sāļiem bija līdzīgs π–π^+ mijiedarbības starp piridīnija katjoniem un fenilaizvietotāju kristālrežģī (3.4. att.). Perhlorāts **42** veidoja pilnīgi paralēlu π–π^+ mijiedarbību starp centroīdiem 3,751 Å attālumā, turpretim hlorīds **43** veidoja gandrīz paralēlu π–π^+ mijiedarbību ar 3,776 līdz 3,900 Å attālumu (3.4. att.). Īsākais π–π^+ attālums perhlorātā **42** veicināja hipsohromo emisijas maksimuma nobīdi salīdzinājumā ar hlorīdu **43** (attiecīgi 417 nm pret 434 nm; sk. 3.5. tabulu). Svarīgi ir tas, ka perhlorāta pretjons savienojumā **42** efektīvi stabilizē π–π^+ mijiedarbības, veidojot ūdeņraža saišu tiltu starp divām blakus esošām molekulām. Savukārt hlorīda anjons veido ūdeņraža saiti tikai ar vienu izstarotāja **43** molekulu, kā rezultātā abi arilgredzeni novietoti dažādās plaknēs, mazinot π–π^+ mijiedarbības efektivitāti (3.4. att.). Nav pārsteidzoši, ka perhlorāts **42** uzrādīja augstāku cietvielas Φ (59,6 %) kā hlorīds (28,5 %; 1., 2. rinda, 3.5. tabula). Tādējādi π–π^+ mijiedarbības stabilizē H-saites veidojošais perhlorāta pretjons, ievērojami uzlabojot cietvielas Φ (3.5. tabula).

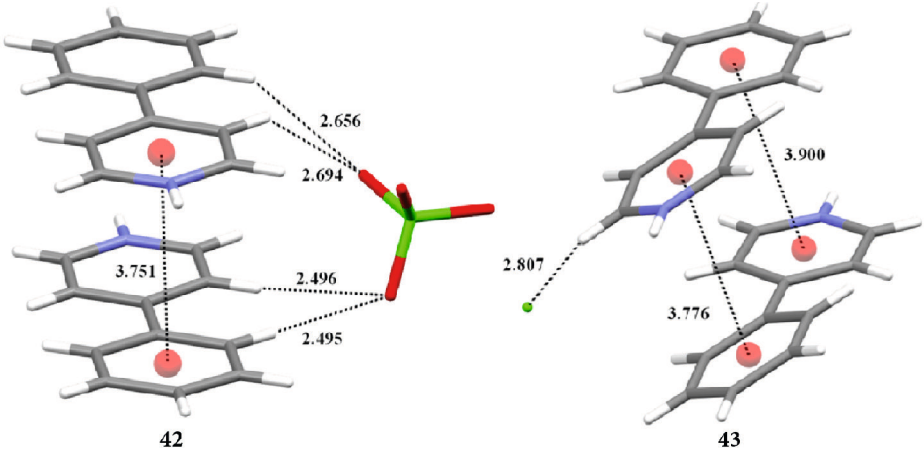

3.4. att. **Starpmolekulārās mijiedarbības savienojumos 42 un 43**

Pētījumu turpinājumā tika pārbaidīta protonēšanas pieeja kā vispārīga metode paaugstinātas cietvielu emisijas nodrošināšanai, kas rastos starpmolekulāru π–π^+ mijiedarbību rezultātā. Protonēšanas pieejā tika izmantoti strukturāli atšķirīgi substrāti. No iepriekš publicētā luminofora **44**,[42] kas saturēja piridīna gredzenu, $HClO_4$ klātienē tika izveidots attiecīgā perhlorāta sāls **45** (3.5. tabula). Gan **44**, gan **45** piemīt vāja emisija MeCN šķīdumos (attiecīgi 2,1 % un 2,8 % Φ). Cietvielā brīvā bāze **44** uzrādīja vāju emisiju (2,0 % Φ; 3.5. tabula, 3. rinda), bet perhlorāta **45** emisijas intensitāte (17,2 % Φ) bija ievērojami augstāka nekā šķīdumā (4. rinda, 3.5. tabula). Turklāt piridīna **44** protonēšana izraisīja batohromisko emisijas maksimuma nobīdi no 414 līdz 524 nm attiecībā pret sāli **45** (3. un 4. rinda, 3.5. tabula).

3.5. tabula. **Savienojumu 42–45 fotofizikālās īpašības**

Nr.	Izstarotājs	Cietv. λ_{Em}, nm	Šķīduma Φ, %	Cietv. Φ, %
1	**42** 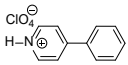	417	30,0	59,6
2	**43** 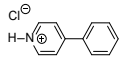	434	24,6	28,5
3	**44** 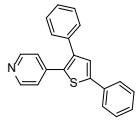	414	2,1	2,0
4	**45** 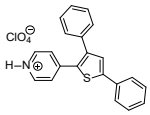	524	2,8	17,2

Paaugstināta cietvielu emisija, kas novērota, protonējot strukturāli atšķirīgus piridīnu saturošus luminoforus, norāda uz to, ka protonēšanas pieeja ir plaši izmantojama metode vēlamo starpmolekulāro π–π$^+$ mijiedarbību un AIE efekta nodrošināšanai. Tātad gan protonēšana, gan kvaternizēšana ir izmantojamas kā stratēģijas AIEgēnu dizainā. Pilns pētījuma pārskats ir apkopots publicētajā rakstā, sk. III pielikumu.

3.4. Starpmolekulāras π–π$^+$ mijiedarbības šķīdumā

Pētījumos tika noskaidrots, ka intensīvu cietvielas CT tipa emisiju var panākt, veidojot lādētas aromātiskas sistēmas, kas palīdz veidot starpmolekulāras π–π$^+$ mijiedarbības. Savukārt emisijas palielināšana šķīdumā, izmantojot π–π$^+$ mijiedarbības, ir panākta tikai iekšmolekulāri. Turpmāko pētījumu gaitā tika izvirzīta hipotēze, ka π–π$^+$ mijiedarbības varētu veidoties šķīdumā arī starpmolekulāri pie nosacījuma, ka šķīdinātājs netraucē mijiedarbībām starp izstarotājiem. Lai pārbaudītu hipotēzi, emisijas spektri tika uzņemti piridīna **30** DMF, DMSO, EtOAc, toluola, $CHCl_3$ un Et_2O šķīdumiem pirms (3.5. A att.) un pēc HCl pārākuma pievienošanas, nodrošinot pilnu piridīna **30** protonēšanu (3.5. B att.).

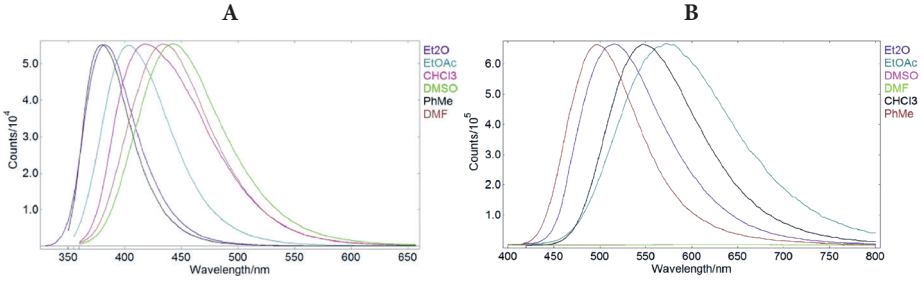

3.5. att. **A: Savienojuma 30 emisija virknē šķīdinātāju; B: savienojuma 30×HCl emisija virknē šķīdinātāju**

Visos pārbaudītajos šķīdinātājos piridīnam **30** piemīt intensīva nestrukturēta emisija ar maksimumu diapazonā no 380 līdz 443 nm (3.5. A att.). Tāpat arī piridīnija sāls **30×HCl** deva plašu, nestrukturētu emisiju Et_2O, EtOAc, $CHCl_3$ un toluola šķīdumos ar emisijas maksimumu diapazonā no 497–574 nm (3.5. B att.). Interesanti, ka emisija netika novērota **30×HCl** aprotonos polāros šķīdinātājos (DMSO un DMF). Atšķirīgās **30×HCl** fotoluminiscences īpašības dažādos šķīdinātājos norāda uz emisijas mehānisma maiņu, mainot šķīdinātājus. Lai gūtu plašāku ieskatu **30×HCl** luminiscences īpašībās, emisiju mērījām 77 K DMSO (3.6. A att.). Atšķirībā no niecīgās emisijas istabas temperatūrā, 77 K pie 483 nm tika nomērīta intensīva emisija ar izteikti ilgu dzīves laiku (1,51 s). Acīmredzot novēroto emisiju 77 K veicina ilgdzīvojoši tripleta stāvokļi, turpretim istabas temperatūrā tripleta stāvokļi spēj relaksēties molekulāro kustību rezultātā, veidojot niecīgu emisiju.

Savienojuma **30×HCl** emisijas mehānisms tika pētīts arī mazāk polāros šķīdinātājos (Et_2O, EtOAc, $CHCl_3$ un toluols) ar vājāk izteiktu sāļu šķīdināšanas spēju. Tika izvirzīta hipotēze, ka piridīnija katjonu pašorganizēšanās vāji koordinējošos šķīdinātājos, kā arī starpmolekulāro π–π^+ mijiedarbību veidošanās varētu būt atbildīga par novēroto plašo nestrukturēto CT tipa emisiju. Dinamiskās gaismas izkliedes (DLS) mērījumi norādīja uz lielu agregātu neesamību **30×HCl** izstarojošajos šķīdumos. Mazāki oligomēri, piemēram, dimēri vai trimēri ir zem DLS noteikšanas robežas, tāpēc starpmolekulāro π–π^+ mijiedarbību klātbūtnes pierādīšanai tika veikti spina režģa relaksācijas laika (T_1) kodolmagnētiskās rezonanses (KMR) eksperimenti $CDCl_3$ un DMSO-d_6 šķīdumos. T_1 relaksācijas laika izmaiņa abos šķīdinātājos tika atainota kā attiecība starp savienojuma **30×HCl** DMSO-d_6 un $CDCl_3$ šķīdumiem katrā no molekulas 1.–8. pozīcijām (numerāciju skatīt 3.6. B att.). Savienojuma **30×HCl** 1. – 4. pozīcijā novērotas būtiskas relaksācijas laika izmaiņas (4 līdz 39 reizes), savukārt 5. – 8. pozīcijā T_1 vērtības DMSO-d_6 bija divas vai mazāk reizes lielākas par vērtībām $CDCl_3$ šķīdumā. Relaksācijas laiku samazināšanās $CDCl_3$, salīdzinot ar DMSO-d_6, liecina, ka $CDCl_3$ šķīdumā ir mazi oligomēri (piemēram, dimēri vai trimēri), kas ir zem DLS noteikšanas robežas. Turklāt 4–39 reizes ilgāks relaksācijas laiks 1. – 4. pozīcijā liecina, ka $CDCl_3$ šķīdumā piridīnija un 1,4-fenilēna molekulu fragmenti ir iesaistīti starpmolekulārās π–π^+ mijiedarbībās. Tādējādi T_1 mērījumi liecina, ka $CHCl_3$, EtOAc, Et_2O un toluola šķīdumā protonētā luminogēna **30×HCl** emisija veidojas starpmolekulāru piridīnija-piridīnija π–π^+ mijiedarbību rezultātā.

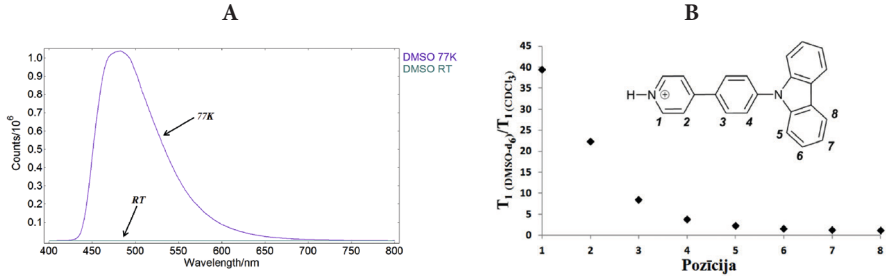

3.6. att. **A: 30×HCl emisija DMSO 77K un istabas temperatūrā; B: Relatīvās T_1 relaksācijas laika izmaiņas DMSO–*d6* un $CDCl_3$ šķīdumos savienojuma 30×HCl 1. – 8. pozīcijā**

Protonēto piridīnija **30** katjonu pašorganizēšanās vāji koordinējošos šķīdinātājos ir piemērota luminiscentu sensoru veidošanas metode. Savienojuma **30** emisijas īpašības

$CHCl_3$ tika pārbaudītas HCl gāzes klātienē (3.7. att.). Piridīna **30** $CHCl_3$ šķīdumu pakļaujot HCl iedarbībai, tas dienas gaismā mainīja krāsu no bezkrāsainas uz bāli zaļu. Izteiktākas krāsas izmaiņas novērojām pie 365 nm ierosmes. Pēc iedarbības ar HCl un attiecīgi **30×HCl** veidošanās piridīna **30** violetā emisija nomainījās uz zaļu. Papildus HCl arī citu spēcīgu skābju, piemēram, MsOH, TsOH, TfOH un TFA klātienē notika līdzīga, vizuāli atpazīstama **30** → **30×H** pārvērtība.

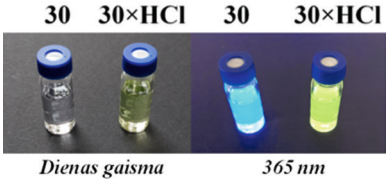

3.7. att. **Savienojuma 30 un 30×HCl dienas gaismā un pie 365 nm ierosmes**

HCl, MsOH, TsOH, TfOH un TFA detektēšanas robeža tika noteikta pie 0,33, 0,06, 0,13, 0,19 un 8,1 miljonajām daļām, attiecīgi. Salīdzinot ar citām skābēm, mazāko jutību piridīns **30** izrādīja pret TFA, tas skaidrojams ar zemāku skābes disociācijas pakāpi ($pK_{a,MeCN}$ = 12,65). Zemāka jutība pret TFA atbilst piedāvātajam sensora mehānismam, kam nepieciešama piridīnija katjonu veidošanās. Iegūtie dati liecina, ka starpmolekulāras π–π^+ mijiedarbības ir labi piemērotas luminogēnu izstrādei, kas ar CT emisijas mehānisma palīdzību izrāda augstu emisiju gan šķīdumā, gan cietvielā. Pilns pētījuma pārskats ir apkopots publicētajā rakstā, sk. IV pielikumu.

4. NODAĻA. FOSFORESCENTU CIETVIELU MATERIĀLU DIZAINS

Tika noskaidrots, ka starpmolekulārās π–π^+ un π^+–π^+ mijiedarbības veiksmīgi izmantojamas kā vispārējs dizaina rīks cietvielu un šķīdinātāju izstarotājos. Darba turpinājumā tika pētītas arī citas starpmolekulārās mijiedarbības, kas kontrolē cietvielu izstarotāju fotofizikālās īpašības. No publicētajiem datiem par cietvielu fosforescējošiem materiāliem var secināt, ka lielākā daļa mēģinājumu paaugstināt fosforescences intensitāti vienlaikus izraisa fosforescences dzīves laika samazināšanos. Saistība starp fosforescences dzīves laiku un intensitāti ir būtisks ierobežojums cietvielu fosforescējošu materiālu dizainā. Pētījumu gaitā tika izstrādāta dizaina stratēģija, kas palīdz atdalīt fosforescences intensitāti un dzīves laiku organiskos fosforescējošos materiālos.

Par darba sākumpunktu tika izmantots plaši pētītais fosforescējošais luminofors **46**. Savienojums **46** izrādīja izteikti garu fosforescences dzīves laiku (619 ms) un zemu fosforescences Φ (0,2 %, 4.1. tabula). Fosforescences Φ tika uzlabots, luminofora molekulā iekļaujot heteroatomu ar nedalītu elektronu pāri. Tādējādi fenilgredzena aizstāšana ar nedalītu elektronu pāri saturošo tiofēna gredzenu gandrīz 30 reizes palielināja fosforescences Φ (5,9 % **52**, salīdzinot ar 0,2 % **46**; 1.–2. rinda 4.1. tabulā). Kā paredzēts, vienlaikus tika novērota arī fosforescences dzīves laika samazināšanās par 30 reizēm (no 619 ms savienojumā **46** līdz 21 ms savienojumā **52**). Savienojumi **46** un **52** uzskatāmi parāda saistību starp fosforescences dzīves laiku un intensitāti. Acīmredzams, ka luminofora **47** kristālrežģī ir ievērojami ātrāks relaksācijas kanāls kā savienojuma **52** kristālrežģī. Tika izvirzīta hipotēze, ka īsākais fosforescences dzīves laiks savienojumā **52** varētu būt saistīts ar spēcīgu starpmolekulāro mijiedarbību, ko rada tiofēna gredzens. Proti, sēra atoma n-orbitāle varētu tikt iesaistīta relatīvi ātrā starpmolekulārā $T_1 \rightarrow S_0$ relaksācijas ceļā, kas notiek caur telpu. Hipotēzes apstiprināšanai sēra atoma n-orbitāle ir jāaizsargā no starpmolekulārām mijiedarbībam. Izmantojot mērķtiecīgu molekulāro dizainu, būtu iespējams sasniegt īpaši ilgu fosforescences dzīves laiku luminoforā **52**. Lai pārbaudītu hipotēzi, mēs izvēlējāmies sintezēt tiofēna luminoforus **52**, **54** un **56**–**58** no attiecīgajiem 2-aminotiofēna karbonskābes esteriem **47**–**51**, izmantojot modificētu *Clauson-Kaas* pirolu sintēzes metodi.[43,44] *Clauson-Kaas* reakcijas standartapstākļos (amīna un 2,5-dimetoksitetrahidrofurāna karsēšana etiķskābē) pirolus bieži iegūst kopā ar indola un karbazola blakusproduktiem. Pēc šādas karbazola cikla sintēzes metodoloģijas produkti iegūstami ar vidējiem iznākumiem (līdz 55 %) pie nosacījuma, ka tiek izmantots liels pārākums dimetoksitetrahidrofurāna (3 un vairāk ekvivalenti) un ilgstoša karsēšana AcOH.[45] Mūsu gadījumā *Clauson-Kaas* apstākļos karbazolkarbonskābes esteri **52**–**56** tika iegūti ar 10–26 % iznākumu (4.1. att.). Lai gan iznākumi nebija augsti, attiecīgos karbazolus **52**–**56** varēja attīrīt ar secīgu tiešās un apgrieztās fāzes kolonnu hromatogrāfiju. Pēc tam etilesteri **53** un **55** divu stadiju procesā, kas ietver saponifikāciju ar NaOH etanolā un secīgu skābes katalizēto esterifikāciju, tika pārveidoti par atbilstošajiem metilesteriem **57**, **58** (4.1. att.). Visi izstarotāji **52**, **54**, **56**–**58** bija kristāliski materiāli. Savienojums **56** tika iegūts divās kristāliskajās formās $\mathbf{56}^{\alpha}$ un $\mathbf{56}^{\beta}$, to apstiprina rentgenstruktūranalīze (4.1. tabula).

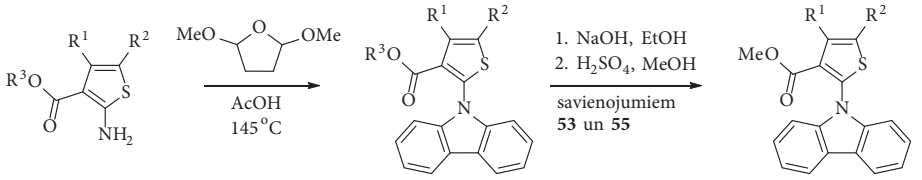

47: R^1=R^2=H; R^3=Me
48: R^1=R^2=Me; R^3=Et
49: R^1,R^2= -$(CH_2)_3$-; R_3=Me
50: R^1,R^2= -$(CH_2)_4$-; R_3=Et
51: R^1,R^2= -$(CH_2)_5$-; R_3=Me

52: 10 % no **47**
53: 17 % no **48**
54: 13 % no **49**
55: 26 % no **50**
56: 21 % no **51**

57: 81 % divos soļos no **53**
58: 89 % divos soļos no **55**

4.1. att. **Izstarotāju 52, 54, 56–58 sintēze**

Cietvielā tiofēna atvasinājumiem **52**, **54** un **56–58** attēlota strukturēta fosforescences emisija ar trim maksimumiem attiecīgi pie 544–549 nm, 585–595 nm un 645–669 nm (4.1. tabula). Iegūto savienojumu līdzīgais emisijas profils liecina, ka alkilaizvietotāji vāji ietekmē **52**, **54** un **56–58** ierosināto stāvokļu īpašības, bet tie ievērojami ietekmēja fosforescences dzīves laiku τ_{phos}. Proti, savienojumam **52** bija salīdzinoši īss τ_{phos} – 21 ms, turpretim alkilaizvietotie analogi **54** un **56–58** uzrādīja ievērojamu dzīves laika τ_{phos} pieaugumu diapazonā no 160 ms līdz 723 ms (4.1. tabula). Svarīgi, ka τ_{phos} palielināšanās **54** un **56–58** neizraisīja vienlaicīgu fosforescences Φ samazināšanos, par ko liecina relatīvi augsti fosforescences Φ savienojumos **54** un **56–58**, kas bija robežās no 3,1 % (**54**) līdz 8,3 % (**57**). Visilgākā fosforescence (723 ms) tika novērota savienojumā **58** (5. rinda), kam arī bija 24 reizes lielāks fosforescences Φ kā standarta emitētājam **46** (5. rinda pret 1., 4.1. tabula). Palielinot aizvietotāju telpisko izmēru tiofēna sēra atoma tuvumā, ir iespējams kavēt ātrus, caur telpu notiekošus, starpmolekulārus relaksācijas kanālus un palielināt fosforescences dzīves laiku, nesamazinot fosforescences Φ (Φ_p).

4.1. tabula. **Savienojumu 46, 52, 54 un 56–58 cietvielu fosforescentās īpašības**

Nr.	Savienojums	Struktūra	Cietvielu λ_{EM}, nm	τ_{phos}, ms	Φ_p, %
1	**46**	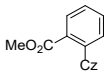	562, 617, 668	619	0,2
2	**52**	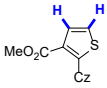	544, 593, 648	21	5,9
3	**57**	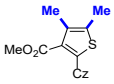	549, 595, 652	322	8,3
4	**54**	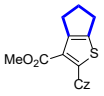	549, 595, 650	160	3,1

Nr.	Savienojums	Struktūra	Cietvielu λ_{EM}, nm	τ_{phos}, ms	Φ_p, %
5	**58**		544, 592, 645	723	4,7
6	**56**$^{\alpha}$		547, 595, 659	360	4,8
7	**56**$^{\beta}$		546, 585, 669	404	3,5

Cz = *N*-karbazolil

Sēra telpiskās aizsargāšanas efektivitāti apstiprināja arī attāluma mērījumi starp tiofēna sēra atomu un tuvākās π-sistēmas S vai C atomiem, izmantojot rentgenstruktūranalīzes datus savienojumos **52**, **54** un **56**–**58** (4.2. A att.). Izmērītie attālumi starp atomiem bija attiecīgi 3,271 Å (**52**), 3,567 Å (**57**), 3,385 Å (**54**), 3,866 Å (**58**), 3,447 Å (**56**$^{\alpha}$) un 3,546 Å (**56**$^{\beta}$). Attālumi būtiski korelēja ar fosforescences dzīves laiku (R^2 = 0,922, 4.2. B att.). Novērotā korelācija liecina, ka sēra n-orbitāle ir iesaistīta starpmolekulārā relaksācijas ceļā, kas spēcīgi ietekmē fosforescences dzīves laiku τ_{phos}.

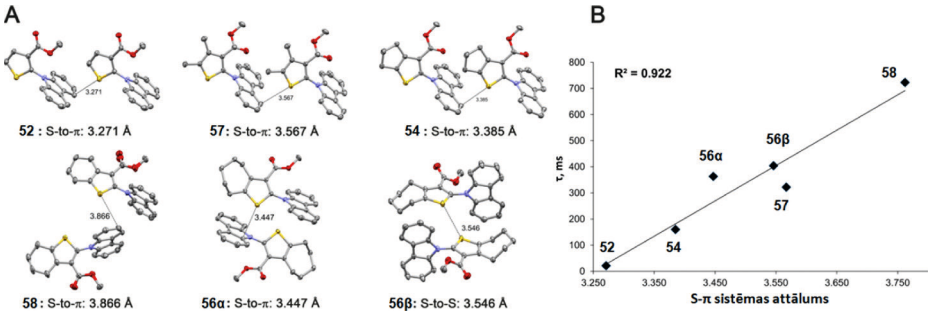

4.2. att. **A: Rentgenstruktūranalīzes aina 52, 54 un 56–58 dimēros; B: korelācijas aina starp S-π/S-S attālumiem un fosforescences dzīves laikiem savienojumos 52, 54 un 56–58**

Novērotā būtiskā korelācija starp τ_{phos} un attālumu starp sēru un tuvāko blakusesošo π-sistēmu tika attiecināta uz CT procesu iesaisti, jo tie ir atkarīgi no attāluma starp akceptoru un donoru. Lai izprastu enerģijas pārneses procesus starp ierosinātu luminoforu un blakus esošām molekulām, savienojumiem **52**, **54** un **56**–**58** tika veikta plaša kristālrežģa CT integrāļu (CTI) analīze. CTI tika aprēķinātas gan elektronu (LUMO, zilie vektori, E_{1-3}), gan caurumu (HOMO, sarkanie vektori, H_{1-3}) pārnesei. Piemēram, savienojumā **54** ir seši unikāli CT vektori, trīs – elektronu un trīs – caurumu pārnesēm (4.3. A att.). Savienojumu **52**, **56α**, **56β**, **57** un **58** kristālrežģī bija attiecīgi desmit, četrpadsmit, desmit, desmit un sešpadsmit CT ceļi. CT efektivitāti katrā no vektoriem var aproksimēt ar tā absolūto V vērtību ($|V|$).

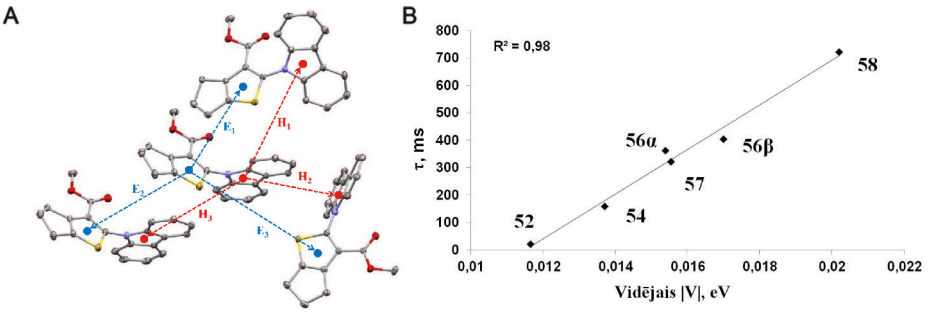

4.3. att. **A: Aprēķinātie elektronu un caurumu CT vektori savienojumā 54; B: korelācijas starp vidējo $|V|$ vērtību un τ_{phos}**

Aprēķinot katra apskatītā CT vektora $|V|$ vērtību, netika ņemtas vērā vērtības, kurām bija niecīga dalība CT procesos. Tie CT vektori, kuru vērtība bija mazāka par 5 % no kopējās $|V|$ summas ($\Sigma|V|$), tika atmesti, iegūstot katra izstarotāja **47**–**51** visiespējamākās CT pārejas kristālrežģī. Tālākos aprēķinos tika izmantoti septiņi CT ceļi savienojumā **47**, pieci savienojumā **48**, pieci savienojumā **49**, četri savienojumā **50**, astoņi savienojuma **51α** formai un pieci savienojuma **51β** formai. Elektroniskās sadarbības vidējā absolūtā vērtība starp visām iespējamām CT pārejām ($\frac{\sum_1^n |V|}{n}$, kur n ir iespējamo ceļu skaits) būtiski korelē ar novēroto katra izstarotāja fosforescences dzīves laiku ($R^2 = 0,98$, 4.3. B att.) un līdz ar to aproksimēja dzīves laiku labāk kā īsākie mijiedarbību attālumi ($R^2 = 0,92$, 4.2. B att.). Aprēķinātā vidējā $|V|$ palielināšanās virzienā no savienojuma **47** uz **51** norāda uz CT pieaugumu starp izstarotājiem, kas uzlabo lādiņa sadalīšanos kristālrežģī un tādējādi noved pie ilgāka emisijas dzīves laika. Galvenais faktors, kas nosaka fosforescences dzīves laiku, ir tīklveida elektroniskā sadarbība starp vairākiem luminoforiem kristālrežģī. Šī molekulārā dizaina pieeja balstās uz telpiski liela aizvietotāja ieviešanu orbitāles tuvumā, kas piedalās ātrā $T_1 \rightarrow S_0$ relaksācijā, to nomācot, bet vienlaikus neietekmējot fosforescences Φ. Pilns pētījuma pārskats ir apkopots V pielikumā.

SECINĀJUMI

1) Piridīnu saturošus luminoforus ar agregācijas izraisītās slāpēšanas efektu var pārvērst agregācijas inducētās emisijas luminoforos, izmantojot kvaternizēšanu, kā rezultātā kristālrežģī veidojas labvēlīgas starpmolekulāras $\pi^+–\pi^+$ un $\pi–\pi^+$ mijiedarbības.

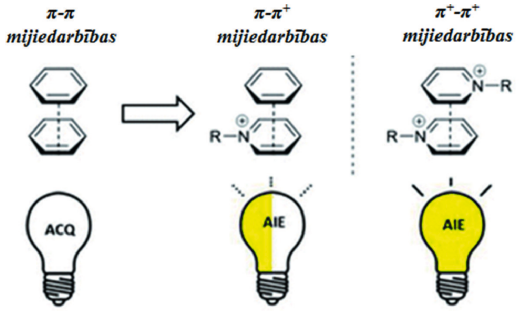

2) Līdzīgi kvaternizēšanai, arī protonēšana nodrošina agregācijas inducētās emisijas efektu piridīnu saturošajos luminoforos.

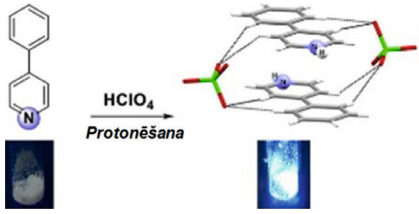

3) Negatīvais pretjons būtiski ietekmē piridīnija sāļu kvantu iznākumu cietvielā. Vispiemērotākais anjons ir perhlorāts, jo tas stabilizē labvēlīgās $\pi–\pi^+$ mijiedarbības.

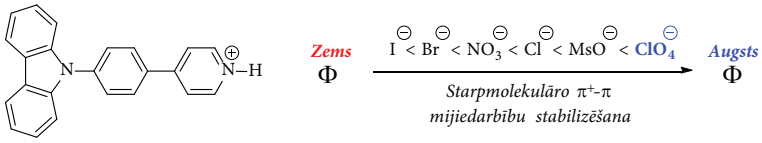

4) Piridīna saturošu luminoforu protonēšana šķīdumā rada oligomērus, kuru veidošanos nodrošina $\pi–\pi^+$ mijiedarbības, kas noved pie starpmolekulāras lādiņa pārneses tipa luminiscences.

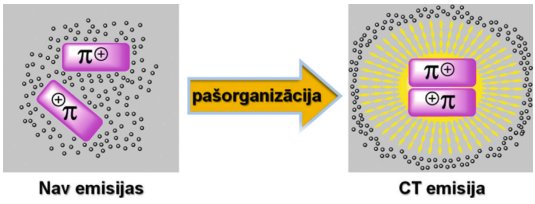

5) Starpmolekulāras π–π^+ mijiedarbības var izmantot plaša pielietojuma luminogēnu, kas izrāda luminiscenci gan šķīdumā, gan cietvielā, dizainā, nemainot emisijas mehānismus.
6) Modificēta *Clauson-Kaas* reakcija ir piemērota karbazola ieviešanai tiofēnu saturošu fosforescējošo materiālu sintēzē.

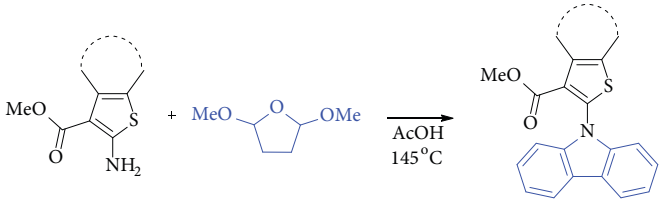

7) Tiofēnu saturošos cietvielu fosforescējošajos materiālos nedalītais sēra atoma elektronu pāris piedalās ātrā $T_1 \rightarrow S_0$ relaksācijas kanālā, kas samazina fosforescences dzīves laiku. Šis relaksācijas ceļš ir atkarīgs no kristālrežģa pakojuma blīvuma, ko apliecina novērotā saistība starp fosforescences dzīves laiku un starpmolekulāro attālumu. Nevēlamo $T_1 \rightarrow S_0$ relaksācijas kanālu var nomākt ar molekulāro dizaina pieeju, kas balstās uz telpiski liela aizvietotāja ievadīšanu sēra atoma tuvumā, tādējādi palielinot starpmolekulāro mijiedarbību attālumu.

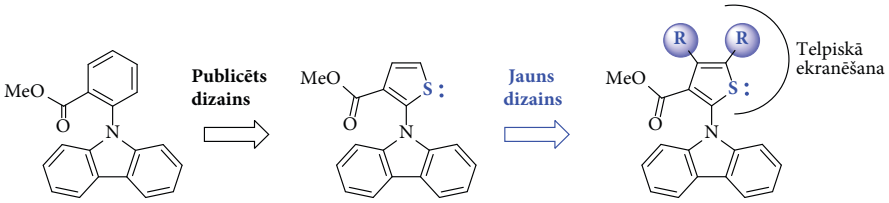

Zems Φ (0,2 %)
Ilgs dzīves laiks (612 ms)

Augsts Φ (5,9 %)
Īss dzīves laiks (21 ms)

Augsts Φ (līdz 8,3 %)
Ilgs dzīves laiks (līdz 723 ms)

LITERATŪRAS ATSAUCES

1. Matsuki, K.; Jiang. P.; Taishi T. "Recent Progress on Light-Emitting Electrochemical Cells with Nonpolymeric Materials" *Adv. Funct. Mater.* **2020**, *30*, 1908641. DOI: 10.1002/adfm.201908641.
2. Shirota, Y. "Organic Materials for Electronic and Optoelectronic Devices" *J. Mat. Chem.* **2000**, *10*, 1–25. DOI: 10.1039/a908130e.
3. Thompson, B. C.; Jean M. J. F. "Polymer-fullerene composite solar cells" *Angew. Chem. Int. Ed.* **2008**, *47*, 58–77. DOI: 10.1002/anie.200702506.
4. Kawata, S.; Kawata, Y. "Three-Dimensional Optical Data Storage Using Photochromic Materials" *Chem. Rev.* **2000**, *100*, 1777–1788. DOI: 10.1021/cr980073p.
5. Murphy A. R.; Frechet, J. M. "Organic Semiconducting Oligomers for Use in Thin Film Transistors" *Chem. Rev.* **2009**, *107*, 1066–1096. DOI: 10.1021/cr0501386.
6. Gu, M.; Li, X.; Cao, Y. "Optical Storage Arrays: A perspective for future Big Data Storage" *Light Sci. Appl.* **2014**, *3*. DOI: 10.1038/lsa.2014.58.
7. Sun, T.; Xu, B.; Chen, B.; Chen, X.; Li, M.; Shi, P.; Wang, F. "Anti-counterfeiting patterns encrypted with multi-mode luminescent nanotaggants" *Nanoscale* **2017**, *9*, 2701–2705. DOI: 10.1039/c6nr09083d.
8. Meruga, J. M.; Cross, W. M.; May, P. S.; Luu, Q. A.; Crawford, G. A.; Kellar, J. J. "Security printing of covert quick response codes using upconverting nanoparticle inks" *Nanotechnology* **2012**, *23*, 395201. DOI: 10.1088/0957-4484/23/39/395201.
9. Cho, U.; Chen, J. K. "Lanthanide-based optical probes of Biological Systems" *Cell Chem. Biol.* **2020**, *27*, 921–936. DOI: 10.1016/j.chembiol.2020.07.009.
10. Quaranta, M.; Borisov, S. M.; Klimant, I. "Indicators for optical oxygen sensors" *Bioanal. Rev.* **2012**, *4*, 115–157. DOI: 10.1007/s12566-012-0032-y.
11. Gee, H.-C.; Lee, C.-H.; Jeong, Y.-H.; Jang, W.-D. "Highly sensitive and selective cyanide detection via cu2+ complex ligand exchange" *Chem. Commun.* **2011**, *47*, 11963–11965. DOI: 10.1039/c1cc14963f.
12. (a) Kenry; Chen, C.; Liu, B. "Enhancing the performance of pure organic room-temperature phosphorescent luminophores" *Nat. Commun.* **2019**, *10*, 2111. DOI: 10.1038/s41467-019-10033-2. (b) Hirata, S. "Recent Advances in Materials with Room-Temperature Phosphorescence: Photophysics for Triplet Exciton Stabilization" *Adv. Opt. Mater.* **2017**, *5*, 1700116. DOI: 10.1002/adom.201700116.
13. (a) Caporale, C.; Massi, M. "Cyclometalated iridium(III) complexes for life science" *Coord. Chem. Rev.* **2018**, *363*, 71–91. DOI: 10.1016/j.ccr.2018.02.006. (b) Shi, H.; Wang, Y.; Lin, S.; Lou, J.; Zhang, Q. "Recent development and application of cyclometalated iridium(iii) complexes as chemical and biological probes" *Dalton Trans.* **2021**, *50*, 6410–6417. DOI: 10.1039/D1DT00592H. (c) Yusoff, A. R. B. M.; Huckaba, A. J.; Nazeeruddin, M. K. "Phosphorescent Neutral Iridium (III) Complexes for Organic Light-Emitting Diodes" *Top. Curr. Chem.* **2017**, *375*. DOI: 10.1007/s41061-017-0126-7.
14. (a)Yang, J.; Zhen, X.; Wang, B.; Gao, X.; Ren, Z.; Wang, J.; Xie, Y.; Li, J.; Peng, Q.; Pu, K.; Li, Z. "The influence of the molecular packing on the room temperature phosphorescence of purely organic luminogens" *Nat. Commun.* **2018**, *9*, 840. DOI: 10.1038/s41467-018-03236-6. (b) Zhou, C.; Zhang, S.; Gao, Y.; Liu, H.; Shan, T.; Liang, X.; Yang, B.; Ma, Y. "Ternary Emission of Fluorescence and Dual Phosphorescence at Room Temperature: A Single-Molecule White Light Emitter Based on Pure Organic Aza-Aromatic Material" *Adv. Funct. Mater.* **2018**, *28*, 1802407. DOI: 10.1002/adfm.201802407. (c) Jia, W.; Wang, Q.; Shi, H.; An, Z.; Huang, W. "Manipulating the Ultralong Organic Phosphorescence of Small

Molecular Crystals" *Chem. Eur. J.* **2020**, *26*, 4437–4448. DOI:10.1002/chem.201904500. (d) Tian, S.; Ma, H.; Wang, X.; Lv, A.; Shi, H.; Geng, Y.; Li, J.; Liang, F.; Su, Z. M.; An, Z.; Huang, W. "Utilizing d–pπ Bonds for Ultralong Organic Phosphorescence" *Angew. Chem. Int. Ed.* **2019**, *58*, 6645–6649. DOI: 10.1002/anie.201901546.

15. (a) Ma, H.; Peng, Q.; An, Z.; Huang, W.; Shuai, Z. "Efficient and Long-Lived Room-Temperature Organic Phosphorescence: Theoretical Descriptors for Molecular Designs" *J. Am. Chem. Soc.* **2018**, *141*, 1010–1015. DOI: 10.1021/jacs.8b11224. (b) Zhao, W.; Cheung, T. S.; Jiang, N.; Huang, W.; Lam, J. W. Y.; Zhang, X.; He, Z.; Tang, B. Z. "Boosting the efficiency of organic persistent room-temperature phosphorescence by intramolecular triplet-triplet energy transfer" *Nat. Commun.* **2019**, *10*, 1595. DOI: 10.1038/s41467-019-09561-8.
16. Wiedemann, E. "Ueber Fluorescenz und Phosphorescenz" *Ann. Phys. Chem.* **1888**, *34*, 446–463. doi.org/10.1002/andp.18882700703.
17. Valeur, B.; Berberan-Santos, M. N. "A Brief History of Fluorescence and Phosphorescence before the Emergence of Quantum Theory" *J. Chem. Educ.* **2011**, *88*, 731–738. DOI: 10.1021/ed100182h.
18. Jaffe, H. H.; Miller, A. L. "The fates of electronic excitation energy" *J. Chem. Educ.* **1966**, *43*, 469–473. DOI:10.1021/ed043p469.
19. Wex, B.; Kaafarani, B. R. "Perspective on carbazole-based organic compounds as emitters and hosts in TADF applications" *J. Mat. Chem. C* **2017**, *5*, 8622–8653. DOI: 10.1039/C7TC02156A.
20. Borisov, S. M. "Quenched-phosphorescence Detection of Molecular Oxygen" **2018**, 1–18. DOI: 10.1039/9781788013451.
21. Kasha, M. "Characterization of electronic transitions in complex molecules" *Discuss. Faraday Soc.* **1950**, *9*, 14–19. DOI: 10.1039/DF9500900014.
22. Wang, X.; Wang, S.; Lv, J.; Shao, S.; Wang, L.; Jing, X.; Wang, F. "Through-space charge transfer hexaarylbenzene dendrimers with thermally activated delayed fluorescence and aggregation-induced emission for efficient solution-processed OLEDs" *Chem. Sci.* **2019**, *10*, 2915–2923. DOI: 10.1039/C8SC04991B.
23. (a) Cebrián, C.; Mauro, M. "Recent advances in phosphorescent platinum complexes for organic light-emitting diodes" *Beilstein J. Org. Chem.* **2018**, *14*, 1459–1481. DOI: 10.3762/bjoc.14.124. (b) Solomatina, A. I.; Su, S.-H.; Lukina, M. M.; Dudenkova, V. V.; Shcheslavskiy, V. I.; Wu, C.-H.; Chelushkin, P. S.; Chou, P.-T.; Koshevoy, I. O.; Tunik, S. P. "Water-soluble cyclometalated platinum(ii) and iridium(iii) complexes: synthesis, tuning of the photophysical properties, and in vitro and in vivo phosphorescence lifetime imaging" *RSC Adv.* **2018**, *8*, 17224–17236. DOI: 10.1039/C8RA02742K. (c) Mao, H.-T.; Li, G.-F.; Shan, G.-G.; Wang, X.-L.; Su, Z.-M. "Recent progress in phosphorescent Ir(III) complexes for nondoped organic light-emitting diodes" *Coord. Chem. Rev.* **2020**, *413*, 213283. DOI: 10.1016/j.ccr.2020.213283. (d) Ho, C.-L.; Li, H.; Wong, W.-Y. "Red to near-infrared organometallic phosphorescent dyes for OLED applications" *J. Organomet. Chem.* **2014**, *751*, 261–285. DOI: 10.1016/j.jorganchem.2013.09.035. (e) Gareth Williams, J.; Develay, S.; Rochester, D.; Murphy, L. "Optimising the luminescence of platinum(II) complexes and their application in organic light emitting devices (OLEDs)" *Coord. Chem. Rev.* **2008**, *252*, 2596–2611. DOI: 10.1016/j.ccr.2008.03.014.
24. (a) Mukherjee, S.; Thilagar, P. "Recent advances in purely organic phosphorescent materials" *Chem. Commun.* **2015**, *51*, 10988–11003. DOI: 10.1039/C5CC03114A. (b) Kenry; Chen, C.; Liu, B. "Enhancing the performance of pure organic room-temperature phosphorescent luminophores" *Nat. Commun.* **2019**, *10*. DOI: 10.1038/s41467-019-10033-2. (c) Karuppannan, S.; Chambron, J.-C. "Supramolecular Chemical Sensors Based on Pyrene Monomer–Excimer Dual Luminescence" *Chem. Asian J.* **2011**, *6*, 964–984. DOI: 10.1002/asia.201000724. (d) Seko, T.; Ogura, K.; Kawakami, Y.; Sugino, H.;

Toyotama, H.; Tanaka, J. "Excimer emission of anthracene, perylene, coronene and pyrene microcrystals dispersed in water" *Chem. Phys. Lett.* **1998**, *291*, 438–444. DOI: 10.1016/s0009-2614(98)00629-0. (e) Katoh, R.; Suzuki, K.; Furube, A.; Kotani, M.; Tokumaru, K. "Fluorescence Quantum Yield of Aromatic Hydrocarbon Crystals" *J. Phys. Chem. C* **2009**, *113*, 2961–2965. DOI: 10.1021/jp807684m.

25. (a) Cai, S.; Shi, H.; Tian, D.; Ma, H.; Cheng, Z.; Wu, Q.; Gu, M.; Huang, L.; An, Z.; Peng, Q.; Huang, W. "Enhancing Ultralong Organic Phosphorescence by Effective π-Type Halogen Bonding" *Adv. Funct. Mater.* **2018**, *28*, 1705045. DOI: 10.1002/adfm.201705045. (b) Huang, L.; Qian, C.; Ma, Z. "Stimuli-Responsive Purely Organic Room-Temperature Phosphorescence Materials" *Chem. Eur. J.* **2020**, *26*, 11914–11930. DOI: 10.1002/chem.202000526.
26. Baba, M. "Intersystem Crossing in the 1nπ* and 1ππ* States" *J. Phys. Chem. A* **2011**, *115*, 9514–9519. DOI: 10.1021/jp111892y.
27. Yamada, S. "Cation–π interactions in organic crystals" *Coord. Chem. Rev.* **2020**, *415*, 213301. DOI: 10.1016/j.ccr.2020.213301.
28. Forster, T.; Kasper K. "Ein Konzentrationsumschlag der Fluoreszenz" *Z. Phys. Chem.* **1954**, *1*, 275–277. DOI: 10.1524/zpch.1954.1.5_6.275.
29. (a) Klymchenko, A. S. "Solvatochromic and Fluorogenic Dyes as Environment-Sensitive Probes: Design and Biological Applications" *Acc. Chem. Res.* **2017**, *50*, 366–375. DOI: 10.1021/acs.accounts.6b00517. (b) Jenekhe, S. A.; Osaheni, J. A. "Excimers and Exciplexes of Conjugated Polymers" *Science* **1994**, 265, 765–768.DOI: 10.1126/science.265.5173.765.
30. Lindquist, R. J.; Lefler, K. M.; Brown, K. E.; Dyar, S. M.; Margulies, E. A.; Young, R. M.; Wasielewski, M. R."Energy Flow Dynamics within Cofacial and Slip-Stacked Perylene-3,4-dicarboximide Dimer Models of π-Aggregates." *J. Am. Chem. Soc.* **2014**, *136*, 14912–14923. DOI: 10.1021/ja507653p.
31. Luo, J.; Xie, Z.; Lam, J. W.; Cheng, L.; Chen, H.; Qiu, C.; Kwok, H. S.; Zhan, X.; Liu, Y.; Zhu, D.;Tang, B. Z. "Aggregation-induced emission of 1-methyl-1,2,3,4,5-pentaphenylsilole" *Chem. Commun.* **2001**, *18*, 1740–1741. DOI: 10.1039/B105159H.
32. Lui J.; Meng Q.; Zhang X.; Lu X.; He P.; Jiang L.; Dong H.; Hu W. "Aggregation-induced emission enhancement based on 11,11,12,12,-tetracyano-9,10-anthraquinodimethane" *Chem. Commun.* **2013**, *49*, 1199–1201. DOI: 10.1039/C2CC38817K.
33. Nie H.; Hu K.; Cai Y.; Peng Q.; Zhao Z.; Hu R.; Chen J.; Su S.-J.; Qin A.; Tang B. Z. "Tetraphenylfuran: aggregation-induced emission or aggregation-caused quenching?" *Mater. Chem. Front.* **2017**, *1*, 1125–1129. DOI: 10.1039/C6QM00343E.
34. Yuan, W. Z.; Shen, X. Y.; Zhao, H.; Lam, J. W.; Tang, L.; Lu, P.; Wang, C.; Liu, Y.; Wang, Z.; Zheng, Q.; Sun, J. Z.; Ma, Y.; Tang, B. Z. "Crystallization-Induced Phosphorescence of Pure Organic Luminogens at Room Temperature" *J. Phys. Chem. C* **2010**, *114*, 6090–6099. DOI: 10.1021/jp909388y.
35. Xie, Y.; Ge, Y.; Peng, Q.; Li, C.; Li, Q.; Li, Z. "How the Molecular Packing Affects the Room Temperature Phosphorescence in Pure Organic Compounds: Ingenious Molecular Design, Detailed Crystal Analysis, and Rational Theoretical Calculations" *Adv. Mater.* **2017**, *29*, 1606829. DOI: 10.1002/adma.201606829.
36. (a) Pan, S.; Chen, Z.; Zheng, X.; Wu, D.; Chen, G.; Xu, J.; Feng, H.; Qian, Z. "Ultralong Room-Temperature Phosphorescence from Supramolecular Behavior via Intermolecular Electronic Coupling in Pure Organic Crystals" *J. Phys. Chem. Lett.* **2018**, *9*, 3939–3945. DOI: 10.1021/acs.jpclett.8b01697. (b) Wang, T.; Hu, Z.; Nie, X.; Huang, L.; Hui, M.; Sun, X.; Zhang, G. "Thermochromic aggregation-induced dual phosphorescence via temperature-dependent sp3-linked donor-acceptor electronic coupling" *Nat. Commun.* 2021, *12*. DOI: 10.1038/s41467-021-21676-5. (c) Tian, Y.; Gong, Y.; Liao, Q.; Wang, Y.; Ren, J.; Fang, M.; Yang, J.; Li, Z. "Adjusting Organic Room-Temperature Phosphorescence with Orderly

Stimulus-Responsive Molecular Motion in Crystals" *Cell Rep. Phys. Sci.* **2020**, *1*, 100052. DOI: 10.1016/j.xcrp.2020.100052.

37. Li, Q.; Li, Z. "Molecular Packing: Another Key Point for the Performance of Organic and Polymeric Optoelectronic Materials" *Acc. Chem. Res.* **2020**, *53*, 962–973. DOI: 10.1021/acs.accounts.0c00060.
38. Song, J.; Muleta, D. Y.; Feng, W.; Song, Y.; Zhou, X.; Li, W.; Wang, L.; Liu, D.; Wang, T.; Hu, W. "Photophysical tuning of small-molecule-doped organic crystals with long-persistent luminescence by variation of dopants" *Dyes Pigm.* **2021**, *193*, 109501. DOI: 10.1016/j.dyepig.2021.109501.
39. Bissesar, S.; Raamsdonk, D. M.; Gibbons, D. J.; Williams, R. M. "Spin Orbit Coupling in Orthogonal Charge Transfer States: (TD-)DFT of Pyrene-Dimethylaniline" *Molecules* **2022**, *27*, 891. DOI: 10.3390/molecules27030891.
40. Shuai, Z.; Li, W.; Ren, J.; Jiang, Y.; Geng, H. "Applying Marcus theory to describe the carrier transports in organic semiconductors: Limitations and beyond" *J. Chem. Phys.* **2020**, *153*, 080902. DOI: 10.1063/5.0018312.
41. (a) Ma, H.; Peng, Q.; An, Z.; Huang, W.; Shuai, Z. "Efficient and Long-Lived Room-Temperature Organic Phosphorescence: Theoretical Descriptors for Molecular Designs" *J. Am. Chem. Soc.* **2018**, *141*, 1010–1015. DOI: 10.1021/jacs.8b11224. (b) Zhao, W.; Cheung, T. S.; Jiang, N.; Huang, W.; Lam, J. W.; Zhang, X.; He, Z.; Tang, B. Z. "Boosting the efficiency of organic persistent room-temperature phosphorescence by intramolecular triplet-triplet energy transfer" *Nat. Commun.* **2019**, *10*. DOI: 10.1038/s41467-019-09561-8.
42. Karpavičienė, I.; Jonušis, M.; Leduskrasts, K.; Misiūnaitė, I.; Suna, E.; Čikotienė, I. "Synthesis and photophysical properties of 3,5-diaryl-2-heteroarylthiophenes" *Dyes Pigm.* **2019**, *170*, 107646. DOI: 10.1016/j.dyepig.2019.107646.
43. Clauson-Kaas, N.; Tyle, Z. "Preparation of Cis- and Trans 2,5-Dimethoxy-2-(acetamidomethyl)-2,5-dihydrofuran, of Cis- and Trans 2,5-Dimethoxy-2-(acetamidomethyl)-tetrahydrofuran and of 1-Phenyl-2-(acetamidomethyl)-pyrrole" *Acta Chem. Scand.* **1952**, *6*, 667–670. DOI: 10.3891/acta.chem.scand.06-0667.
44. Clauson-Kaas Reaction. In Comprehensive Organic Name Reactions and Reagents; John Wiley & Sons, Inc.: Hoboken, NJ, USA, **2010**; p conrr146. DOI: 10.1002/9780470638859.conrr146.
45. Lee, D.H.; Lee, S.G.; Jung, D.I.; Hahn. J.T. "Synthesis of Heteroaromatic Derivatives with Nitrogen Atoms: Tripyrrolyl Pyrimidine and Tripyrrolyl[1,3,5]Triazine" *Asian J. Chem.* **2013**, *25*, 501–504. DOI: 10.14233/ajchem.2013.13307.

PIELIKUMI

P-1

Leduskrasts, K.; Sūna, E.
"Aggregation induced emission by pyridinium–pyridinium interactions"
RSC Advances **2019**, 9, 460–465.
DOI:10.1039/C8RA08771G.

RSC Advances

PAPER

View Article Online
View Journal | View Issue

Cite this: *RSC Adv.*, 2019, **9**, 460

Received 23rd October 2018
Accepted 18th December 2018

DOI: 10.1039/c8ra08771g

rsc.li/rsc-advances

Aggregation induced emission by pyridinium–pyridinium interactions†

Kaspars Leduskrasts and Edgars Suna *

Non-covalent intermolecular interactions between pyridinium subunits in a crystal-state are an efficient means to accomplish aggregation induced emission and avoid aggregation caused quenching.

Introduction

Organic luminescent molecules (luminophores) have found widespread applications in the design of optoelectronic devices and sensors.[1] In the majority of applications, organic luminophores are either used as thin solid films or they are doped into a polymer matrix (host material). In thin films and in polymer matrices highly aggregated luminophore molecules may experience intermolecular π–π aromatic interactions. The non-covalent π–π interactions usually lead to decay of the excited-state energy of organic luminophores *via* non-radiative intermolecular energy transfer, thus resulting in decrease of emissive properties in the solid state. This phenomenon is well-known as aggregation caused quenching (ACQ).[2] Due to the ACQ, the majority of organic luminophores feature considerably reduced emission or even lack of emission in the solid state, while being highly emissive in diluted solutions.

A traditional approach to minimize the detrimental intermolecular π–π stacking relies on a decrease of planarity of organic luminophores. This has been achieved by out-of-plane twisting of aromatic subunits in luminophores as well as by incorporation of steric bulk[3] or an anionic moiety[4] in proximity to the π-system. Combined with a restriction of intramolecular motions (to minimize the non-radiative dissipation of exciton energy), these approaches have resulted in the design of organic emitters that feature higher emission in the solid-state as compared to solution (known as aggregation induced emission or AIE). First introduced by Tang,[5] AIE luminogens (AIEgens) have become a hot topic in materials science during the last decade,[6] and they have found ample application in materials science.[7] It should be noted, however, that AIEgens may lose the solid state emission if intermolecular non-covalent π–π interactions between emitter molecules can take place.[8] Clearly, the search for a new type of interactions that would help to avoid the detrimental intermolecular π–π stacking would facilitate the development of AIEgens with improved emissive properties.

It has been demonstrated that the undesired π–π stacking can be avoided by increasing the distance between interacting π-systems in the solid state.[8a] We hypothesized that other interactions that are effective at longer distances and are more flexible with respect to mutual spatial orientation[9] of the interacting π-systems can be utilized to avoid the undesired π–π stacking. This has led us to propose that interactions between heteroaromatic cationic π-systems can be employed in the design of solid-state luminogens (AIEgens). Interestingly, the pyridinium cation–arene π system interactions have been used by Bull and Fossey to generate luminescent responses in solution.[10] In addition, Lu and coworkers reported a fluorescence turn-on in polymer matrices *via* cation-π interactions.[11] However, to the best of our knowledge, interactions between two heteroaromatic cationic π-systems has not been used in the design of AIEgens. Herein we demonstrate that non-covalent intermolecular interactions between two neighboring pyridinium subunits in solid-state is an efficient means to accomplish the solid-state emission (Fig. 1).

Results and discussion

Synthesis of quaternary pyridinium salts 1–5

N-Benzyl pyridinium bromide **1** was obtained by alkylation of pyridine with benzyl bromide (Fig. 2). The synthesis of pyridinium carbazoles **2a** and **2b** involved reduction of aldehyde **6** to benzylic alcohol **7**, followed by conversion to benzyl chloride and reaction with pyridine (Fig. 2). The corresponding tosylate **2b** was prepared from benzyl alcohol **7** and TsCl in the presence of pyridine as a base. In addition, pyridinium carbazoles **3**, **4** possessing substituents in position 4 of the pyridine ring were also synthesized to evaluate influence of steric bulk on the interaction between pyridinium subunits of neighboring molecules in the solid-state (Fig. 2). Finally, 1,4-butylene linker-

Latvian Institute of Organic Synthesis, Aizkraukles 21, LV-1006, Riga, Latvia. E-mail: edgars@osi.lv

† Electronic supplementary information (ESI) available: Experimental procedures, photophysical properties, X-ray crystallographic data (CIF files), ^{1}H and ^{13}C NMR data. CCDC 1873711–1873715. For ESI and crystallographic data in CIF or other electronic format see DOI: 10.1039/c8ra08771g

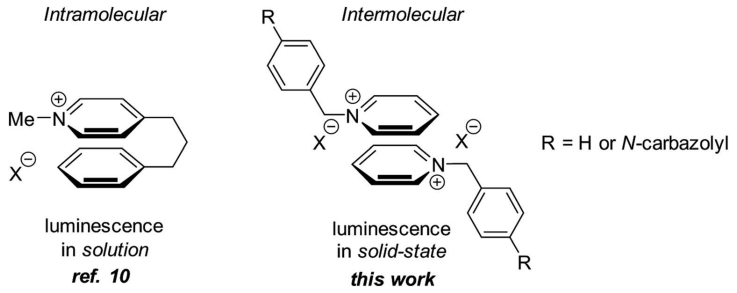

Fig. 1 Design of the solid-state AIEgens based on pyridinium–pyridinium interactions.

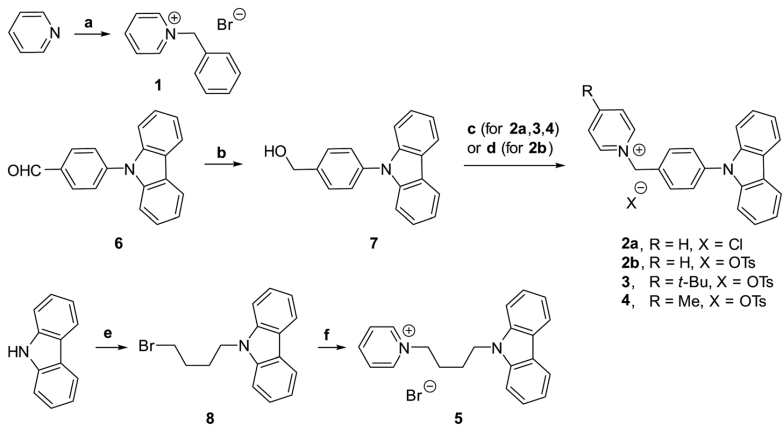

Fig. 2 Synthesis of pyridinium salts **1–5**. Reagents and conditions: (a) BnBr, acetone, reflux, 1 h, 94%. (b) $NaBH_4$, THF, MeOH, rt, 16 h, 87%. (c) TsCl, pyridine (for **2a**), 4-*t*Bu-pyridine (for **3**) or 4-Me-pyridine (for **4**), CH_2Cl_2, rt, 24 h, 57% (**2a**), 63% (**3**), 53% (**4**). (d) $SOCl_2$, CH_2Cl_2, rt, 30 min, then pyridine, MeCN, 80 °C, 1 h, 70%. (e) $Br(CH_2)_4Br$, KOH, DMSO, rt, ultrasound, 30 min, 48%, (f) pyridine, MeCN, 90 °C, 16 h, 69%.

containing pyridinium carbazole **5** was prepared by double substitution of 1,4-dibromobutane with carbazole and pyridine (Fig. 2). All obtained pyridinium salts **1–5** were crystalline materials and they were characterized by ^1H and ^{13}C NMR spectra as well as by HRMS and IR techniques.

Luminescence data

UV-vis absorption spectra of **1–5** were measured in MeCN solutions (at *ca.* 10^{-6} mol L^{-1} concentration) at room temperature and under ambient atmosphere. All synthesized materials displayed absorption peaks in 235–360 nm range (Fig. 3A), which were attributed to the π–π^* transitions. Pyridinium salt **1** showed a narrow absorption band in MeCN solution with a maximum at 285 nm (entry 1, Table 1). Intense solid-state absorbance in the 250–350 nm region with sharply decreasing absorbance intensity above 350 nm was observed for the crystalline salt **1** (see ESI, page S10†). The salt also displayed an emission in MeCN solution (see ESI, page S9†) with photoluminescence quantum yield (PLQY) of 1.9% (entry 1, Table 1). Notably, excitation of the crystalline pyridinium salt **1** at 393 nm resulted in a solid-state emission with PLQY of 5.3% (entry 1, Table 1) and the maximum at 520 nm (see ESI, page S9†). The observed 2.8-fold increase of PLQY in the solid-state as compared to that in the MeCN solution pointed to the AIE properties of pyridinium salt **1**. Next, emission properties of pyridinium salts **2–5** with attached carbazole luminophore were evaluated.

All pyridinium carbazoles **2–5** were virtually non-emissive in solutions with photoluminescence quantum yields (PLQY) below 0.1%. In sharp contrast, the solid state PLQY for pyridinium salts **2–5** were measured to be in the range from 9.7 to 18.7%. Hence, pyridinium salts featured up to 187 times increase of emission in the solid state as compared to that in MeCN solution (Table 1). These results clearly indicated that pyridinium salts **2–5** possess AIE properties. Interestingly, the solid state emission intensity was not influenced by the

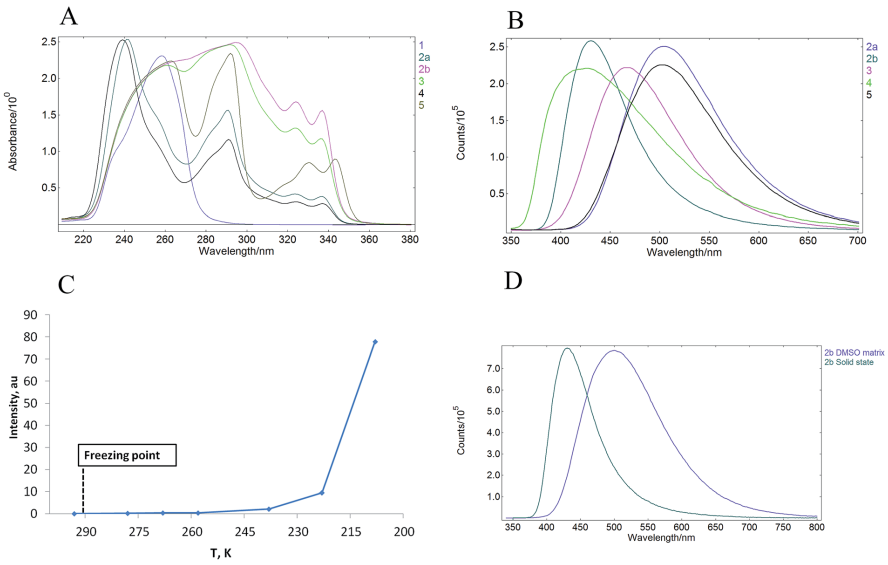

Fig. 3 (A) UV-vis spectra of **1–5** in MeCN solutions; (B) solid state emission of **2–5**; (C) emission of **2b** in DMSO as a function of temperature; (D) normalized intensity of emission of **2b** in the solid state and in the DMSO matrix.

Table 1 Photoluminescent properties of pyridinium salts **1–5**

Entry	Compound	λ_{Abs}, nm	Solid λ_{Em}, nm	Solution φ (%)	Solid φ (%)	α_{AIE}
1	**1**	258	520[a]	1.9	5.3	2.8
2	**2a**	241, 290, 325, 337	505[b]	<0.1	17.3	>173
3	**2b**	264, 295, 324, 337	432[b]	<0.1	18.7	>187
4	**3**	260, 294, 325, 337	465[b]	<0.1	18.5	>185
5	**4**	240, 292, 324, 337	442[b]	<0.1	9.7	>97
6	**5**	263, 292, 330, 343	503[b]	<0.1	15.9	>159

[a] Excited at 393 nm. [b] Excited at 325 nm.

structure of the anion as evidenced by comparable solid state PLQY for pyridinium chloride **2a** (entry 2, Table 1) and pyridinium tosylate **2b** (entry 3). Introduction of bulky *t*-Bu substituent in the position 4 of pyridinium subunit did not affect the solid state PLQY of **3** (entry 4 *vs.* entry 3), however the corresponding 4-methyl substituted analogue **4** showed the lowest PLQY values in the carbazole series (entry 5). Finally, AIEgen **5** with a flexible butylene linker between carbazole subunit and pyridinium moiety featured only slightly reduced solid state PLQY as compared to **2b** (entry 6 *vs.* entry 3). This is notable given a higher degree of freedom for intramolecular motions in **5** as compared to **2b** due to the long alkyl chain, which may consume the excited-state through non-radiative relaxation. All AIEgens **2–5** showed a broad emission peak in the solid state with no distinctive bands except the maximum in the range of 432–520 nm (Fig. 3B). Importantly, wavelength of the solid-state emission maximum depended on the counterion in pyridinium salts **1–5**. Higher energy emission peaks in the range of 432–465 nm were observed for AIEgens **2b**, **3** and **4**, which possess tosylate as the counter ion (Table 1, entries 3–5). In contrast, lower energy emission (503–520 nm) was measured for chloride or bromide counterion-containing AIEgens **1**, **2a** and **5** (Table 1, entries 1, 2 and 6). Finally, pyridinium carbazoles **2–5** displayed intense solid-state absorbance in the 250–350 nm region with sharply decreasing absorbance intensity above 350 nm. The solid-state absorbance of **2–5** was consistent with that in MeCN solution (see ESI, page S10†).

Photoluminescence behaviour of **2a** in various solvent mixtures was investigated to get an additional insight in AIE properties of **2a**. Lack of the emission was observed for **2a** in acetonitrile (a good solvent). In contrast, enhanced emission was observed in mixtures containing high (90–95% v/v) fraction

of Et_2O (a poor solvent) in MeCN (see ESI, page S13†). The dynamic light scattering (DLS) measurements indicated that pyridinium salt **2a** did not form aggregates in solvent mixtures that contained less than 90% of Et_2O in acetonitrile (see ESI, page S13†). Notably, the lack of emission was observed for **2a** in these solvent mixtures. In contrast, the formation of aggregates could be observed even by the naked eye if 90–95% (v/v) of Et_2O in acetonitrile was used as the solvent. In the latter case, the size of aggregates was larger than 10 μm, thus exceeding limits of DLS measurements. The apparent correlation between the formation of aggregates and luminescence provided an additional support for AIE properties of pyridinium salt **2a**.

We have also examined whether AIE properties of pyridinium salts **1–5** originate from restriction of intramolecular rotation (RIR) phenomena.[12] To this end we measured a relationship between emission of **2b** in DMSO solution and temperature in the range from 293 K to 208 K (Fig. 3C). A solution of **2b** in DMSO did not display observable emission at 293 K. Importantly, the emission increase could not be determined after freezing of the DMSO solution of **2b**, as well as upon further cooling to 238 K. The emission only started to appear at temperatures below 238 K and the intensity increased considerably at 208 K (Fig. 3C). Lack of the emission for **2b** in the DMSO matrix points against the RIR mechanism as the origin of AIE properties of **2b**, because considerable enhancement of the emission in solid matrices is usually observed for most of AIEgens that benefit from RIR effect.[13] Furthermore, the emission peak for **2b** in frozen DMSO matrix showed bathochromic shift as compared to that in the solid state (Fig. 3D). Finally, the solid state emission intensity for crystalline **2b** remained unchanged in the temperature range from 293 K to 193 K. These data provide evidence that the luminogens **1–5** show AIE properties in crystalline form.

Single crystal X-ray analysis

Single crystal X-ray analysis of luminogens **2–5** provided important insight into intermolecular interactions that result in AIE properties (Table 2). Single crystals of pyridinium salts **2–5** suitable for X-ray crystallography could be obtained by vapor diffusion from various solvents systems such as acetone/EtOH, DCM/hexane, EtOAc/MeCN, toluene/DCM or Et_2O. In a crystal lattice pyridinium salts **2a**, **2b**, **3** and **5** feature intermolecular π^+–π^+ interactions between the charged pyridinium rings. This is evidenced by a strictly parallel off-center orientation of neighboring pyridinium rings with the distance between them spanning a range from 3.686 Å (for **5**) to 4.211 Å (for **2a**; see Table 2). In contrast, pyridinium salt **4** does not have the π^+–π^+ interactions between the charged pyridinium rings. Instead, interactions between pyridinium ring and 1,4-disubstituted phenylene moiety can be observed for **4** as evidenced by a relatively close distance (from 3.803 Å to 4.027 Å) between the two nonparallel-oriented π-systems (Table 2).[14] It should be noted that pyridinium salt **4** demonstrated lower PLQY as compared to other AIEgens **2a**, **2b**, **3** and **5** (see Table 1), suggesting that pyridinium–pyridinium interactions are important to achieve greater AIE properties in the crystalline state.[15]

In addition to the intermolecular pyridinium–pyridinium interactions in the crystal lattice of **2b**, the aromatic system of tosylate anion is positioned in a non-parallel off-center orientation with respect to pyridinium ring (3.843–4.186 Å distance, see ESI, page S9†). However, the latter interaction apparently does not influence the AIE properties of **2b**, as evidenced by similar PLQY values for **2b** and the analogous AIEgen **2a**, possessing chloride as the counter-ion (see entries 2 and 3, Table 1). The other tosylate-containing AIEgens **3** and **4** do not show the face-to-face interactions between pyridinium cation and π-

Table 2 Crystal packing and expanded views of π^+–π^+ and π^+–π interactions for pyridinium salts **2–5**

Compound **2a**	Compound **2b**	Compound **3**	Compound **4**	Compound **5**
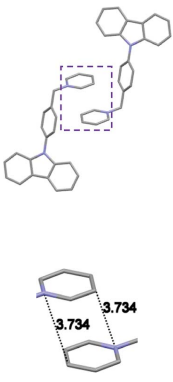	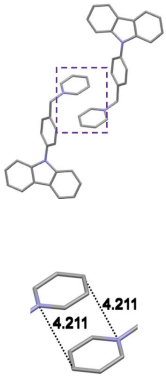	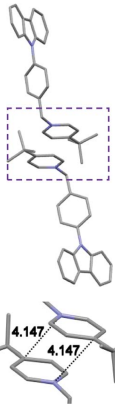	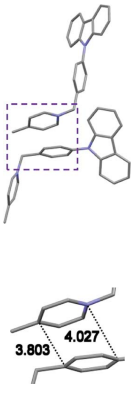	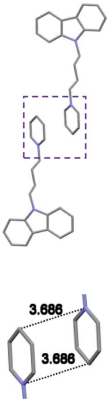

system of the tosylate anion. Hence, these data demonstrate that the crystal-state AIE effect can be achieved using chloride, bromide and tosylate as the counter-ion for pyridinium. Importantly, nature of counter-ion influences the solid-state emission maximum of AIEgens. Thus, change of the counter-ion in AIEgen **2** from tosylate (**2b**) to chloride (**2a**) resulted in a noticeable bathochromic shift of more than 70 nm (Fig. 3B.). The dependence of the solid-state emission maximum on the nature of the counter-ion simplifies the design of AIEgens with the desired emission wavelength.

Conclusions

All synthesized pyridinium salts **1–5** demonstrate AIE properties with up to 187 times emission increase in the crystal-state as compared to solution. Lack of emission for **2b** in solution and frozen DMSO matrix (solid amorphous state) speaks against the RIR effect as the origin of the AIE properties for pyridinium salt **2b**. Single crystal X-ray analyses provide clear evidence for the presence of non-covalent intermolecular pyridinium–pyridinium and pyridinium–π interactions in the crystal-state of AIEgens **2–5**. Consequently, crystal-state AIE effect can be attributed to the intermolecular π^{+}–π^{+} and π^{+}–π interactions involving pyridinium cations. Hence, non-covalent interactions between two neighboring pyridinium subunits in a crystal-state are an efficient means to accomplish AIE. The nature of counter-ion in pyridinium salts **2–5** does not affect emission efficiency (PLQY) of the crystal-state AIEgens, however, the counter-ion does influence the crystal-state emission maximum of AIEgens. The use of the non-covalent pyridinium–pyridinium or pyridinium–π interactions in the design of AIEgens is alternative and complementary approach to routinely used means to avoid the ACQ effect.[3,4] Further studies on the design of the crystal-state AIEgens based on interactions between cationic π systems will be reported in due course.

Conflicts of interest

There are no conflicts to declare.

Acknowledgements

This work was funded by Taiwan–Lithuania–Latvia Tripartite Cooperation Fund (Project "New materials and technologies for very-high color rendering and high sunlight spectrum resemblance OLED lighting sources"). We thank Dr A. Mishnev and Dr D. Stepanovs for X-ray crystallographic analysis and P. Dimitrijevs for DLS measurements.

References

1 (*a*) D. Volz, *J. Photonics Energy*, 2016, **6**, 020901; (*b*) X.-D. Wang, O. S. Wolfbeis and R. J. Meier, *Chem. Soc. Rev.*, 2013, **42**, 7834–7869.

2 (*a*) A. S. Klymchenko, *Acc. Chem. Res.*, 2017, **50**, 366; (*b*) S. A. Jenekhe and J. A. Osaheni, *Science*, 1994, **265**, 765; (*c*) Solid-state luminescence enhancement has been also observed: J. Shi, L. E. Aguilar Suarez, S.-J. Yoon, S. Varghese, C. Serpa, S. Y. Park, L. Lüer, D. Roca-Sanjuán, B. Milián-Medina and J. Gierschner, *J. Phys. Chem. C*, 2017, **121**, 23166–23183.

3 (*a*) J. E. Anthony, J. S. Brooks, D. L. Eaton and S. R. Parkin, *J. Am. Chem. Soc.*, 2001, **123**, 9482–9483; (*b*) Z.-F. Yao, J.-Y. Wang and J. Pei, *Cryst. Growth Des.*, 2018, **18**, 7–15.

4 J. Wang, X. Gu, P. Zhang, X. Huang, X. Zheng, M. Chen, H. Feng, R. T. K. Kwok, J. W. Y. Lam and B. Z. Tang, *J. Am. Chem. Soc.*, 2017, **139**, 16974–16979.

5 J. Luo, Z. Xie, J. W. Y. Lam, L. Cheng, H. Chen, C. Qiu, H. S. Kwok, X. Zhan, Y. Liu, D. Zhuc and B. Z. Tang, *Chem. Commun.*, 2001, 1740–1741.

6 (*a*) T. Butler, W. A. Morris, J. Samonina-Kosicka and C. L. Fraser, *ACS Appl. Mater. Interfaces*, 2016, **8**, 1242; (*b*) Z. S. Wang, B. S. Gelfand, P. C. Dong, S. Trudel and T. Baumgartner, *J. Mater. Chem. C*, 2016, **4**, 2936; (*c*) O. Shynkaruk, G. He, R. McDonald, M. J. Ferguson and E. Rivard, *Chem.–Eur. J.*, 2016, **22**, 248; (*d*) M. T. Gabr and F. C. Pigge, *RSC Adv.*, 2015, **5**, 90226; (*e*) W. A. Morris, T. D. Liu and C. L. Fraser, *J. Mater. Chem. C*, 2015, **3**, 352; (*f*) K. R. Ghosh, S. K. Saha and Z. Y. Wang, *Polym. Chem.*, 2014, **5**, 5638; (*g*) N. B. Shustova, A. F. Cozzolino, S. Reineke, M. Baldo and M. Dinca, *J. Am. Chem. Soc.*, 2013, **135**, 13326; (*h*) F. Hu, G. X. Zhang, C. Zhan, W. Zhang, Y. L. Yan, Y. S. Zhao, H. B. Fu and D. Q. Zhang, *Small*, 2015, **11**, 1335; (*i*) C. Wang, H. Zhang, L. Tian, W. Zhu, Y. Lan, J. Li, H. Wang, G. X. Zhang, D. Q. Zhang, S. L. Yuan and G. T. Li, *Sci. China: Chem.*, 2016, **59**, 89.

7 (*a*) Y. Hong, J. W. Y. Lam and B. Z. Tang, *Chem. Soc. Rev.*, 2011, **40**, 5361; (*b*) J. Mei, N. L. C. Leung, R. T. K. Kwok, J. W. Y. Lam and B. Z. Tang, *Chem. Rev.*, 2015, **115**, 11718; (*c*) X. Z. Yan, H. Z. Wang, C. E. Hauke, T. R. Cook, M. Wang, M. L. Saha, Z. X. Zhou, M. M. Zhang, X. P. Li, F. H. Huang and P. J. Stang, *J. Am. Chem. Soc.*, 2015, **137**, 15276; (*d*) X. Z. Yan, M. Wang, T. R. Cook, M. M. Zhang, M. L. Saha, Z. X. Zhou, X. P. Li, F. H. Huang and P. J. Stang, *J. Am. Chem. Soc.*, 2016, **138**, 4580; (*e*) A. D. Shao, Y. S. Xie, S. J. Zhu, Z. Q. Guo, S. Q. Zhu, J. Guo, P. Shi, T. D. James, H. Tian and W. H. Zhu, *Angew. Chem., Int. Ed.*, 2015, **54**, 7275; (*f*) C. Wang, B. J. Xu, M. S. Li, Z. G. Chi, Y. J. Xie, Q. Q. Li and Z. Li, *Mater. Horiz.*, 2016, **3**, 220; (*g*) Z. L. Xie, C. J. Chen, S. D. Xu, J. Li, Y. Zhang, S. W. Liu, J. R. Xu and Z. G. Chi, *Angew. Chem., Int. Ed.*, 2015, **54**, 7181; (*h*) Y. T. Gao, G. X. Feng, T. Jiang, C. C. Goh, L. G. Ng, B. Liu, B. Li, L. Yang, J. L. Hua and H. Tian, *Adv. Funct. Mater.*, 2015, **25**, 2857; (*i*) W. Dong, T. Fei, A. Palma-Cando and U. Scherf, *Polym. Chem.*, 2014, **5**, 4048.

8 (*a*) M. Mohan, S. Pangannaya, M. N. Satyanarayan and D. R. Trivedi, *ChemistrySelect*, 2018, **3**, 3803–3813; (*b*) N. Han, H. Kun, X. Yuanjing, P. Qian, Z. Zujin, H. Rongrong, C. Junwu, S. Shi-Jian, Q. Anjun and B. Z. Tang, *Mater. Chem. Front.*, 2017, **1**, 1125–1129.

9 M. S. Marshall, R. P. Steele, K. S. Thanthiriwatte and C. D. Sherrill, *J. Phys. Chem. A*, 2009, **113**, 13628–13632.

10 W. Chen, S. A. Elfeky, Y. Nonne, L. Male, K. Ahmed, C. Amiable, P. Axe, S. Yamada, T. D. James, S. D. Bull and J. S. Fossey, *Chem. Commun.*, 2011, **47**, 253–255.
11 J. Zhong, Z. Li, W. Guan and C. Lu, *Anal. Chem.*, 2017, **89**, 12472–12479.
12 J. Chen, C. C. W. Law, J. W. Y. Lam, Y. Dong, S. M. F. Lo, I. D. Williams, D. Zhu and B. Z. Tang, *Chem. Mater.*, 2003, **15**, 1535–1546.
13 Y. Hong, J. W. Y. Lam and B. Z. Tang, *Chem. Commun.*, 2009, 4332–4353.
14 Similar interactions between pyridinium cation and aromatic or heteroaromatic π-system have been observed by X-ray analysis: (*a*) X.-H. Jin, C. Chen, C.-X. Ren, L.-X. Cai and J. Zhang, *Chem. Commun.*, 2014, 15878–15881; (*b*) C. Chen, X.-H. Jin, X.-J. Zhou, L.-X. Cai, Y.-J. Zhang and J. Zhang, *J. Mater. Chem. C*, 2015, **3**, 4563–4589; (*c*) Y. Gu, Z. Zhao, H. Su, P. Zhang, J. Liu, G. Niu, S. Li, Z. Wang, R. T. K. Kwok, X.-L. Ni, J. Sun, A. Qin, J. W. Y. Lam and B. Z. Tang, *Chem. Sci.*, 2018, **9**, 6497–6502.
15 9-(4-Benzylphenyl)-9*H*-carbazole **10** (see ESI, page S7†), an analog of **2a**,**b** with benzene ring instead of the pyridinium subunit does not possess AIE properties. It features high solution-state emission (39.9% PLQY) and reduced solid-state emission (35.5% PLQY). For photophysical properties of **10**, see ESI.†

P-2

Leduskrasts, K.; Kinēns, A.; Sūna, E.
"Cation–π interactions secure aggregation induced emission of Planar Organic Luminophores"
Chem. Commun. **2019**, 55, 12663–12666.
DOI:10.1039/C9CC06829E.

ChemComm

COMMUNICATION

View Article Online
View Journal | View Issue

Cite this: *Chem. Commun.*, 2019, 55, 12663

Received 2nd September 2019,
Accepted 23rd September 2019

DOI: 10.1039/c9cc06829e

rsc.li/chemcomm

Cation–π interactions secure aggregation induced emission of planar organic luminophores†

Kaspars Leduskrasts, Artis Kinens and Edgars Suna *

The use of non-covalent intermolecular π^+–π interactions between quaternary pyridinium or imidazolium cations and aromatic π systems is an efficient approach to achieve AIE in planar purely organic luminophores.

Organic luminophores that are highly emissive in dilute solutions frequently experience decrease or even loss of the emission upon aggregation. This phenomenon is known as aggregation-caused quenching (ACQ).[1] The ACQ is a major hurdle in many practical applications, which require emission in the aggregated state (thin films, polymer matrices, *etc.*) or in the solid state.[2–6] In 2001 Tang discovered aggregation induced emission luminogens (AIEgens) that featured increased emission in the solid state as compared to that in dilute solution.[7] Since then AIEgens have found ample applications in various optoelectronic devices such as OLEDs,[8] organic field-effect transistors[5,9] and photovoltaic devices[10] as well as in artificial photosynthesis[11] and photon refining.[12] AIEgens have also been widely used as chemical sensors,[13] biosensors,[14] stimuli sensors[15] and as luminescent probes in biomedical applications.[16]

The working principle underlying the emission of AIEgens is proposed to be a restriction of intramolecular motions (RIM), vibrations (RIV) and rotations (RIR) to minimize the non-radiative dissipation of exciton energy.[16b,17] In addition, the design of AIEgens also frequently features out-of-plane twisting of aromatic subunits and incorporation of a steric bulk to avoid the detrimental intermolecular π–π stacking interactions between planar aromatic luminophores, which results in the ACQ effect. These structural requirements usually lead to a relatively complex design of purely organic AIEgens.[16a,b,18] Clearly, a new type of interaction that would help to achieve AIE in structurally simple purely organic molecules is highly desired for the development of AIEgens.

Latvian Institute of Organic Synthesis, Aizkraukles 21, Riga, LV-1006, Latvia.
E-mail: edgars@osi.lv

† Electronic supplementary information (ESI) available: Experimental procedures, photo physical properties, X-ray crystallographic data (CIF files), DFT calculations, and ^{1}H and ^{13}C NMR spectra. CCDC 1949701–1949703. For ESI and crystallographic data in CIF or other electronic format see DOI: 10.1039/c9cc06829e

Recently we have demonstrated that non-covalent intermolecular interactions between pyridinium (Py^+) cations (π^+–π^+ interactions) leads to a solid state luminescence (SSL) with up to 19% PLQY (see Fig. 1).[19] In this study we report on a further development of the conceptual approach to achieve AIE. Specifically, we show herein that a mechanistically related interaction between quaternary Py^+ or imidazolium (Im^+) cations and aromatic π systems (π^+–π interactions) results in remarkable SSL (up to 80% PLQY). Furthermore, the quaternization of nitrogen atoms turns on the SSL even in planar heteroaromatic molecules (Fig. 1). The performed DFT calculations suggest that the observed SSL results from intermolecular charge transfer (ICT) between heteroaromatic (Py^+ and Im^+) cations and aromatic π systems.

Py^+ and Im^+ perchlorates **3a–d** were obtained by *N*-alkylation of the commercially available heterocycles **1a–d** with MeI, followed by the exchange of iodide for perchlorate (Fig. 2). Pyridines **5a,b** were synthesized from the commercially available **4** and pyridine boronic acids under Suzuki reaction conditions. Subsequent *N*-alkylation with MeI was followed by iodide-to-perchlorate exchange to afford Py^+ salts **7a,b**. The synthesis of heterocycles **5c** and **5d** required Cu(I)-catalyzed *N*-arylation of carbazole by the commercially available bromides **8** and **9**, respectively. A subsequent *N*-alkylation and anion exchange sequence provided **7c,d** (Fig. 2). All heteroaromatic quaternary salts **3a–d**, **6a** and **7a–d** were crystalline materials.

UV-vis spectra of all synthesized quaternary salts and parent heterocycles were measured in MeCN solutions (at *ca.* 10^{-5} mol L^{-1}) at room temperature and under an ambient atmosphere.

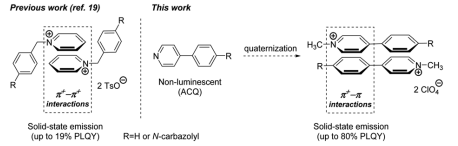

Fig. 1 Design of the solid state AIEgens by intermolecular cation–π interactions.

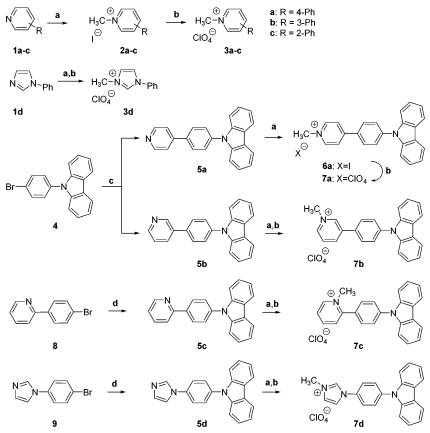

Fig. 2 Synthesis of heteroaromatic salts **2a**, **3a–d**, **6a** and **7a–d**. *Reagents and conditions*: (a) CH_3I, MeCN, 80 °C, 16 h, 96% (**2a**), 94% (**6a**). (b) $AgClO_4$, MeCN, r.t., 15 min, 70% (**3a**), 61% (**3b**), 88% (**3c**), 64% (**3d**), 98% (**7a**), 94% (**7b**), 54% (**7c**), 94% (**7d**). (c) Pyridine-4-boronic acid (for **5a**) or pyridine-3-boronic acid (for **5b**), $Pd(dppf)Cl_2$ × DCM (5 mol%), K_2CO_3, 1 : 6 water–MeCN, 90 °C, 1 h, 75% (**5a**), 72% (**5b**). (d) Carbazole, CuI (15 mol%), L-Pro (30 mol%), K_2CO_3, DMSO, 120–140 °C, 16–72 h, 22% (**5c**), 47% (**5d**).

For analysis of absorption spectra, see Table 1 and the ESI,† page S16. Heteroarenes **1a–d** did not show any measurable emission in solution and in the solid state with <0.1% photoluminescence quantum yields (PLQYs). The lack of emission for **1a–d** was not surprising because these molecules do not possess any of the traditional luminophore moieties such as carbazole. Alkylation of **1a** with MeI afforded Py^+ iodide **2a**, which displayed a broad non-structured emission band at λ_{max} = 372 nm in MeCN solution with 36.8% PLQY (entry 1, Table 1).[20] Unfortunately, Py^+ salt **2a** was non-emissive in the solid state, and the lack of SSL for Py^+ iodides has been reported earlier by Fossey.[21] We were pleased to find that a simple exchange of iodide **2a** to perchlorate **3a** enabled high SSL (λ_{max} = 346 nm, 52.7% PLQY), while retaining the emission in MeCN solution (broad emission band at λ_{max} = 372 nm with 37.9% PLQY; entry 2). Isomeric perchlorates **3b,c** also displayed observable emission in solution (at λ_{max} = 390 nm and 380 nm with PLQYs of 21.1% and 3.5%, respectively) and high SSL with PLQYs of 42.1% (λ_{max} = 350 nm) and 39.1% (λ_{max} = 341 nm), respectively (entries 3 and 4). Decreased PLQY for **3c** both in solution and in the solid state could be possibly attributed to the decreased conjugation due to the presence of a *N*-methyl substituent. We were also pleased to find that SSL can be achieved using cationic heteroaromatic subunits other than Py^+ salts. Thus, Im^+ perchlorate **3d** showed luminescence both in solution (λ_{max} = 380 nm, 16.1% PLQY) and in the solid state (λ_{max} = 315 nm, 19.8% PLQY; entry 5). Notably, all perchlorates **3a–d** featured AIE properties as evidenced by higher PLQY in the solid state as compared to solution (α_{AIE} up to 11.2; see Table 1). The observed SSL levels for **3a–d** (up to 53% PLQY for **3a**) are remarkable given the structural simplicity of salts **3a–d** and the absence of a luminophore moiety in their structure.

Next, we incorporated carbazole into AIEgens **3a–d** to increase their luminescence efficiency. Highly intense SSL was observed for perchlorates **7a** (79.8% PLQY at λ_{max} = 489 nm), **7b** (72.2% PLQY at λ_{max} = 446 nm) and **7c** (46.9% PLQY at λ_{max} = 465 nm; entries 11–13). Strikingly, Py^+ perchlorates **7a–c** were non-emissive in MeCN solution with PLQY < 0.1%. The observed up to 800-fold increase of PLQY in the solid state as compared to that in the MeCN solution confirms the AIE nature of **7a–c**. Perchlorate **7d** demonstrated slightly reduced SSL (11.0% PLQY at λ_{max} = 498 nm; entry 14) *vs.* parent **3d** (entry 5). In contrast to perchlorate **7a**, the corresponding iodide **6a** showed luminescence neither in the MeCN solution nor in the solid state (entry 10). The observed lack of the luminescence for iodides **2a** and **6a** demonstrates the importance of the counter-ion in the quaternized luminophores. Finally, the luminescence properties of parent **5a–d** were also determined. All non-charged heterocycles **5a–d** featured high emission intensity in MeCN solutions (entries 6–9) with **5a** showing the highest PLQY (73.1%). In contrast, considerably reduced SSL was observed for **5a–d**. Thus, **5b** showed up to 80-fold decrease of PLQY in the solid state as compared to the MeCN solution (entry 7). Evidently, the reduced SSL is a result of the ACQ effect in the highly planar luminophores **5a–d**, which experience intermolecular π–π aromatic interactions leading to decay of the

Table 1 Photoluminescence properties of luminophores **2a–7d**

Entry	Compound	λ_{abs}, nm	Solution λ_{em}, nm	Solid λ_{em}, nm	Solution, ϕ (%)	Solid, ϕ (%)	α_{AIE}
1	**2a**	247, 293	372	—	36.8	<0.1	<0.1
2	**3a**	231, 294	372	346	37.9	52.7	1.4
3	**3b**	237, 257, 292	390	350	21.2	42.1	2.0
4	**3c**	239, 282	380	341	3.5	39.1	11.2
5	**3d**	235	353	315	16.1	19.8	1.2
6	**5a**	238, 292, 322	442	371, 387, 407	73.1	5.7	0.1
7	**5b**	240, 292, 338	408	368	46.5	0.6	<0.1
8	**5c**	240, 292, 315	416	378, 436	74.6	16.8	0.2
9	**5d**	240, 292, 326, 339	347, 361	371	33.2	17.8	0.5
10	**6a**	237, 282, 376	—	473	<0.1	0.40	>4
11	**7a**	239, 282, 379	—	489	<0.1	79.8	>800
12	**7b**	236, 289, 339	—	446	<0.1	72.2	>700
13	**7c**	237, 279, 337	—	465	<0.1	46.9	>470
14	**7d**	241, 291, 336	498	369	1.6	11.0	6.9

excited-state energy *via* non-radiative energy transfer.[22] In contrast, ACQ does not affect the structurally related planar salts **7a–d** as evidenced by the pronounced AIE properties of these luminophores. Furthermore, the change in structured emission for **5a** in the solid state to a broad featureless solid state emission of perchlorate **7a** indicates distinct emission mechanisms for **5a** and **7a.**

The AIE properties of perchlorates **7a–d** were further corroborated by the observed correlation between the emission and formation of aggregates (see the ESI,† page S27, for details). In addition, lack of emission for **7a** in solution and the frozen DMSO matrix (solid amorphous state) speaks against the RIR effect as the origin of the AIE properties of quaternary salts **3a–d** and **7a–d** (see the ESI,† page S29, for details). A notable feature of perchlorates **3a–d** and **7d** is the SSL in the UV region (315–369 nm; entries 2–5 and 14), a property that has been rarely observed for AIE materials.[23] The attachment of the carbazole moiety to **3a–d** resulted in a substantial (54–143 nm) red-shift of the SSL. Hence, the introduction of electron donating moieties in **3a–d** shifts the emission maxima, allowing for direct control of the emission wavelength.

Single crystal X-ray analysis of **3a**, **6a** and **7a** provided important insight into the intermolecular interactions that lead to the SSL (Table 2). In a crystal lattice, salts **3a**, **6a** and **7a** showed close interactions between charged Py^+ cations and π systems (π^+–π interactions), which ranged from 3.500 Å (**6a**) to 3.760 Å (**3a**; Table 2). However, the distance between centroids does not correlate with the emission efficiency. Thus, very low PLQY (0.4%) was observed for **6a** in the solid state despite the short distances for π^+–π interactions (3.500 Å and 3.652 Å). Salt **7a** also featured short distance between Py^+ cations and carbazole π-systems (3.525 Å), whereas the corresponding distance in **3a** was longer (3.760 Å). Nevertheless, both **3a** and **7a** were superior to **6a** with respect to the SSL efficiency (52.7% and 79.8% PLQY, respectively). The interacting Py^+ and carbazole planar rings are nearly parallel in **6a** and **7a** (5.65° and 3.73° angles between the planes of heterocycles, respectively), and the angle between the Py^+ subunit and arene ring in **3a** is 19.1°. Despite the apparent similarity between the packing mode of **6a** and **7a,** the remarkable difference in the solid state PLQY suggests that the iodide ion quenches the emission in **6a** by mechanisms other than steric or electronic hindrance of the π^+–π interactions.

Additional support for the relationship between π^+–π interactions (involving Py^+ cations and carbazole π systems) and the SSL was obtained by time-dependent density functional theory (TDDFT) calculations of the emission spectra for **7a** at the B3LYP/6-31G(d) level of theory (see the ESI,† page S33). As Py^+ perchlorate **7a** did not display emission in solution, the emission spectra of **7a** were calculated using geometry from the crystalline state. Furthermore, only singlet states S_n were used for calculations because oxygen quenching experiments in the suspensions of **7a** did not show any emission intensity change, thus providing evidence against triplet state emission.

First, the feasibility of intramolecular CT character of the SSL in cation **7a** was examined at the single molecule level. The calculated emission spectra (Fig. 3A) displayed two distinct emission peaks at λ_{max} = 341 nm and 740 nm with high oscillatory force (f = 0.3387 and f = 0.3063; see Fig. 3A). Molecular orbitals (MO) associated with the electronic transitions were localized in the carbazole moiety (HOMO) and in the Py^+ moiety with lesser intensity occupying also the phenylene linker (LUMO; see Fig. 3C and the ESI,† page S33, for the representation of frontier MO). The emission peak at λ_{max} = 341 nm corresponded to transition from HOMO−4 to the LUMO and from the HOMO to LUMO+3. The emission peak at λ_{max} = 740 nm corresponded to transition from the HOMO to LUMO (see Fig. 3B and the ESI†). Notably, the calculated emission peaks did not match the experimentally observed one at λ_{max} = 489 nm (Table 1, entry 11). Consequently, an intramolecular CT apparently does not account for the observed SSL of **7a.**

Next, the emission spectra for the symmetric dimer of **7a** were calculated, resulting in a broad emission peak at λ_{max} = 495 nm with a large oscillatory force (f = 0.3784; Fig. 3C). MO associated with the electronic transitions was localized in two regions of the dimer: the HOMO was located on the carbazole moiety, whereas the LUMO was mostly localized on the Py^+ moiety with lesser intensity occupying also the phenylene linker (see Fig. 3C and the ESI† for the representation of the frontier MO). Calculations show that multiple CT (from HOMO−3 to the LUMO, from HOMO−2 to LUMO+1, from HOMO−1 to LUMO and from HOMO to LUMO+1; see the ESI†) are responsible for the emission at λ_{max} = 495 nm. Such a type of symmetric

Table 2 Crystal packing of salts **3a**, **6a** and **7a**

3a	**6a**	**7a**
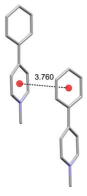	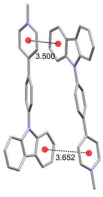	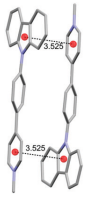

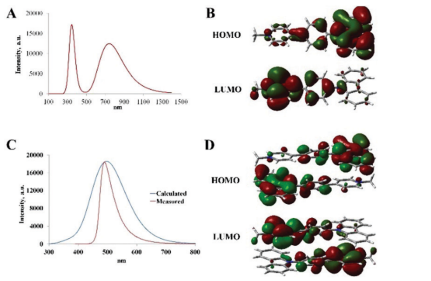

Fig. 3 (A) Calculated UV-Vis spectrum of **7a** (single molecule). (B) Frontier MO for **7a** (single molecule). (C) Calculated UV-Vis spectrum of the dimer of **7a**. (D) Frontier MO for the dimer of **7a**.

through-space CT has been reported for the SSL.[24] Notably, the calculated emission at λ_{max} = 495 nm for the dimer of **7a** was consistent with that observed experimentally (λ_{max} = 489 nm; entry 11). However, the observed SSL peak for **7a** was narrower compared to the calculated one. This difference could be possibly attributed to the additional stabilizing interactions in the crystal lattice for **7a**. Consequently, the TDDFT calculations provide evidence that an emissive intermolecular through-space CT band is responsible for the SSL of cationic perchlorates **3a–d** and **7a–d**.

In summary, a series of highly emissive planar AIEgens has been designed by utilizing non-covalent intermolecular π^+–π interactions between Py^+ or Im^+ cations and aromatic π systems. Structurally simple salts **3a–d** lacking any conventional luminophore moiety demonstrated high SSL (up to 53% PLQY) in the UV region (315–350 nm). The introduction of electron donating moieties in **3a–d** resulted in bathochromic shifts of the emission maxima, thus allowing for direct control of emission wavelength. Carbazole-containing perchlorates **7a–d** also demonstrated a remarkable (up to 800-fold) increase of PLQY as compared to that in MeCN solution. The presence of iodide ions led to the quenching of the SSL. Single crystal X-ray analyses confirm the presence of non-covalent intermolecular interactions between Py^+ or Im^+ cations and aromatic π systems in the crystal state of AIEgens **3a** and **7a**. TDDFT calculations provide strong evidence that the observed SSL of **3a–d** and **7a–d** is a result of intermolecular π^+–π interactions that generate through-space CT bands in the crystal state. The use of the non-covalent π^+–π interactions in the design of AIEgens is a complementary approach to routinely used means to achieve AIE properties and to avoid the ACQ effect. We believe that our study will expand the scope of structural motifs that previously could not be used due to the ACQ and will open a new avenue for the rational design of AIEgens.

This work was funded by ERDF project No. 1.1.1.1/18/A/063. We thank Dr S. Belyakov and Dr A. Mishnev for X-ray crystallographic analysis and P. Dimitrijevs for DLS measurements.

Conflicts of interest

There are no conflicts to declare.

Notes and references

1 (*a*) A. S. Klymchenko, *Acc. Chem. Res.*, 2017, **50**, 366; (*b*) S. A. Jenekhe and J. A. Osaheni, *Science*, 1994, **265**, 765.
2 R. B. Thompson, *Fluorescence Sensors and Biosensors*, CRC/Taylor & Francis, Boca Raton, 2006.
3 C. D. Geddes and J. R. Lakopwicz, *Advanced Concepts in Fluorescence Sensing*, Springer, New York, 2005.
4 A. Buckley, *Organic light-emitting diodes (OLEDs): materials, devices and applications*, Woodhead Publishing, Oxford, 2013.
5 S. G. Surya, H. N. Raval, R. Ahmad, P. Sonar, K. N. Salama and V. R. Rao, *TrAC, Trends Anal. Chem.*, 2019, **111**, 27.
6 E. Fresta and R. D. Costa, *J. Mater. Chem. C*, 2017, **5**, 5643.
7 J. Luo, Z. Xie, J. W. Y. Lam, L. Cheng, H. Chen, C. Qiu, H. S. Kwok, X. Zhan, Y. Liu, D. Zhu and B. Z. Tang, *Chem. Commun.*, 2001, 1740.
8 (*a*) Z. Ning, Z. Chen, Q. Zhang, Y. Yan, S. Qian, Y. Cao and H. Tian, *Adv. Funct. Mater.*, 2007, **17**, 3799; (*b*) J. Huang, N. Sun, Y. Dong, R. Tang, P. Lu, P. Cai, Q. Li, D. Ma, J. Qin and Z. Li, *Adv. Funct. Mater.*, 2013, **23**, 2329.
9 (*a*) Z. Zhao, Z. Li, J. W. Y. Lam, J.-L. Maldonado, G. Ramos-Ortiz, Y. Liu, W. Yuan, J. Xu, Q. Miao and B. Z. Tang, *Chem. Commun.*, 2011, **47**, 6924; (*b*) M. P. Aldred, G.-F. Zhang, C. Li, G. Chen, T. Chen and M.-Q. Zhu, *J. Mater. Chem. C*, 2013, **1**, 6709.
10 (*a*) B. Mi, Y. Dong, Z. Li, J. W. Y. Lam, M. Haussler, H. H. Sung, H. S. Kwok, Y. Dong, I. D. Williams, Y. Liu, Y. Luo, Z. Shuai, D. Zhu and B. Z. Tang, *Chem. Commun.*, 2005, 3583; (*b*) Y. Li, Z. Li, Y. Wang, A. Compaan, T. Ren and W.-J. Dong, *Energy Environ. Sci.*, 2013, **6**, 2907.
11 (*a*) M. Zhang, X. Yin, T. Tian, Y. Liang, W. Li, Y. Lan, J. Li, M. Zhou, Y. Ju and G. Li, *Chem. Commun.*, 2015, **51**, 10210; (*b*) Y. Zeng, P. Li, X. Liu, T. Yu, J. Chen, G. Yang and Y. Li, *Polym. Chem.*, 2014, **5**, 5978.
12 (*a*) P. Duan, D. Asthana, T. Nakashima, T. Kawai, N. Yanai and N. Kimizuka, *Faraday Discuss.*, 2017, **196**, 305; (*b*) L. Li, Y. Zeng, T. Yu, J. Chen, G. Yang and Y. Li, *ChemSusChem*, 2017, **10**, 4610.
13 (*a*) X. Wang, J. Hu, T. Liu, G. Zhang and S. Liu, *J. Mater. Chem.*, 2012, **22**, 8622–8628; (*b*) Y. Chen, W. Zhang, Y. Cai, R. T. K. Kwok, Y. Hu, J. W. Y. Lam, X. Gu, Z. He, Z. Zhao, X. Zheng, B. Chen, C. Gui and B. Z. Tang, *Chem. Sci.*, 2017, **8**, 2047.
14 X. Xue, Y. Zhao, L. Dai, X. Zhang, X. Hao, C. Zhang, S. Huo, J. Liu, C. Liu, A. Kumar, W. Q. Chen, G. Zou and X. J. Liang, *Adv. Mater.*, 2014, **26**, 712.
15 (*a*) J. Q. Shi, W. J. Zhao, C. H. Li, Z. P. Liu, Z. S. Bo, Y. P. Dong, Y. Q. Dong and B. Z. Tang, *Chin. Sci. Bull.*, 2013, **58**, 2723; (*b*) Q. Qi, X. Fang, Y. Liu, P. Zhou, Y. Zhang, B. Yang, W. Tian and S. X.-A. Zhang, *RSC Adv.*, 2013, **3**, 16986.
16 (*a*) Y. Tang and B. Z. Tang, *Principles and Applications of Aggregation-Induced Emission*, Springer International Publishing, New York, 2019; (*b*) J. Mei, N. L. C. Leung, R. T. K. Kwok, J. W. Y. Lam and B. Z. Tang, *Chem. Rev.*, 2015, **115**, 11718.
17 (*a*) C. Yuan, S. Saito, C. Camacho, T. Kowalczyk, S. Irle and S. Yamaguchi, *Chem. – Eur. J.*, 2014, **20**, 2193; (*b*) L. Yao, S. Zhang, R. Wang, W. Li, F. Shen, B. Yang and Y. Ma, *Angew. Chem., Int. Ed.*, 2014, **53**, 2119; (*c*) J. Liu, X. Zhang, X. Lu, P. He, L. Jiang, H. Dong and W. Hu, *Chem. Commun.*, 2013, **49**, 1199.
18 (*a*) X. Wang, S. Wang, J. Lv, S. Shao, L. Wang, X. Jing and F. Wang, *Chem. Sci.*, 2019, **10**, 2915; (*b*) S.-K. Kim, S.-Y. Oh and J.-W. Park, *Thin Solid Films*, 2008, **517**, 1349.
19 K. Leduskrasts and E. Suna, *RSC Adv.*, 2019, **9**, 460.
20 W. Chen, S. A. Elfeky, Y. Nonne, L. Male, K. Ahmed, C. Amiable, P. Axe, S. Yamada, T. D. James, S. D. Bull and J. S. Fossey, *Chem. Commun.*, 2011, **47**, 253.
21 I. Richter, M. R. Warren, J. Minari, S. A. Elfeky, W. Chen, M. F. Mahon, P. R. Raithby, T. D. James, K. Sakurai, S. J. Teat, S. D. Bull and J. S. Fossey, *Chem. – Asian J.*, 2009, **4**, 194.
22 See the ESI,† page S23, for further discussions.
23 (*a*) C.-Q. Ye, L.-W. Zhou, C.-B. Fan, G.-L. Dai, X.-M. Wang, X.-T. Tao, P.-Y. Tang and W.-M. Su, *ChemistrySelect*, 2019, **4**, 2044; (*b*) Z. Gan, M. Meng, Y. Di and S. Huang, *New J. Chem.*, 2016, **40**, 1970.
24 X.-H. Jin, C. Chen, C.-X. Ren, L.-X. Cai and J. Zhang, *Chem. Commun.*, 2014, **50**, 15878.

P-3

Leduskrasts, K.; Sūna, E.
"Aggregation Induced Emission in One Easy Step: Pyridinium AIEgens and Counter Ion Effect."
RSC Adv. **2020**, 10, 38107–38113.
DOI:10.1039/D0RA07137D.

RSC Advances

PAPER

View Article Online
View Journal | View Issue

Cite this: *RSC Adv.*, 2020, **10**, 38107

Aggregation induced emission in one easy step: pyridinium AIEgens and counter ion effect†

Kaspars Leduskrasts and Edgars Suna *

Received 19th August 2020
Accepted 10th October 2020

DOI: 10.1039/d0ra07137d

rsc.li/rsc-advances

Protonation of pyridines with a strong acid is a general and straightforward approach to achieve efficient aggregation induced emission (AIE) in structurally remarkably simple organic molecules that lack any of the conventional luminophores. The relationship between the nature of counter ion and the AIE efficiency is demonstrated. The superiority of the perchlorate counter ion is attributed to efficient stabilization of the key intermolecular $\pi^{+}-\pi$ interactions between neighboring luminophore molecules in the crystal lattice.

A large variety of optoelectronic appliances such as photovoltaic devices,[1] organic light emitting diodes,[2] and organic field-effect transistors[3] as well as a number of light harvesting applications including artificial photosynthesis[4] and photon refining,[5] rely on solid state luminophores. In 2001, Tang introduced a general method to achieve highly efficient solid state luminescence (SSL) in purely organic molecules, generally known as aggregation induced emission (AIE).[6] The vast majority of AIE luminogens (AIEgens) are based on sterically hindered, bulky propeller-like molecular structures to reduce the planarity of luminophore,[7] because the planar architecture is known to be detrimental to the AIE efficiency.[8,7a] In the meantime, the majority of luminophores with high emission intensity in solution feature a planar structure, so an approach that would allow for the design of the solid state luminogens based on the planar architecture of the known solution state emitters is highly desirable.

We have recently demonstrated that the formation of intermolecular interactions between quaternary nitrogen-containing heteroaromatic cations and aromatic π-system in the solid state is a convenient and general approach to achieve AIE and to turn-on high SSL in planar organic molecules.[9] The high SSL has been attributed to intermolecular charge transfer (ICT) between quaternary heteroaromatic subunits such as *N*-methyl pyridinium and *N*-methyl imidazolium cations and aromatic π-systems.[9b] Herein we report on a further development of the conceptual approach to achieve AIE. Specifically, we demonstrate that efficient AIE can be achieved in planar organic luminophores by simple protonation of pyridine with a suitable acid (Fig. 1). Furthermore, our study provides an important insight into the relationship between the nature of counter ion and the AIE efficiency of pyridinium salts.

The relationship between the structure of counter ion and luminescence efficiency has been studied in several pyridinium-containing AIE luminogens.[10] The highest luminescence efficiency was observed for pyridinium salts possessing a counter ion that helped to avoid the detrimental aggregation-induced quenching (ACQ) effect by minimizing intermolecular π–π interactions between planar luminophore molecules (eqn (1) and (3), Fig. 1)[10a,b] or by stabilizing twisted conformation of luminogens (eqn (2), Fig. 2).[10c] In sharp contrast, a completely opposite counter ion effect has been observed in this study. Specifically, counter ions that contributed to strengthening the intermolecular interactions between planar pyridinium luminophores have helped to achieve the highest SSL efficiency (eqn (4), Fig. 1). Perchlorate was found to be superior as the counter-ion, whereas the corresponding mesylate, nitrate as well as halides were inferior. The latter showed apparent negative correlation between the polarizability of the counter ion and SSL emission intensity (Cl > Br > I; see eqn (4), Fig. 1.). The superiority of perchlorate has been rationalized based on X-ray crystallographic analysis as demonstrated below. The striking difference of counter-ion effects in this work (eqn (4)) and in the earlier studies (eqn (1)–(3)) points to an apparent difference in mechanisms that are responsible for the AIE (Fig. 1).

Pyridinium salts **2a,b** were obtained by protonation of commercially available 4-phenylpyridine **1** with aqueous $HClO_4$ and hydrochloric acid, respectively. The protonation of previously reported **3**[9b] with $HClO_4$, HCl, HBr, HI, MsOH and HNO_3 resulted in the formation of pyridinium salts **4a–f** (Fig. 2). All pyridinium salts **2a,b** and **4a–f** were crystalline materials.

UV-vis spectra of all pyridinium salts **2a,b** and **4a–f** and parent heteroaromatic compounds **1** and **3** were measured in MeCN solutions at room temperature under ambient atmosphere at *ca.* 10^{-5} M concentration (see ESI, pages S11–S28†). Pyridine **1** displayed one absorption band at 251 nm (Table 1,

Latvian Institute of Organic Synthesis, Aizkraukles 21, LV-1006, Riga, Latvia. E-mail: edgars@osi.lv

† Electronic supplementary information (ESI) available. CCDC 1988911–1988916. For ESI and crystallographic data in CIF or other electronic format see DOI: 10.1039/d0ra07137d

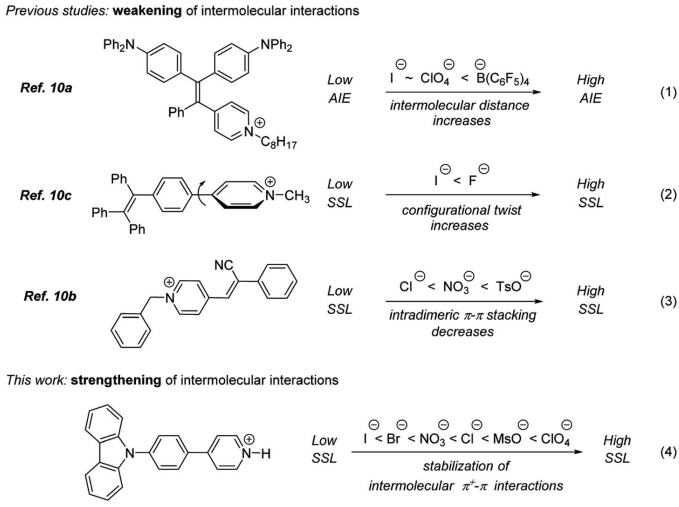

Fig. 1 Effect of counter ions on AIE and SSL.

entry 1). This single absorption band was red-shifted by 40 nm in the corresponding pyridinium salts **2a,b** (Table 1, entries 2 and 3). Pyridine **3** displayed 3 absorption bands at 238, 292 and 322 nm (Table 1, entry 4). The absorption band of pyridine **3** at 238 nm did not change upon protonation, and remained in the range of 236–238 nm for salts **4a–f** (Table 1 entries 7–14). The absorption band of free-base **3** at 292 nm experienced slight hypsochromic shift to 281–288 nm in protonated forms **4a–c,e,f**. However, the largest difference was observed for the absorption band at 322 nm, which featured bathochromic shift of 52–56 nm in salts **4a–c,e,f**. Pyridinium iodide **4d** displayed two absorption bands at 314 and 338 nm (Table 1, entry 12).

Pyridine **1** was not emissive in solution, whereas the corresponding protonated species **2a,b** displayed high emission in MeCN solution at 378 nm with 30.0% and 24.6% photoluminescence quantum yield (PLQY), respectively (Table 1, entries 2 and 3). Pyridine **1** did not display any observable emission also in the solid state. In sharp contrast, pyridinium

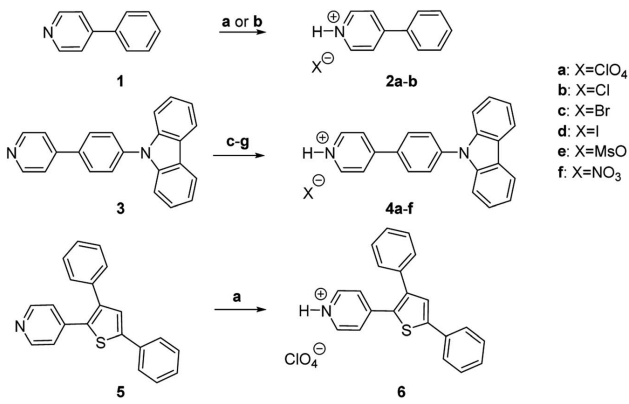

Fig. 2 Synthesis of pyridinium salts **2a**,**b** and **4a**–**f**. Reagents and conditions: (a) aq. $HClO_4$, MeOH or MeCN, rt, 10 min, 83% (**2a**); 99% (**4a**); 32% (**6**). (b) 4 M HCl in dioxane, EtOAc, rt, 10 min, 97% (**2b**). (c) 4 M HCl in dioxane, 1 : 2 CH_2Cl_2 : hexane, rt, 10 min, 93% (**4b**). (d) aq. HBr, MeOH, rt, 10 min, 91% (**4c**). (e) aq. HI, EtOH, rt, 1 h, 61% (**4d**). (f) $MeSO_3H$, MeCN, rt, 10 min, 94% (**4e**). (g) HNO_3, MeCN, rt, 30 min, 99% (**4f**).

Table 1 Photoluminescent properties of luminophores **1–6**

Entry	Compound	Additive	λ_{abs}, nm	Solution λ_{em}, nm	Solid λ_{em}, nm	Solution, φ (%)	Solid, φ (%)
1	**1**	—	251[a]	—	—	<0.1	<0.1
2	**2a**	—	291[a]	378	417	30.0	59.6
3	**2b**	—	291[a]	378	434	24.6	28.5
4	**3**	—	238, 292, 322[a]	442	371, 387, 407	73.1	5.7
5	**3**	$HClO_4$ (500 equiv.)	—	—	n/a	<0.1	n/a
6	**3**	Bu_4NClO_4 (500 equiv.)	—	442	n/a	62.1	n/a
7	**4aA**[b]		237, 281, 377[a]	442[c]	496	n/a	5.5
8	**4aB**[d]	—	237, 281, 377[a]	442[c]	503	n/a	24.1
9	**4aC**[e]		237, 281, 377[a]	442[c]	492	n/a	54.6
10	**4b**	—	238, 288, 374[a]	442[c]	496	n/a	42.4
11	**4c**	—	236, 282, 378[a]	442[c]	514	n/a	18.2
12	**4d**	—	238, 292, 314, 338[a]	442[c]	—	n/a	<0.1
13	**4e**	—	238, 287, 376[a]	442[c]	484	n/a	45.8
14	**4f**	—	237, 288, 377[a]	442[c]	468	n/a	33.4
15	**5**	—	265, 329[a]	416	414	2.1	2.0
16	**6**	—	254, 275, 388[a]	489	524	2.8	17.2

[a] Corresponds to wavelength of excitation. [b] Salt **4a** was obtained by evaporating 10 : 1 MeCN : water solution of **4a** under the reduced pressure at 20 °C. [c] Equilibrium concentration of free base **3** is responsible for the emission in the MeCN solution. [d] A batch of **4a** that was recrystallized from MeCN. [e] Crystalline batch of **4a** obtained by vapor diffusion from Et_2O/MeOH.

salts **2a,b** featured high SSL at 417 and 434 nm respectively. Notably, the solid state PLQY for salts **2a,b** (59.6% and 28.5%, respectively) were higher than those in MeCN solution (Table 1, entries 2 and 3), and this observation highlights AIE enhancement properties of pyridinium salts **2a,b**. Pyridine **3** and its salts **4a–f** displayed identical emission wavelength at 442 nm in MeCN solution, suggesting that the same species might be responsible for the solution-state emission of both **3** and **4a–f**. We hypothesized that the dissociation of salts **4a–f** generates equilibrium concentration of free-base **3** that is responsible for the observed non-structured emission band at 442 nm. To verify this hypothesis, a large excess (500 equiv.) of $HClO_4$ was added to the solution of **3** in MeCN to ensure that all pyridine **3** is protonated. Gratifyingly, a complete quench of the emission was observed for the acidified solution suggesting that protonated pyridines are non-emissive in MeCN solution (Table 1, entry 5). Excess of Bu_4N–ClO_4 (500 equiv.) was also added to a solution of **3** to verify whether perchlorate anion would affect the solution-state emission. Modest drop of the emission efficiency from 73.1 to 62.1% PLQY was observed when excess Bu_4N–ClO_4 (500 equiv.) was added to a solution of **3**, however the emission spectra did not change (Table 1, entry 6). These experiments provide strong evidence that the equilibrium concentration of free base **3** is responsible for the observed solution state emission of pyridinium salts **4a–f**.

Pyridine **3** displayed a structured vibronic emission in the solid state at 371, 387 and 407 nm. The considerable reduction of emission efficiency in the solid state (5.7% PLQY) as compared to that in the solution (73.1% PLQY) points to the aggregation caused quenching (ACQ) properties of luminophore **3** (Table 1, entry 4). The corresponding perchlorate **4a** showed a broad non-structured charge transfer (CT) type[11] solid state emission with maxima spanning the range from 492 to 503 nm (entries 7–9). Notably, efficiency of the SSL of perchlorate **4a** highly depended on crystallinity of the solid material as well as on the properties of crystal lattice. Thus, a batch of perchlorate **4aA** that was obtained by concentrating 10 : 1 MeCN : water solution of **4a** under the reduced pressure at 20 °C showed a relatively low emission efficiency (5.5% PLQY; entry 7). X-Ray powder diffraction (XRPD) spectra of **4aA** featured a distorted baseline, which is indicative of semi-crystalline character of the solid material (see ESI, page S30†). Notably, recrystallization of solid **4a** from MeCN afforded crystalline **4aB** that demonstrated considerably higher emission efficiency (24.1%, entry 8). Furthermore, when crystals of **4a** were grown by vapour diffusion from Et_2O/MeOH, the corresponding material **4aC** featured the highest emission efficiency among all prepared salts of **3** (54.6% PLQY, entry 9). Importantly, XRPD spectra confirmed that **4aB** and **4aC** were different polymorphs (see ESI, page S30–S31†). These data show that the efficiency of SSL depends on the degree of crystallinity and on the properties of crystal lattice. It should be also noted that the solid state emission spectra of all batches **4aA–4aC** were similar.

Pyridinium salts **4b,c,e,f** displayed broad non-structured CT type emission[11a] in the solid state[11b] at 496, 514, 484 and 468 nm (entries 10, 11, 13 and 14, respectively). Pyridinium mesylate **4e** showed the second highest emission efficiency after perchlorate **4aC** (45.8% PLQY; entry 13). Pyridinium chloride **4b**, bromide **4c** and nitrate **4f** were inferior with PLQY of 42.4, 18.2 and 33.4, respectively (entries 10, 11, 14), whereas pyridinium iodide **4d** was completely non-emissive (<0.1% PLQY) in the solid state (entry 12). Notably, our data demonstrates an apparent negative correlation between solid state PLQY and the polarizability of the halide counter ion.[12] It should be also noted, that the lack of solid-state emission for iodide-containing pyridinium salts has been observed previously.[13,9b] Importantly, the highest intensity of SSL has been observed for pyridinium salts **2a** and **4aC** possessing perchlorate counter ion (Table 1).

To demonstrate the scope and generality of the protonation approach as a means to achieve AIE and high SSL, perchlorate salt **6** of a known luminophore **5** (ref. 14) possessing a pyridine core with 3,5-diphenylthiophene substituent was prepared (Fig. 2). Pyridine **5** displayed two absorption bands at 265, 329 nm and perchlorate **6** showed 3 absorption bands at 254, 275 and 388 nm in MeCN solution. A broad non-structured emission at 416 nm was observed for pyridine **5** in the solution. Protonation of **5** resulted in a red-shift of the emission to 489 nm in perchlorate **6**. Pyridine **5** showed low emission efficiency both in solution and in the solid state with PLQY of 2.1% (at 416 nm) and 2.0% (at 414 nm), respectively (Table 1, entries 15 and 16). In sharp contrast, pyridinium perchlorate **6** featured pronounced AIE properties, as evidenced by the increased SSL (17.2% PLQY) as compared to the emission efficiency in the solution (2.8% PLQY). Furthermore, noticeable red-shift of 35 nm was also observed for the solid state emission maxima (524 nm) *vs.* that in the solution (489 nm; entry 14). The observed AIE properties and increased SSL upon the protonation of **5** by perchloric acid has confirmed that the protonation is a general approach to achieve AIE and high SSL in pyridine-containing organic luminophores.

X-ray crystallography provided an important insight into key interactions underlying the observed AIE properties and high SSL for pyridinium luminophores (Table 2). Single crystals of **2a**, **2b**, **4aB**, **4aC**, **4b**, **4f** and **6** suitable for X-ray crystallography were obtained by Et_2O vapour diffusion into the corresponding MeCN and MeOH solutions or by crystallization from MeCN. Importantly, all pyridinium salts **2a**, **2b**, **4aB**, **4aC**, **4b**, **4f** and **6** featured π^+–π interactions between pyridinium cation and aromatic π-system in the crystal lattice (Table 2). For example, pyridinium salt **2a** formed a strictly parallel head-to-tail packing with 3.751 Å distance for the π^+–π interactions of pyridinium subunit with phenyl ring. Likewise, pyridinium salt **2b** formed a near parallel head-to-tail packing with 3.776 and 3.900 Å distances between the pyridinium and phenyl ring centroids (Table 2). Similar head-to-tail packing was also observed for pyridinium salt **4aC**, which feature nearly parallel off-center π^+–π interactions between the charged pyridinium subunit and electron rich carbazole moiety. Furthermore, molecules of **4aC** formed stacked dimers in the crystal lattice, where every molecule was engaged in two distinct π^+–π interactions at 3.618 and 3.655 Å distances between respective carbazole and pyridinium moieties (Table 2). In contrast, the corresponding polymorph **4aB** formed parallel displaced packing with only one intermolecular π^+–π interactions at 4.215 Å distance between the pyridinium ring and the phenylene linker. Similar packing was also observed for pyridinium nitrate **4f** with the corresponding π^+–π interactions at 3.927 Å distance. Chloride **4b** featured 3.535 Å distance for the off-center π^+–π interactions between pyridinium and carbazole subunit, whereas non-parallel off-centered π^+–π interactions between pyridinium heterocycle and phenyl moiety (3.714 Å distance) were observed for pyridinium perchlorate **6** (Table 2).

X-ray crystallography data has also provided an evidence that perchlorate counter ion provides an important stabilization of the key π^+–π interactions between pyridinium subunit and aromatic π system. Thus, the perchlorate forms a hydrogen–bonded bridge between two molecules of **2a** in the crystal lattice as evidenced by the short H-bond contacts spanning a range from 2.495 to 2.694 Å (Table 2). The symmetric nature of these interactions not only helps to stabilize the intermolecular π^+–π interactions, but also ensures the coplanar conformation around the biaryl bond in **2a**. In contrast, the chloride in **2b** is involved in hydrogen bonding with only one pyridinium subunit (2.807 Å bond length), which leads to 22.7° biaryl dihedral angle in **2b**. The bridging effect of perchlorate apparently contributes to the higher crystal lattice energy for **2a** *vs.* **2b**, as evidenced by the considerably higher melting point for **2a** (145 °C) as compared to that for **2b** (74 °C). Notably, perchlorate **2a** featured remarkably high SSL efficiency (59.6% PLQY), whereas chloride **2a** was less efficient (28.5% PLQY; see entry 3 *vs.* 2, Table 1). The propensity of perchlorate ion to form the hydrogen–bonded bridge between two molecules in the crystal lattice has been also observed for luminogens **4aB** (range of contacts from 2.428 to 2.678 Å), **4aC** (2.613–2.635 Å) and **6** (2.391 and 2.602 Å). Among them, the perchlorate-bridged dimer **4aC** possessed the highest SSL efficiency (54.6% PLQY, entry 9, Table 1). The corresponding chloride **4b**, bromide **4c** and mesylate **4e** were less efficient (entries 10, 11, 13 *vs.* 9). Surprisingly, the hydrogen–bonded bridging interactions were not observed for nitrate **4f** (Table 2). The lack of intermolecular stabilization in the crystal lattice has obviously resulted in inferior SSL for **4f** as compared to perchlorate **4aC** (entry 14 *vs.* 9, Table 1). Hence, among all single crystals of pyridinium salts examined, only the perchlorate counter ion contributes to stabilization of the key π^+–π interactions, and this effect results in the higher SSL efficiency for perchlorates as compared to chlorides and bromides. The apparent relationship between the intermolecular π^+–π interactions and SSL has been also demonstrated in previous study for structurally closely related *N*-methyl pyridinium perchlorate,[9b] and TDDFT calculations provided strong evidence that the π^+–π interactions generated through-space CT bands in the crystal state, resulting in SSL.

Additional support for the involvement of through-space CT in the SSL of **2a**, **2b**, **4aB**, **4aC**, **4b**, **4f** and **6** was obtained by a series of control experiments. Thus, the emission of **3** + **HCl**[15] in MeCN solution was measured at 298 K, 190 K and 77 K. At room temperature MeCN solution of **3** + **HCl** featured lack of emission (see also entry 5, Table 1), whereas in a frozen MeCN matrix at 190 K intense emission was observed for **3+HCl** with maxima at 545 nm. Notably, a remarkable blue shift of emission maxima to 452 nm was measured upon further cooling to 77 K (Fig. 3A). The observed pronounced rigidochromic effect is characteristic of CT-type emission due to the polarization flip between ground and excited states.[16] Furthermore, the observed hypsochromic shift also speaks against the possible involvement of excimers in the SSL of the protonated pyridine **3** + **HCl**, because eximer-driven emission typically features a batochromic shift of the emission maxima.[17] An additional evidence against eximer formation was obtained by measuring the emission spectra of protonated pyridine **2a** in MeCN at various concentrations. Pyridinium perchlorate **2a** was chosen due to the relatively high solubility in organic solvents and observable emission in the monomeric state (entry 2, Table 1). The emission maxima for **2a** did not change at

Table 2 X-ray single crystal representations of **2a**, **2b**, **4aB**, **4aC**, **4b**, **4f** and **6**

2a	**2b**
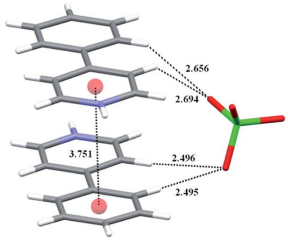	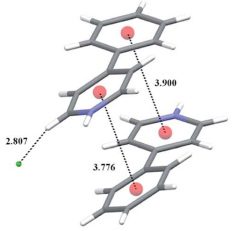
4aB	**4aC**
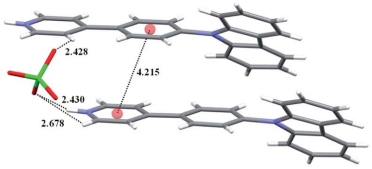	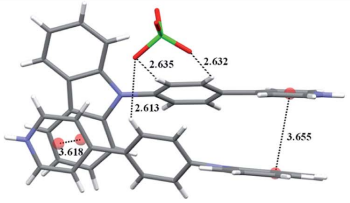
4b	**4f**
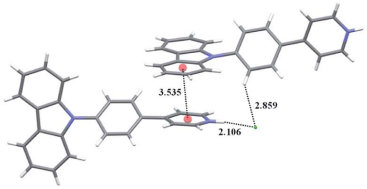	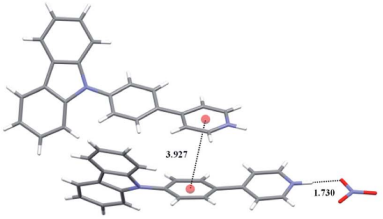
6	
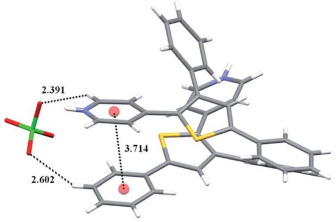	

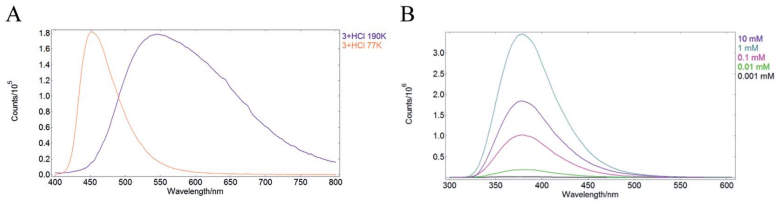

Fig. 3 (A) Solid state emission of **3** + **HCl** in MeCN at 190 K (purple) and 77 K (pale red); (B) emission spectra of **2a** in MeCN solution at various concentrations.

concentrations in the range from 0.001 mM to 10 mM indicating that excimer formation is not responsible for the luminescence of **2a** (Fig. 3B).

In summary, this study demonstrates a straightforward and versatile approach to achieve efficient AIE in structurally diverse purely organic luminogens. The developed method relies on a simple protonation of pyridine derivatives by a strong acid to generate pyridinium cation for the key non-covalent π^{+}–π interactions with aromatic π-system that leads to high SSL through the intermolecular charge transfer (ICT) mechanism.[9b] Hence, the protonation of pyridines is a highly straightforward and complementary approach to the previously developed *N*-alkylation/ion exchange sequence as a means of achieving the SSL. High solid state emission efficiency (up to 60% PLQY) has been attained by the protonation of structurally remarkably simple organic molecules such as 4-phenyl pyridine that lacks any of the conventional luminophores. The versatility of the protonation approach is demonstrated in three structurally distinct series of pyridine-containing luminogens with both planar and twisted architectures. The solid state emission efficiency depends strongly on the degree of crystallinity of the solid luminogens as well as on the structure of the pyridinium counter ion. Perchlorate as the counter ion was superior in terms of SSL efficiency as compared to chloride, bromide, mesylate and nitrate whereas iodide affected complete luminescence quench. X-Ray crystallographic analysis provided evidence that perchlorate counter-ion can increase AIE effect by (a) forming a H-bonded bridge between the neighbouring luminophore molecules in the crystal lattice, thus providing an additional stabilization of the key intermolecular π^{+}–π interactions, (b) enabling H-bond assisted planarization of the luminophore molecule. Hence, these insights together with control experiments provide an evidence against the RIM AIE mechanism as well as excimer formation in protonated pyridine luminophores. We believe that the remarkable operational simplicity of the protonation as a general approach to achieve high SSL and the elucidation of counter-ion effect will provide ample opportunities for the rational design and development of solid state emitters.

Conflicts of interest

There are no conflicts to declare.

Acknowledgements

This work was funded by ERDF (project no. 1.1.1.1/18/A/063 "Next Generation Aggregation Induced Emission Luminogens for Artificial Lighting Sources"). We thank Dr S. Belyakov for X-ray crystallographic and XRPD analysis.

References

1 (*a*) B. Mi, Y. Dong, Z. Li, J. W. Y. Lam, M. Haussler, H. H. Sung, H. S. Kwok, Y. Dong, I. D. Williams, Y. Liu, Y. Luo, Z. Shuai, D. Zhu and B. Z. Tang, *Chem. Commun.*, 2005, 3583–3585; (*b*) Y. Li, Z. Li, Y. Wang, A. Compaan, T. Ren and W.-J. Dong, *Energy Environ. Sci.*, 2013, **6**, 2907–2911.

2 (*a*) Z. Ning, Z. Chen, Q. Zhang, Y. Yan, S. Qian, Y. Cao and H. Tian, *Adv. Funct. Mater.*, 2007, **17**, 3799–3807; (*b*) W. Qin, Z. Yang, Y. Jiang, J. W. Y. Lam, G. Liang, H. S. Kwok and B. Z. Tang, *Chem. Mater.*, 2015, **27**, 3892–3901; (*c*) J. Huang, N. Sun, Y. Dong, R. Tang, P. Lu, P. Cai, Q. Li, D. Ma, J. Qin and Z. Li, *Adv. Funct. Mater.*, 2013, **23**, 2329–2337; (*d*) J. N. Moorthy, P. Venkatakrishnan, P. Natarajan, Z. H. Lin and T. J. J. Chow, *J. Org. Chem.*, 2010, **75**, 2599–2609; (*e*) J. Huang, N. Sun, J. Yang, R. Tang, Q. Li, D. Ma and Z. Li, *Adv. Funct. Mater.*, 2014, **24**, 7645–7654.

3 (*a*) S. G. Surya, H. N. Raval, R. Ahmad, P. Sonar, K. N. Salama and V. R. Rao, *TrAC, Trends Anal. Chem.*, 2019, **111**, 27–36; (*b*) Z. Zhao, Z. Li, J. W. Y. Lam, J.-L. Maldonado, G. Ramos-Ortiz, Y. Liu, W. Yuan, J. Xu, Q. Miao and B. Z. Tang, *Chem. Commun.*, 2011, **47**, 6924–6926; (*c*) M. P. Aldred, G.-F. Zhang, C. Li, G. Chen, T. Chen and M.-Q. Zhu, *J. Mater. Chem. C*, 2013, **1**, 6709–6718.

4 (*a*) M. Zhang, X. Yin, T. Tian, Y. Liang, W. Li, Y. Lan, J. Li, M. Zhou, Y. Ju and G. Li, *Chem. Commun.*, 2015, **51**, 10210–10213; (*b*) Y. Zeng, P. Li, X. Liu, T. Yu, J. Chen, G. Yang and Y. Li, *Polym. Chem.*, 2014, **5**, 5978–5984; (*c*) F. Qiao, L. Zhang, Z. Lian, Z. Yuan, C.-Y. Yan, S. Zhuo, Z.-Y. Zhou and L.-B. Xing, *J. Photochem. Photobiol., A*, 2018, **355**, 419–424.

5 (*a*) P. Duan, D. Asthana, T. Nakashima, T. Kawai, N. Yanai and N. Kimizuka, *Faraday Discuss.*, 2017, **196**, 305–316; (*b*)

L. Li, Y. Zeng, T. Yu, J. Chen, G. Yang and Y. Li, *ChemSusChem*, 2017, **10**, 4610–4615.

6 J. Luo, Z. Xie, J. W. Y. Lam, L. Cheng, H. Chen, C. Qiu, H. S. Kwok, X. Zhan, Y. Liu, D. Zhu and B. Z. Tang, *Chem. Commun.*, 2001, 1740.

7 (*a*) Y. Tang and B. Z. Tang, *Principles and Applications of Aggregation-Induced Emission*, Springer International Publishing, New York, 2019; (*b*) J. Mei, N. L. C. Leung, R. T. K. Kwok, J. W. Y. Lam and B. Z. Tang, *Chem. Rev.*, 2015, **115**, 11718.

8 (*a*) T. Forster and K. Z. Kasper, *J. Phys. Chem.*, 1954, **1**, 275; (*b*) J. B. Birks, *Photophysics of aromatic molecules*, Wiley-Interscience, London, 1970.

9 (*a*) K. Leduskrasts and E. Suna, *RSC Adv.*, 2019, **9**, 460–465; (*b*) K. Leduskrasts, A. Kinens and E. Suna, *Chem. Commun.*, 2019, **55**, 12663–12666.

10 (*a*) N. Adarsh and A. S. Klymchenko, *Nanoscale*, 2019, **11**, 13977–13987; (*b*) G. Zhang, X. Zhang, L. Kong, S. Wang, Y. Tian, X. Tao and J. Yang, *Sci. Rep.*, 2016, **6**, 37609; (*c*) M. Bineci, M. Bağlan and S. Atılgan, *Sens. Actuators, B*, 2016, **222**, 315–319.

11 (*a*) X. Wang, S. Wang, J. Lv, S. Shao, L. Wang, X. Jing and F. Wang, *Chem. Sci.*, 2019, **10**, 2915–2923; (*b*) X.-H. Jin, C. Chen, C.-X. Ren, L.-X. Cai and J. Zhang, *Chem. Commun.*, 2014, 15878.

12 E. V. Anslyn and D. A. Dougherty, *Modern physical chemistry,* University Science, Sausalito, CA, 2004.

13 I. Richter, M. R. Warren, J. Minari, S. A. Elfeky, W. Chen, M. F. Mahon, P. R. Raithby, T. D. James, K. Sakurai, S. J. Teat, S. D. Bull and J. S. Fossey, *Chem.–Asian J.*, 2009, **4**, 194–198.

14 I. Karpaviciene, M. Jonusis, K. Leduskrasts, I. Misiunaite, E. Suna and I. Cikotiene, *Dyes Pigm.*, 2019, **170**, 107646.

15 Anhydrous HCl in dioxane (20 equiv.) was added to a solution of 3 in MeCN (*ca.* 10^{-5} mol L^{-1}).

16 A. J. Lees, *Comments Inorg. Chem.*, 1995, **17**, 319–346.

17 The formation of eximers was proposed to be responsible for the observed AIE effect in certain planar protonated pyridinium salts based on the large batochromic shift (50 nm) of the emission in thin films as compared to that in solution: X. Cui, Y. Hao, W. Guan, L. Liu, W. Shi and C. Lu, *Adv. Opt. Mater.*, 2020, 2000125.

P-4

Leduskrasts, K.; Sūna, E.
"Intermolecular Charge-Transfer Luminescence by Self-Assembly of Pyridinium Luminophores in Solutions"
ChemistryOpen, **2021**, 10, 1081–1086.
DOI:10.1002/open.202100191.

Intermolecular Charge-Transfer Luminescence by Self-Assembly of Pyridinium Luminophores in Solutions

Kaspars Leduskrasts and Edgars Suna*[a]

Designing a luminophore for application both in solution and in the solid state is a highly challenging task given the distinct nature of intermolecular interactions in these phases. In this context, we demonstrate that self-assembly of non-emissive charged pyridinium luminophores enables luminescence in solutions through a mechanism that is characteristic for the crystal state. Specifically, protonation of pyridine luminophore subunits in a solution promotes oligomer formation through intermolecular π^{+}-π interactions, leading to an intermolecular charge-transfer type luminescence. The luminescence turn-on by protonation is utilized for a highly efficient solution-state luminescent sensing of hydrogen chloride and sulfonic acids (TfOH, TsOH and MsOH) with detection limits spanning the range from 0.06 to 0.33 ppm. The protonation followed by self-assembly results in a bathochromic shift of the emission from 420 nm to 550 nm.

1. Introduction

A wide range of sensing applications in solutions as well as modern solid state lighting devices is based on light-emitting molecules (luminophores).[1] The vast majority of luminophores feature distinct luminescence mechanisms in solution and in the crystal state.[2a,b] This distinction has been a focus of considerable research efforts during the last two decades.[2] In the crystal state, numerous static intermolecular interactions,[3] such as H-bonds,[4] halogen bonds,[4b,5] π-π interactions,[6] cation-π stacking[7] and electrostatic interactions,[8] greatly impact the luminescence emission pathways, resulting in aggregated luminophore mechanisms (Figure 1). In sharp contrast, the intermolecular interactions in solution are highly dynamic and significantly weakened due to Brownian motion.[9] The weakened intermolecular interactions in solution lead to an emission by isolated luminophore mechanisms. Apparently, the distinct nature of intermolecular interactions in solution and in the crystal state is responsible for the different luminescence mechanisms.

A rare example of a luminescence mechanism that does not differ between the phases is associated with luminophores that exert luminescence through the excited dimer (excimer) mechanism (Figure 1).[10] Excimer emission relies on the formation of a meta-stable excited dimer, which upon emission dissociates into its parent luminophores.[10a,c,e] The excimer emission of purely organic luminophores in the crystal state is promoted by intermolecular π orbital overlap.[10b] A similar π orbital overlap is also achievable in solutions, provided that high enough concentration of the luminophore can be obtained,[11] resulting in excimer-type emission. Unfortunately, the excimer emission cannot be maintained in diluted solutions due to the low collision likelihood between luminophores. Accordingly, achieving intermolecular interactions that are persistent in both the solid and the solution state would open a path to obtain exceptional luminophores with consistent luminescent mechanisms between the phases.

Recently, we have demonstrated that enhanced solid-state emission can be achieved by simple protonation of highly planar conjugated pyridines.[12] The mechanism of the solid-

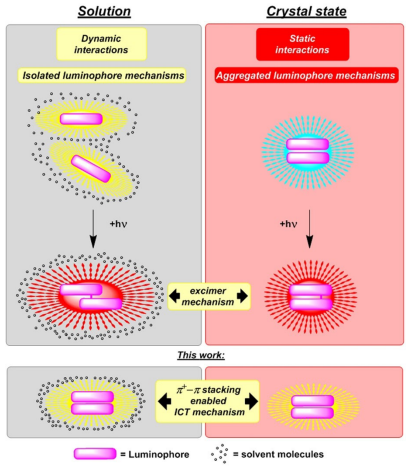

Figure 1. Luminescent properties in solution and in the crystal state.

[a] K. Leduskrasts, Prof. Dr. E. Suna
Latvian Institute of Organic Synthesis
Aizkraukles 21
1006 Riga (Latvia)
E-mail: edgars@osi.lv

Supporting information for this article is available on the WWW under https://doi.org/10.1002/open.202100191

state luminescence involved intermolecular π^+-π and π^+-π^+ interactions.[13] We envisioned that the protonation of planar conjugated pyridine subunits could lead to enhanced emission also in solution, provided that the solvent does not interfere with the key intermolecular π^+-π and π^+-π^+ interactions.[7,14] Herein, we disclose that protonation of pyridine-containing luminophores in diluted solutions of toluene, Et_2O, $CHCl_3$ and EtOAc effects the desired intermolecular π^+-π interactions by self-assembly of the protonated species. The self-assembly in solution leads to emission turn-on through intermolecular charge-transfer (ICT) type luminescence mechanism (Figure 1). Hence, the key intermolecular π^+-π interactions are well-suited for the design of versatile luminogens that exert luminescence both in solution and in the solid state through similar emission mechanisms. The application of the pyridine-containing luminogens for the detection of hydrogen chloride and sulfonic acid in solutions with sensing limits well below 1 ppm is also reported.

2. Results and Discussion

2.1. Spectral Characterization of 3 and 3×HCl in Various Solvents

Pyridine **3** was synthesized from 9-(4-bromophenyl)-9H-carbazole **1** and pyridine-4-boronic acid hydrate **2** (Supporting Information, page S3) by a previously reported protocol.[13a] The UV-Vis absorption and emission spectra of pyridine **3** were recorded in DMF, DMSO, EtOAc, toluene, $CHCl_3$ and Et_2O solutions at room temperature and under ambient atmosphere. The concentration of samples was 10^{-5} M. Pyridine **3** displayed three distinct absorption maxima at 242–262 nm, 290–294 nm and 320–329 nm, respectively, in DMSO, EtOAc, $CHCl_3$ and Et_2O. The absorption maxima could not be measured in the 240–280 nm region for toluene and in the 240–260 nm region for DMF due to the competing absorption by these solvents (Supporting Information, page S5). Additionally, the broad featureless emission maxima of **3** underwent a bathochromic shift from 380 nm in toluene to 443 nm in DMSO (Figure 2A). Next, the UV-Vis absorption and emission spectra of pyridine **3×HCl**[15] were recorded in DMF, DMSO, EtOAc, toluene, $CHCl_3$ and Et_2O solutions. Accordingly, **3×HCl** displayed absorption peaks at 239–263 nm, 278–287 nm and 367–397 nm in DMSO, EtOAc, $CHCl_3$ and Et_2O. The absorption in DMF and toluene could not be measured up to 260 nm and 275 nm, respectively, due to the intrinsic solvent absorption (Supporting Information, page S5). Significant red-shifts were observed for the absorption peaks in all examined solvents upon the protonation of pyridine **3** by hydrogen chloride. For example, a 53 nm bathochromic shift of the absorption peak from 319 nm to 372 nm was measured in Et_2O for **3** in the presence of HCl (Figure 2B).

Notably, lack of emission was observed for pyridine salt **3×HCl** in highly polar solvents such as DMF and DMSO. This observation is in agreement with the previously reported poor luminescence of **3×HCl** in MeCN solution.[12] To gain insight into the origins of the observed emission lack in polar solvents, the luminescence of **3×HCl** in DMSO was compared at room

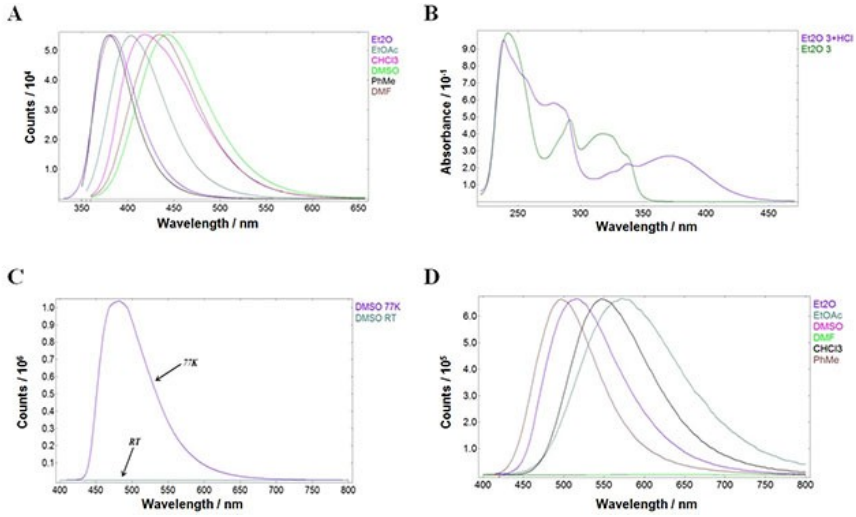

Figure 2. [A] Emission of **3** in various solvents; [B] Absorbtion of **3** and **3×HCl** in Et_2O; [C] Emission of **3×HCl** in DMSO at room temperature and 77 K; [D] Emission of **3×HCl** in various solvents.

temperature to that at 77 K. In sharp contrast to the lack of emission at room temperature, intense luminescence at 483 nm was observed in a frozen DMSO matrix upon cooling **3×HCl** to 77 K (Figure 2C). Importantly, the emission at 77 K displayed a clear afterglow that was observable even with the naked eye. The measured lifetime value for the emission ($\tau = 1.51$ s; Supporting Information, page S6) suggests that long-lived triplet states are responsible for the luminescence at 77 K. The strength of the emission intensity at 77 K is associated with the high triplet state population, apparently because of the highly efficient and rapid intersystem crossing in **3×HCl**. Hence, the lack of emission in DMSO solution at room temperature can be most likely attributed to the non-radiative relaxation of the highly solvated **3×HCl** through molecular motion.

In contrast to the non-luminescent properties of **3×HCl** in highly polar solvents such as DMSO and DMF, an intense emission was observed for **3×HCl** at room temperature in less polar solvents. Specifically, an intense, broad and featureless emission with a strong solvatochromic effect was observed in toluene (emission maximum at 497 nm), Et_2O (at 516 nm), $CHCl_3$ (at 548 nm) and EtOAc (at 574 nm; Figure 2D). The observed distinct luminescence behavior of **3×HCl** in high- and low-polarity solvents could be attributed to their different solvating ability. Thus, the polar solvents (DMSO, DMF) of high solvating ability stabilize monomers of **3×HCl**. The lack of the emission for **3×HCl** in DMSO and DMF at room temperature suggests that monomeric species of **3×HCl** are non-emissive. In contrast, solvents of a lesser solvating ability, such as EtOAc, $CHCl_3$, Et_2O and toluene, should favor the formation of intermolecular interactions between **3×HCl**. We hypothesized that the observed room temperature emission of **3×HCl** in EtOAc, $CHCl_3$, Et_2O and toluene may be attributed to the formation of aggregates. Dynamic light scattering (DLS) measurements were employed to verify whether aggregates are responsible for the observed emission. However, DLS measurements did not support the presence of higher aggregates in the luminescent solutions of **3×HCl**. Since smaller oligomers such as dimers or trimers fall below the detection limits of DLS, additional experiments were required to verify the possible involvement of small oligomers in the emission of **3×HCl**.

2.2. T_1 NMR Experiments

Strong evidence supporting the presence of small oligomers (dimers or trimers) in $CHCl_3$ solutions of **3×HCl** was obtained by longitudinal relaxation time (T_1) nuclear magnetic resonance (NMR) experiments. In the experiment, a decrease in spin lattice relaxation time (T_1) is observed for those molecules that feature intermolecular interactions, because the resulting aggregated species possess larger size and stronger inertia moments.[9] Accordingly, the spin lattice relaxation time (T_1) was measured for **3×HCl** in DMSO-d_6 and $CDCl_3$ solutions (Supporting Information, page S6). For a better representation of changes in T_1 relaxation times in the two solvents, the measured T_1 values in DMSO-d_6 were divided by the respective T_1 values in $CDCl_3$ for each of positions 1–8 in the luminophore molecule **3×HCl** (for the numbering, see Figure 3A). Notably, a significant drop (from 4 to 39 times) of T_1 values was observed for protons in positions 1–4 in $CDCl_3$ solution as compared to those in DMSO-d_6 as the solvent. In contrast, smaller (less than 2 times) differences in T_1 values in the two solvents were measured for

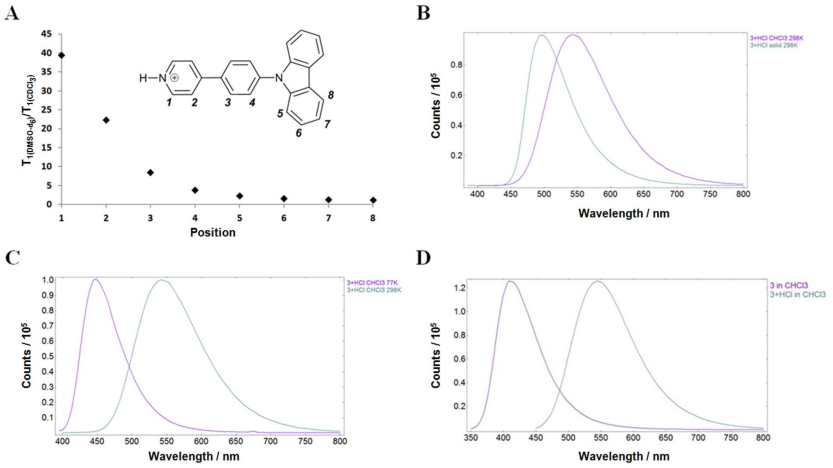

Figure 3. [A] Relative change of T_1 relaxation times at positions 1–8 of **3×HCl** in DMSO-d_6 and $CDCl_3$ solutions; [B] Emission of **3×HCl** in solid state and solution; [C] Emission of **3×HCl** in $CHCl_3$ at 298 K and 77 K; [D] Emission spectra of **3** in $CHCl_3$ before (left), after (right) addition of HCl;

positions 5–8. These results provide strong evidence for the presence of intermolecular interactions between protonated pyridine species **3×HCl** in $CDCl_3$ solution. Furthermore, only the pyridinium subunit and the phenylene linker appear subjected to these intermolecular interactions. In contrast, the carbazole moiety is not involved as evidenced by the NMR experiments. Hence, the spin lattice relaxation time measurements suggest that the observed luminescence in $CHCl_3$, EtOAc, Et_2O and toluene is a result of intermolecular pyridinium-pyridinium π^+-π interactions of protonated luminogen **3×HCl** in solution.[12,13]

2.3. Charge-Transfer Emission

Additional indirect support for the formation of intermolecular pyridinium-pyridinium π^+-π interactions in $CHCl_3$ solution of protonated luminogen **3×HCl** was provided by the comparison of its luminescent properties in the solid state with those in the solution. It has been demonstrated earlier that the observed broad featureless emission of pyridinium salts such as **3×HCl** in the solid state is indicative of intermolecular π^+-π charge-transfer (ICT) mechanism for the luminescence.[12,13,16] Importantly, featureless emission for **3×HCl** was also observed in $CHCl_3$ solution. Furthermore, a red-shift of emission maximum from 496 nm in the solid state to 548 nm in the $CHCl_3$ solution was measured (Figure 3B). In the meantime, cooling the $CHCl_3$ solution of **3×HCl** from 293 K to 77 K resulted in a blue-shift from 548 nm to 448 nm, respectively (Figure 3C). The apparent dependence of the luminescence maximum on the rigidity of molecular environment (rigidochromism) points to the ICT mechanism for **3×HCl** due to a polarization flip between ground and excited states.[17] The observed blue-shift for **3×HCl** is associated with the reduced degree of stabilization of the luminophore excited state by solvent molecules in a frozen matrix at 77 K. An additional evidence for the CT emission for **3×HCl** was also obtained from the observed strong solvatochromic effect between PhMe, $CHCl_3$, EtOAc and Et_2O (Figure 2D).[18] Finally, the observed emission for **3×HCl** in weakly coordinating solvents at concentrations as low as 10^{-7} M helped to rule out the excimer-type emission that usually requires much higher concentrations, typically around 10^{-3} M.[11b] Hence, the luminescence data provide strong support for the ICT emission mechanism enabled by π^+-π interactions between the protonated species of **3×HCl** in relatively non-polar solvents such as $CHCl_3$, EtOAc, Et_2O and PhMe.

2.4. Sensing of HCl

The observed bathochromic shift of the emission maximum from 418 nm for **3** to 548 nm for **3×HCl** (Figure 3D) in the presence of hydrogen chloride is a result of a two-step process: 1) protonation of the pyridine luminophore resulting in a non-emissive monomer, and 2) the formation of oligomers through π^+-π interactions, which leads to the intermolecular CT emission. We realized that such an emission mechanism is well-suited for the design of luminescent sensors. The luminescence response and emission properties of **3** in $CHCl_3$ were examined in the presence of HCl vapours (see Figure 4 and Videos S1 and S2 in the Supporting Information). Gratifyingly, a distinct emission change from colourless to pale green was observed under ambient light after the $CHCl_3$ solution of **3** was subjected to hydrogen chloride vapours. The colour change was more pronounced when observed under UV light (365 nm). Accordingly, the $CHCl_3$ solution of **3** emits violet light, and a change to green emission occurred upon exposure to HCl vapours (Figure 4; see also Supporting Information, page S17). A similar sensory response was observed for MsOH, TsOH, TfOH and TFA by pyridine-derived luminogen **3** (Supporting Information, pages S7–S9). Hence, the solution of **3** demonstrates a response to the presence of various strong acids. The sensory response time towards acids is as fast as the diffusion of the acid within the solution (Video 2 in Supporting Information).

2.5. Determining the Limit of Detection (LoD)

A statistical approach was used at the 95% confidence level to determine the limit of detection (LoD) for HCl, MsOH, TsOH, TfOH and TFA by pyridine-derived luminogen **3**. Assuming that the Gaussian distribution holds true,[19] the LoD was determined from the linear range of the calibration plot (Eq. (1); see also Supporting Information pages S9–S16).

$$LoD = \frac{m_{blank} + 3.29 \times \sigma_{(blank)}}{b} \quad (1)$$

where $m_{(blank)}$ = the mean value of blank measurements; $\sigma_{(blank)}$ = standard deviation of blank measurements; b = the slope of the linear equation.

The linear range of the calibration plot was obtained by conducting additional measurements for each of the acids (Supporting Information, pages S10–S15). The obtained $\sigma_{(blank)}$ was in the range from 23–33 counts per second (Supporting Information, pages S9–S10). Accordingly, the calculated LoD for the tested acids decrease in the following order (Supporting Information, pages S15–S16): MsOH (0.06 ppm) > TfOH (0.13 ppm) > TsOH (0.19 ppm) > HCl (0.33 ppm) > TFA (8.1 ppm)

The determined detection limits for sulfonic acids (TfOH, TsOH and MsOH) were similar to that for hydrochloric acid,

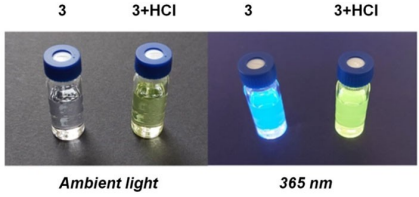

Figure 4. $CHCl_3$ solution of **3** before and after exposure to HCl vapours at ambient light and at 365 nm excitation.

falling within the range from 0.06 ppm to 0.33 ppm. However, luminophore **3** was less sensitive (by two orders of magnitude) towards TFA (8.1 ppm). Notably, the detection limit for acids correlated well with their equilibrium acidity values. Thus, luminophore **3** demonstrated highest sensitivity towards strong acids such as hydrogen chloride ($pK_{a,MeCN} = 10.3$),[20] MsOH ($pK_{a,MeCN} = 9.97$),[20] TsOH ($pK_{a,MeCN} = 8.45$)[21] and TfOH ($pK_{a,\ MeCN} = 2.6$).[21] In contrast, **3** featured reduced sensitivity towards TFA ($pK_{a,MeCN} = 12.65$),[21] which is the weakest among all tested acids. The observed correlation between the equilibrium acidity values and the LoD is consistent with the proposed sensing mechanism that relies on the protonation of the pyridine subunit in luminophore **3**, leading to intermolecular pyridinium-pyridinium π^+-π interactions of **3**×**HCl**. Notably, the pyridine **3**-derived hydrogen chloride sensor features considerably higher (more than two orders of magnitude) sensitivity when compared to that of most potent Schiff-base sensors (54 ppm).[22]

3. Conclusion

Intermolecular charge transfer type (ICT) emission in solution can be achieved by self-assembly of individually non-emissive pyridinium-containing luminophores. Spin-lattice relaxation (T_1) time NMR experiments in $CDCl_3$ solution provided strong evidence for the self-assembly and oligomer formation through intermolecular π^+-π interactions. The proposed ICT mechanism for the luminescence is consistent with the non-emissive nature of the pyridinium luminophore in polar solvents such as DMSO and DMF, where the highly solvated monomeric luminophore undergoes non-radiative relaxation through molecular motions. Additional support for the ICT mechanism was also obtained from the observed solvatochromism and emission dependence on the rigidity of molecular environment. Importantly, the intermolecular interactions of non-excited pyridine luminophores that are observable by NMR methods together with the emission in highly diluted (as low as 10^{-7} M) solutions speak against the excimer emission mechanism. The ICT luminescence in solutions allows for the use of easy-to-synthesise, robust and inexpensive planar pyridine-derived luminophore 3 as a sensor for the detection of hydrogen chloride as well as other relatively strong acids such as sulfonic acids (TfOH, TsOH and MsOH) with sensing limits (LoD) spanning the range from 0.06 ppm to 0.33 ppm. Less acidic carboxylic acids such as TFA could be also determined, however with reduced sensitivity (8.1 ppm LoD). The exposure of solutions of luminophore 3 in EtOAc, toluene, $CHCl_3$ or Et_2O to HCl gas and organic acids brings about a rapid emission increase at 550 nm. The importance of the pyridinium salt formation for the luminescent response is corroborated by the observed correlation between LoD and the thermodynamic acidity (pK_a) values for various acids. Overall, the use of intermolecular π^+-π CT type interactions in solutions opens ample opportunities for the rational design of luminescent materials and sensors.

Acknowledgements

This work was funded by ERDF (project No. 1.1.1.1/18/A/063 "Next Generation Aggregation Induced Emission Luminogens for Artificial Lighting Sources"). We thank Prof. Dr. K. Jaudzems for assistance with NMR experiments.

Conflict of Interest

The authors declare no conflict of interest.

Keywords: aggregation-induced emission · intermolecular interactions · luminescent property transfer · self-assembly · sensors

[1] a) Y. Zhou, J. Yoon, *Chem. Soc. Rev.* **2012**, *41*, 52; b) Y. Liu, C. Li, Z. Ren, S. Yan, M. R. Bryce, *Nat. Rev. Mater.* **2018**, *3*, 18020; c) S. Kanagaraj, A. Puthanveedu, Y. Choe, *Adv. Funct. Mater.* **2019**, *30*, 1907126; d) S. Chowdhury, B. Rooj, A. Dutta, U. Mandal, *J. Fluoresc.* **2018**, *28*, 999.
[2] For representative reviews, see: a) S. Mukherjee, P. Thilagar, *Chem. Commun.* **2015**, *51*, 10988; b) Kenry, C. Chen, B. Liu, *Nat. Commun.* **2019**, *10*, 1; c) J. Mei, N. L. Leung, R. T. Kwok, J. W. Lam, B. Z. Tang, *Chem. Rev.* **2015**, *115*, 11718; d) Z. Zhao, H. Zhang, J. W. Lam, B. Z. Tang, *Angew. Chem. Int. Ed.* **2020**, *59*, 9888; e) J. Yang, M. Fang, Z. Li, *InfoMat* **2020**, *2*, 791; f) W. Jia, Q. Wang, H. Shi, Z. An, W. Huang, *Chem. Eur. J.* **2020**, *26*, 4437; g) A. D. Nidhankar, Goudappagouda, V. C. Wakchaure, S. S. Babu, *Chem. Sci.* **2021**, *12*, 4216; h) J. Mei, Y. Hong, J. W. Lam, A. Qin, Y. Tang, B. Z. Tang, *Adv. Mater.* **2014**, *26*, 5429.
[3] J.-P. Zhang, P.-Q. Liao, H.-L. Zhou, R.-B. Lin, X.-M. Chen, *Chem. Soc. Rev.* **2014**, *43*, 5789.
[4] a) T. Zhang, H. Gao, A. Lv, Z. Wang, Y. Gong, D. Ding, H. Ma, Y. Zhang, W. Z. Yuan, *J. Mater. Chem. C* **2019**, *7*, 9095; b) L. Xiao, H. Fu, *Chem. Eur. J.* **2018**, *25*, 714.
[5] W. Wang, Y. Zhang, W. J. Jin, *Coord. Chem. Rev.* **2020**, *404*, 213107.
[6] a) A. S. Klymchenko, *Acc. Chem. Res.* **2017**, *50*, 366; b) S. A. Jenekhe, J. A. Osaheni, *Science* **1994**, *265*, 765.
[7] S. Yamada, *Coord. Chem. Rev.* **2020**, *415*, 213301.
[8] a) B. A. Naqvi, M. Schmid, E. Crovini, P. Sahay, T. Naujoks, F. Rodella, Z. Zhang, P. Strohriegl, S. Bräse, E. Zysman-Colman, W. Brütting, *Front. Chem.* **2020**, *8*, 750; b) J. Wang, X. Gu, P. Zhang, X. Huang, X. Zheng, M. Chen, H. Feng, R. T. Kwok, J. W. Lam, B. Z. Tang, *J. Am. Chem. Soc.* **2017**, *139*, 16974.
[9] V. I. Bakhmutov, *Practical NMR relaxation for chemists*, Wiley, Chichester, West Sussex, England, **2004**.
[10] a) V. Tkachenko, *Optical Spectroscopy: Methods and Instrumentations*, Elsevier, **2006**; b) Y. Ge, Y. Wen, H. Liu, T. Lu, Y. Yu, X. Zhang, B. Li, S.-T. Zhang, W. Li, B. Yang, *J. Mater. Chem. C* **2020**, *8*, 11830; c) J. B. Birks, *Rep. Prog. Phys.* **1975**, *38*, 903; d) G. W. Gokel, L. J. Barbour, *Comprehensive Supramolecular Chemistry II*, Elsevier, Amsterdam, Netherlands, **2017**; e) J. C. Lindon, G. E. Tranter, D. W. Koppenaal, *Encyclopedia of Spectroscopy and Spectrometry*, Academic Press, Amsterdam, **2017**.
[11] a) R. Katoh, K. Suzuki, A. Furube, M. Kotani, K. Tokumaru, *J. Phys. Chem. C* **2009**, *113*, 2961; b) P. C. Johnson, H. W. Offen, *J. Chem. Phys.* **1973**, *59*, 801.
[12] K. Leduskrasts, E. Suna, *RSC Adv.* **2020**, *10*, 38107.
[13] a) K. Leduskrasts, A. Kinens, E. Suna, *Chem. Commun.* **2019**, *55*, 12663; b) K. Leduskrasts, E. Suna, *RSC Adv.* **2019**, *9*, 460.
[14] a) I. Richter, J. Minari, P. Axe, J. P. Lowe, T. D. James, K. Sakurai, S. D. Bull, J. S. Fossey, *Chem. Commun.* **2008**, 1082; b) W. Chen, S. A. Elfeky, Y. Nonne, L. Male, K. Ahmed, C. Amiable, P. Axe, S. Yamada, T. D. James, S. D. Bull, J. S. Fossey, *Chem. Commun.* **2011**, *47*, 253; c) Y.-J. Huang, Y.-B. Jiang, S. D. Bull, J. S. Fossey, T. D. James, *Chem. Commun.* **2010**, *46*, 8180; d) Excimer emission mechanism through intermolecular π^+-π interactions has also been proposed in certain pyridinium salts in the solid state: X. Cui, Y. Hao, W. Guan, L. Liu, W. Shi, C. Lu, *Adv. Opt. Mater.* **2020**, *8*, 2000125.
[15] 50 equiv. of HCl were added to the solution of **3** in various solvents.

[16] a) S. Sasaki, G. P. Drummen, G.-I. Konishi, *J. Mater. Chem. C* **2016**, *4*, 2731; b) F. B. Dias, S. Pollock, G. Hedley, L.-O. Pålsson, A. Monkman, I. I. Perepichka, I. F. Perepichka, M. Tavasli, M. R. Bryce, *J. Phys. Chem. B* **2006**, *110*, 19329; c) A. Petrozza, F. Laquai, I. A. Howard, J.-S. Kim, R. H. Friend, *Phys. Rev. B* **2010**, *81*, 205421.
[17] A. J. Lees, *Comments Inorg. Chem.* **1995**, *17*, 319.
[18] a) B. Carlotti, R. Flamini, I. Kikaš, U. Mazzucato, A. Spalletti, *Chem. Phys.* **2012**, *407*, 9; b) V. Martínez-Martínez, J. Lim, J. Bañuelos, I. López-Arbeloa, O. Š. Miljanić, *Phys. Chem. Chem. Phys.* **2013**, *15*, 18023; c) E. Sucre-Rosales, R. Fernández-Terán, N. Urdaneta, F. E. Hernández, L. Echevarria, *Chem. Phys.* **2020**, *537*, 110854.
[19] D. A. Armbruster, T. Pry, *Clin. Biochem. Rev.* **2008**, *29*, (Suppl 1) S49.
[20] A. Kütt, T. Rodima, J. Saame, E. Raamat, V. Mäemets, I. Kaljurand, I. A. Koppel, R. Y. Garlyauskayte, Y. L. Yagupolskii, L. M. Yagupolskii, E. Bernhardt, H. Willner, I. Leito, *J. Org. Chem.* **2011**, *76*, 391.
[21] F. Eckert, I. Leito, I. Kaljurand, A. Kütt, A. Klamt, M. Diedenhofen, *J. Comput. Chem.* **2009**, *30*, 799.
[22] X.-C. Li, C.-Y. Wang, Y. Wan, W.-Y. Lai, L. Zhao, M.-F. Yin, W. Huang, *Chem. Commun.* **2016**, *52*, 2748.

Manuscript received: August 5, 2021
Revised manuscript received: October 5, 2021

P-5

Mazarevičs, A.; Kinēns, A.; Leduskrasts, K.; Sūna, E.
"Ultra-long Room Temperature Phosphorescence: Decoupling Lifetimes and Quantum Yields in Purely Organic Emitters"
Manuskripts iesniegts

Ultra-Long Room Temperature Phosphorescence: Decoupling Lifetimes and Quantum Yields in Purely Organic Emitters.

Arturs Mazarevics,[a]‡ Artis Kinens,[a] Kaspars Leduskrasts[a]‡* and Edgars Suna[a]*

AUTHOR ADDRESS: [a]Latvian Institute of Organic Synthesis, Aizkraukles 21, LV-1006, Riga, Latvia

KEYWORDS: room temperature phosphorescence, solid state, intermolecular interactions, molecular engineering

ABSTRACT: A general strategy to achieve ultra-long phosphorescence lifetimes without compromising quantum yields is demonstrated in simple purely organic solid-state emitters using steric shielding approach. The steric shielding of n-type orbital in a sulfur-containing luminophore helps to increase the inter-emitter distances in a crystal lattice. The increased distance hinders the fast intermolecular ISC channel and $T_1 \rightarrow S_0$ pathways while triggering multiple slower through-space ISC and $T_1 \rightarrow S_0$ alternatives. The steric shielding approach allowed for 35-fold extension of the phosphorescence lifetime (from 21 ms to 723 ms) without sacrificing phosphorescence quantum yields.

Introduction

Phosphorescent materials display afterglow with relatively long lifetimes (up to seconds) after the cease of excitation,[1] and they have found numerous applications in optoelectronic and biological areas.[2] The most efficient phosphorescent materials are based on transition metal complexes. However, the metal-containing emitters feature high manufacturing costs[3] and short lifetimes for phosphorescence (microsecond range).[4] Purely organic phosphorescent materials have emerged as considerably less expensive alternatives with much longer (millisecond range) phosphorescence lifetimes[5] as compared to the metal-based emitters. Despite the apparent advantages of metal-free emitters, achieving room temperature phosphorescence (RTP) remains a challenge because of the slow intersystem crossing (ISC) due to weak spin-orbit coupling (SOC) in organic molecules.[6] Typical approaches to achieve RTP in purely organic luminophore molecules rely on host-guest assemblies,[7] matrix induced rigidification,[8] intermolecular interaction control[9] and heavy-atom effect.[10] Arguably, the most frequently used design of metal-free organic phosphorescent materials employs the introduction of heteroatoms as a source of lone pair electrons.[11]

The introduction of the lone pair electrons enhances the ISC rate through transitions between $\pi\pi^*$ and $n\pi^*$ states.[3b,7c,12] Such a cross orbital excitation increases the rate of singlet to triplet ($S \rightarrow T$) transitions leading to greater phosphorescence quantum yields (QYs).[13] Importantly, the increase of phosphorescence QY in the solid state is typically accompanied by reduced phosphorescence lifetime.[13a,13b,14] The intertwined relationship between the phosphorescence lifetime and QY constitutes a fundamental challenge for the design of solid state phosphorescent materials that would feature *both* high phosphorescence QY and ultra-long lifetimes (>100 milliseconds). Herein, we demonstrate a design strategy that helps to decouple the phosphorescence QY and lifetime in purely organic phosphorescent materials. Our design strategy is demonstrated on a prototypical solid-state phosphorescent emitter **1**[15] that features long phosphorescence lifetime and poor QY (Figure 1). A 30-fold increase in QY could be readily achieved by replacing arene subunit in **1** with a lone-pair containing thiophene moiety (emitter **2**). As anticipated, the growth in solid state phosphorescence QY was accompanied by a sharp drop in lifetime (29-fold decrease). However, we found that the introduction of a steric bulk in a close proximity to the sulfur lone pair in luminophore **2** helps to accomplish ultra-long phosphorescence lifetimes (up to 723 ms) while retaining high phosphorescence QY (up to 8.3%; see Figure 1). The experimental evidence suggests that the increased steric bulk apparently hinders the detrimental intermolecular through-space relaxation channels that lead to a sharp drop in phosphorescence lifetime for luminogen **2** in the crystal lattice (*vide infra*). Furthermore, calculations using the crystal lattice geometries provided evidence that the measured phosphorescence lifetimes are proportional to the average electronic coupling between the luminophores. Since the vast majority of purely organic phosphorescent materials possess heteroatoms with electron lone pair, the proposed steric shielding approach offers a general strategy to achieve ultra-long emission lifetimes and good phosphorescence quantum yields.

Results and discussion

Initially, we elected to verify whether the replacement of phenyl moiety in the phosphorescent emitter **1** by the lone-pair containing thiophene subunit could be related to the increase of the excited state triplet population in

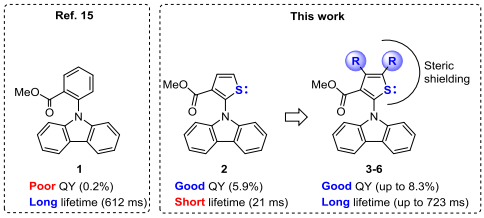

Figure 1. Steric shielding approach to decouple the phosphorescence lifetime and QY.

luminophore **2**. To this end, we measured the emission spectra of **1** and **2** at 77K in a hexane matrix[16] and observed fluorescence peaks at about 400 nm and a phosphorescent component at about 550 nm (Figure 2A,B) with lifetimes in the range of 4–5 ms (see Table 1, entries 1 and 3; see also SI, pages S15–16). The measured broad intense emission for **2** at 550 nm (Figure 2B) indicated considerably higher triplet state population for thiophene-containing emitter as compared to that for **1**, for which lack of emission at 550 nm was observed (Figure 2A). Hence, the 77K hexane matrix experiments provided strong evidence that the presence of a thiophene subunit in **2** increases the ISC rate as compared to that for **1**.

Next, luminescent behavior of **1** and **2** was evaluated in the crystalline state. Both **1** and **2** possessed fluorescence peaks in the 370–450 nm region (Figure 2C–D). Importantly, emitter **1** displayed weak phosphorescent emission in the 500–800 nm region with less than 0.2% phosphorescence QY (entry 2, Table 1). In sharp contrast, crystals of **2** showed intense emission at 544, 593 and 648 nm with phosphorescence QY of 5.9% (entry 4, Table 1). The observed 30-fold higher crystal state phosphorescence QY for **2** as compared to **1** is consistent with results from 77K hexane matrix experiments and provides an additional evidence for the increased ISC rate in emitter **2**.[17]

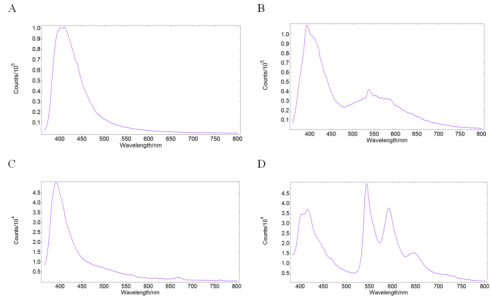

Figure 2. A:Emission of emitter 1 in hexane matrix at 77K; B: Emission of emitter **2** in hexane matrix at 77K; C: Crystal state emission of **1**; D: Crystal state emission of **2**.

Notably, the phosphorescence lifetime in the crystalline state for emitter **2** was measured to be considerably shorter than that of carbazole **1** (21 ms vs 619 ms; entry 2 and 4, Table 1). The apparent inverse correlation between phosphorescence lifetime and QY for luminophores **1** and **2** in the crystalline state follows the well-known notion that the increase of ISC rate leads to the drop in the lifetime.[14]

The increased phosphorescence lifetime in the crystal state as compared to that in the frozen hexane matrix for both emitters (619 ms vs 5 ms for **1** and 21 vs 4 ms for **2**; see Table 1) can be attributed to the stabilization of triplet excitons via inherent rigidification of luminophore molecules through ubiquitous low energy interactions, such as H–heteroatom and H–π bonds.[15b,18] In fact, the phosphorescence lifetime is known to be affected by the intermolecular interactions in the crystal lattice.[15b,18,19] Furthermore, previous reports indicate that strong intermolecular interactions can enable both radiative[1b,20] and non-radiative[1a,21] through-space relaxation pathways. In this regard, it has been demonstrated that the variation of intermolecular interaction distance between luminophores can change emission intensity, emission wavelength and emission lifetime.[22] Since luminophore **2** apparently possesses much faster relaxation channel as compared to that of **1** in the crystal lattice, we hypothesized that the shorter phosphorescence lifetimes for **2** may be attributed to stronger intermolecular interactions, facilitated by the thiophene subunit. Specifically, the n-orbital of the sulfur atom is most likely involved in the relatively fast intermolecular through-space $T_1 \rightarrow S_0$ relaxation pathway. If this holds true, shielding the n-orbital of the sulfur atom from intermolecular interactions through molecular engineering should help to achieve ultra-long phosphorescence lifetimes in luminophore **2**. In the meantime, the presence of the sulfur atom n-orbitals would help to maintain the fast ISC rate and, hence, high phosphorescence QY. Eventually, such on-site shielding of the n-orbital would help to accomplish *both* high phosphorescence QY and ultra-long lifetimes without compromising each other.

The on-site shielding hypothesis was examined by increasing steric hindrance at positions 4 and 5 of the thiophene ring. To this end, a series of thiophene derivatives **3–6** with was synthesized with the substituent volume spanning the range from 4.8 Å^3 in **2** to 76.9 Å^3 in **6** (Table 1; see also SI for the synthesis of **2–6**). All emitters **2–6** turned out to be crystalline materials. Interestingly, two polymorph forms could be obtained for luminophore **6** (entries 8 and 9, Table 1) as evidenced by X-Ray crystallography (*vide infra*). All thiophene derivatives **2–6** featured similar structured phosphorescent emission in the solid state with three distinct emission maxima at 544–549, 585–595 and 645–669 nm (see Table 1 and SI, page S17).[23] The highly similar emission spectrum highlights the minor influence of the introduced alkyl substituents on the excited state properties in **2–6**. In the solid state, all thiophene derivatives **2–6** displayed significantly increased phosphorescence QY (3.1–8.3%) when compared to the phenyl group-containing emitter **1** (0.2%, entry 2, Table 1). The highest phosphorescence QY (8.3%, entry 5, Table 1) in the solid state was measured for dimethyl substituted thiophene derivative **3**, whereas the lowest phosphorescence QY was observed for luminophore **4** (3.1%, entry 6, Table 1).

Table 1. Crystal state phosphorescence data for emitters **1–6**.

#	Compound	subst.vol. (Å^3)[b]	Solid λ_{EM} (nm)[c]	τ (ms)[d]	QY (%)
1[a]	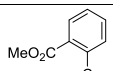 **1**	n/a	n/a	5	-
2			562, 617, 668	619	0.2
3[a]	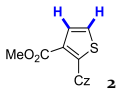 **2**	4.8	n/a	4	-
4			544, 593, 648	21	5.9
5	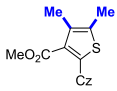 **3**	37.5	549, 595, 652	322	8.3
6	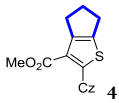 **4**	42.9	549, 595, 650	160	3.1
7	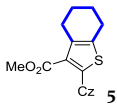 **5**	58.7	544, 592, 645	723	4.7
8[e]	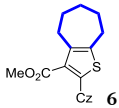 **6**	76.9	547, 595, 659	360	4.8
9[f]			546, 585, 669	404	3.5

[a]Emission spectra and lifetime in hexane matrix at 77K. [b]The substituent volume was calculated for optimized structures using *VEGA ZZ* software.[24] [c] At 370 nm excitation. [d]Measured at 550 nm emission and 370 nm excitation. [e]Polymorph α, see X-ray, SI page S22. [f]Polymorph β, see X-ray, SI page S23.

The thiophene derivative **2** displayed the shortest phosphorescence lifetime among all emitters tested (21 ms at 550 nm; entry 4, Table 1 and SI, page S15). In sharp contrast, the phosphorescence of sterically hindered 4,5-disubstituted analogs **3–6** could easily be visualized even by the naked eye after the cease of excitation. Specifically, the introduction of methyl substituents in the thiophene moiety resulted in more than 15-fold increase of phosphorescence lifetime (from 21 ms to 322 ms; entry 4 vs. entry 5, Table 1). Interestingly, the phosphorescence lifetime did not correlate with calculated volume of substituents at thiophene ring: the sterically largest cyclohepta[b]thiophene subunit-containing emitter **6** displayed the lifetime comparable to that of the less hindered dimethyl analog **3** (entry 8 vs entry 5). Furthermore, cyclopenta[b]thiophene derivative **4** featured two-fold shorter lifetime as compared to **3** despite the similar steric between the two emitters (entry 6 vs entry 5). The highest phosphorescence lifetimes (723 ms) were measured for 4,5,6,7-tetrahydro-1-benzothiophene derivative **5** (entry 7). Notably, not only compound **5** surpassed the phosphorescence lifetime of **1**, but it also featured 24-fold higher phosphorescence QY than the benchmark emitter **1** (entry 7 vs. entry 2). Hence, the increased steric bulk in the close proximity to the thiophene sulfur atom apparently helps to hinder the detrimental intermolecular through-space relaxation channels and leads to the increase of the phosphorescence lifetimes without compromising QY.

X-ray data analysis.

The efficiency of the sulfur on-site shielding approach to suppress the detrimental intermolecular non-radiative relaxation routes was further corroborated by single crystal X-ray data for emitters **2–6**. Single crystals of **2–6** suitable for X-ray analysis were obtained by vapor diffusion from MeCN for **2**, heptane for **3**, a mixture of heptane, EtOAc and Et_2O for **4**, a mixture of hexane and EtOAc for **5**, a mixture of heptane and Et_2O for α-polymorph **6**$^{\alpha}$ and heptane for β-polymorph **6**$^{\beta}$ (Figure 3A). Compounds **2–4** crystallized as orthorhombic colorless blocks with *Pbca* space group, compound **5** was obtained as monoclinic colorless plates with $P2_1/c$ space group and polymorphs **6**$^{\alpha}$ and **6**$^{\beta}$ crystallized as triclinic colorless prisms and needles, respectively, with $P\bar{1}$ space group. The lattice dimensions were found to be similar for **2**, **3**, **4** and **6b**. In contrast, 2-3 fold reduced unit cell volume was observed for **5** and **6a** as compared to the aforementioned emitters. Thiophene derivatives **2–4** featured dimeric structures with very similar parallel-displaced stacking arrangement induced by S–π system interactions, whereas both

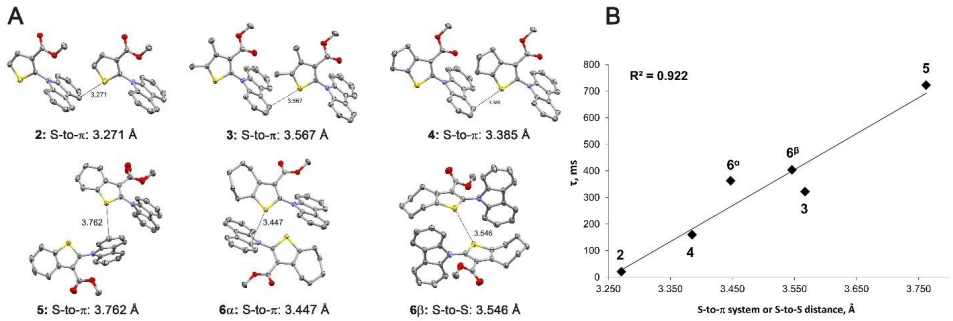

Figure 3. A: X-ray representations of emitters **2–6** (carbon, oxygen, nitrogen and sulfur are shown as grey, red, blue and green ellipsoids, respectively, at the 50% probability level; hydrogens are removed for clarity). Shown are the shortest distances between thiophene S atom and the closest π-system of the neighboring luminophore. B: Correlation plot of the S-to-π and S-to-S distances and phosphorescence lifetimes for emitters **2–6**.

polymorphs of **6** displayed head-to-tail arrangements, induced either by S–π system or S–S interactions. Finally, **5** displayed a distorted tail-to-tail arrangement, however the S–π system interaction was still present. To investigate the packing arrangement and intermolecular interactions between molecules in a crystal lattice, three types of adjacent dimers were extracted for the in-depth analysis.

It was hypothesized that the variation of a steric bulk next to the sulfur atom of the thiophene subunit in emitters **2–6** should influence the packing arrangement in the crystal lattice. Indeed, dimers **2–6** featured different distances between the thiophene S atom and the *closest* π-system (carbazole moiety for emitters **2–5** and **6$^{\alpha}$** or π-system of thiophene moiety for emitter **6$^{\beta}$**) of the neighboring luminophore. Thus, 4,5-nonsubstituted thiophene derivative **2** displayed the shortest intermolecular S-to-π system distance of 3.271 Å (Figure 3A). The introduction of fused cyclopentene moiety (emitter **4**) and methyl groups (emitter **3**) resulted in the distance increase to 3.385 Å and 3.567 Å, respectively (Figure 3A). The longest intermolecular S-to-π system or S-to-S distances were measured for cyclohepta[b]thiophene-containing emitter **6** (3.447 Å for **6$^{\alpha}$** and 3.546 Å for **6$^{\beta}$**) and 4,5,6,7-tetrahydro-1-benzothiophene derivative **5** (3.762 ; see Figure 3). Importantly, the distances correlated well with the respective phosphorescence lifetimes for emitters **2–6** (R^2 = 0.92, Figure 3B). The observed correlation is notable, as it provides a strong evidence for the involvement of the sulfur n-orbital in an *intermolecular* radiative relaxation pathway that apparently has strong impact on phosphorescence lifetimes.

Additionally, we also examined other crystal state parameters for emitters **2–6** that could have an impact on the phosphorescence lifetimes (see SI, pages S24–26 for detailed data). First, torsion angles between the carbazole and thiophene moieties were measured. The thiophene moiety was twisted out of the carbazole plane and the torsion angles were found to be 86.2° for **2**, 65.1° for **3**, 63.4° for **4**, 77.8° for **5**, 51.4° for **6$^{\alpha}$** and 87.6° for **6$^{\beta}$**. Next, close contacts from the oxygen of the carbonyl group (C=O) were evaluated. In all materials, one to three hydrogen bonds between adjacent molecules and the carbonyl oxygen were present with distances spanning the range from 2.39 to 2.66Å. Finally, the orientation of the C=O group within the molecule was also inspected. The C=O group was pointed to the same direction as the carbazole moiety in emitters **2** and **5**. However, opposite orientations of the C=O group and carbazole were observed in **3**, **4**, **6$^{\alpha}$** and **6$^{\beta}$**. Notably, no correlation between the phosphorescence lifetime or QY and torsion angles as well as hydrogen bond distances was found.

Density functional theory calculations.

To gain a deeper insight into the excited state behavior, time dependent density functional theory (TD-DFT and DFT) calculations were employed at the B3LYP/6-311++g(2df,p) level of theory[25] using geometries obtained from X-ray analyses. First, the highest occupied molecular orbital (HOMO) and lowest unoccupied molecular orbital (LUMO) energy levels were calculated for both singlet (S_n) and triplet (T_n) states of monomers **2–6**. LUMO in **2–5** and **6$^{\beta}$** were localized mainly on the carbazole moiety and to a much lesser degree on the thiophene ring (Figure 4). In contrast, HOMO in **2–5** and **6$^{\beta}$** were predominantly spread on the thiophene ring and the ester moiety. Interestingly, both LUMO and HOMO were largely localized on both carbazole and thiophene moieties only for **6$^{\alpha}$**. Consequently, the n-orbitals of both sulfur and oxygen atoms participate in the excited state.

Next, energy gaps between ground and singlet as well as triplet excited states were calculated. The transition between ground singlet state (S_0) to the lowest excited singlet state (S_1) was calculated to be in the range from 3.61 to 3.27 eV (Figure 4, also see SI, pages S27–32). The low-lying T_n states that feature lower energy than S_1 state were also analyzed. Accordingly, compounds **2**, **3**, **6$^{\alpha}$** and **6$^{\beta}$** possessed three low-lying triplet states ($T_{1–3}$), whereas emitters **4** and **5** featured two low-lying triplet states ($T_{1–2}$). The energy gaps between S_1 and the highest of the low-lying T_n states ($\Delta E_{S_1T_n}$, where n = 2 or 3) for **2**, **3**, **4**, **5**, **6$^{\alpha}$** and **6$^{\beta}$** were calculated to be 0.05, 0.12, 0.12, 0.18, 0.31 and

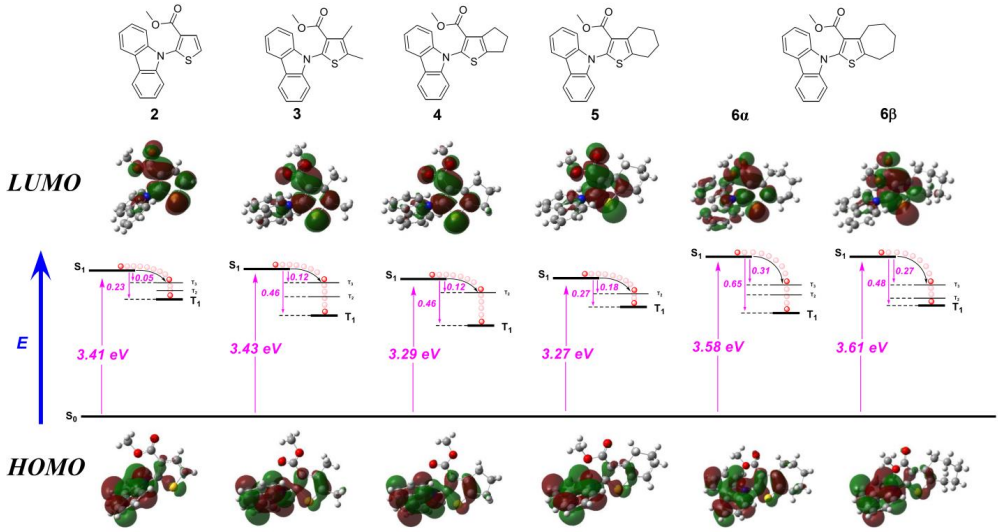

Figure 4. HOMO and LUMO (S_1 and T_n) representations for emitters **2–6**.

0.27 eV, respectively. The energy gap between S_1 and T_1 states ($\Delta E_{S_1T_1}$) for compounds **2**, **3**, **4**, **5**, **6**$^{\alpha}$ and **6**$^{\beta}$ was 0.23, 0.46, 0.46, 0.27, 0.65 and 0.48 eV, respectively. The relatively high $\Delta E_{S_1T_n}$ and $\Delta E_{S_1T_1}$ values for **6**$^{\alpha}$ can be rationalized by the high degree of HOMO and LUMO overlap.

Generally, high $\Delta E_{S_1T_1}$ values are known to reduce the ISC rate leading to low phosphorescence quantum yields.[15a] However, in our case emitter **6**$^{\alpha}$ with the highest $\Delta E_{S_1T_1}$ and $\Delta E_{S_1T_n}$ values ($\Delta E_{S_1T_n}$ = 0.31 eV and $\Delta E_{S_1T_1}$ = 0.65 eV) displayed higher phosphorescence QY than its counterparts **4**, **5** and **6**$^{\beta}$ that feature relatively smaller energy gaps between S_1 and T_1/T_n states ($\Delta E_{S_1T_n}$ = 0.12, 0.18, 0.27 and $\Delta E_{S_1T_n}$ = 0.46, 0.27, 0.48 eV, respectively). In addition, identical $\Delta E_{S_1T_1}$ and $\Delta E_{S_1T_n}$ values were calculated for **3** and **4**; however these emitters displayed the highest disparity in phosphorescence QYs among these materials (see Table 1, entries 5 and 6). Evidently, the phosphorescence QY for emitters **2–6** cannot be estimated merely by TD-DFT calculations of $\Delta E_{S_1T_1}$ and $\Delta E_{S_1T_n}$ values for *individual* molecules without taking into the consideration intermolecular interactions in the crystal state. Apparently, intermolecular interactions for emitters **2–6** play significant role in determining the ISC rate and phosphorescence QY as opposed to archetypal emitter **1**, for which a good correlation between ISC and $\Delta E_{S_1T_n}$ gap[15a] was observed without considering intermolecular processes.

Additional calculations were performed to identify key intermolecular processes in the crystal state that may contribute to the phosphorescence QY and lifetimes of emitters **2–6**. The observed correlation of the crystal state phosphorescence lifetime and distance between neighboring luminophores **2–6** (see Figure 3B) led us to hypothesize that the sought-after mechanism is the charge transfer (CT) process, which effectiveness is well-known to be dependent on the inter-emitter distance.[26] Accordingly, a thorough charge transfer integral (CTI) analysis of **2–6** was conducted to account for all possible CT vectors between the excited luminophore and all adjacent molecules in the crystal lattice. CTIs were calculated for both electron transfer (LUMO, blue vectors, E_{1-3}) and hole transfer (HOMO, red vectors, H_{1-3}) using CATNIP[27] software (Figure 5). For example, compound **4** possessed six CT pathways, three for electron transfer and three for hole transfer (Figure 5A), whereas ten CT pathways were identified for **2**, fourteen for **3**, ten for **5**, ten for **6**$^{\alpha}$ and sixteen for emitter **6**$^{\beta}$, respectively (see SI S33–36). The effectiveness of the CT in each of the vectors was approximated by the intermolecular electronic coupling $\boldsymbol{V}$ (see SI, page S33) between the two luminophores.[28] Importantly, recent works have identified that the increase of $\boldsymbol{V}$ plays a crucial role in ensuring long and intense solid state emission.[12,29] Specifically, strong intermolecular $\boldsymbol{V}$ between ππ* and nπ* states is required to achieve ultra-long room temperature phosphorescence in the crystal state.[9f] Higher absolute values of $\boldsymbol{V}$ ($|\boldsymbol{V}|$) ensure stronger intermolecular interactions, and hence a more plausible CT.

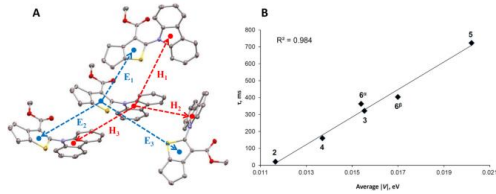

Figure 5. A: Every considered electron and hole CT pathway for **4**; B: Correlation between the average value of $|V|$ and phosphorescence lifetime.

Having calculated $|\boldsymbol{V}|$ values for each of CT vectors under consideration, we disregarded those with negligible

participation in the CT processes. Specifically, CT vectors with $|V|$ value contributing below 5% of the total sum of $|V|$ ($\sum|V|$) values were omitted to obtain the most probable CT pathways for each of emitters **2–6** in the crystal lattice. Accordingly, seven CT pathways for **2**, five **3**, five **4**, four **5**, eight $\mathbf{6}^{\alpha}$ and five $\mathbf{6}^{\beta}$ were employed in further calculations (See SI S37–40). The $|V|$ values for each plausible pathway for **2–6** were in the range between 0.001 and 0.062 eV. Notably, the average absolute value of electronic coupling ($|V|$) for all plausible CT pathways ($\frac{\sum_1^n|V|}{n}$, where n is the number of plausible pathways) correlated extremely well with the observed phosphorescence lifetimes for each of the emitters (R^2=0.98, **Error! Reference source not found.**B), and hence, approximated the lifetime even better than did the shortest contact distances (R^2=0.92, **Error! Reference source not found.**B). Apparently, the increase of a distance between luminophores in a crystal lattice hinders the dominant *intermolecular* $T_1 \rightarrow S_0$ relaxation channel and triggers multiple alternative through-space $T_1 \rightarrow S_0$ pathways, thus stabilizing excitons and leading to ultra-long phosphorescence lifetimes. Exciton stabilization depends on the rates of CT processes (charge separation and recombination). Notably, recent studies clearly demonstrated that charge separation and recombination rates of the triplet states are governed by the electronic coupling $\boldsymbol{V}$.[30] Overall, the CTI calculations provide compelling evidence that both electron and hole mobility has strong impact on the phosphorescence lifetime for emitters **2–6** in the crystal lattice.

Having identified CT as the key intermolecular process that affects the crystal state emission properties of **2–6**, we revisited the DFT calculations of phosphorescence QYs for these emitters (B3LYP/6-311++g(2df,p) level of theory). Accordingly, energy levels for both singlet (S_n) and triplet (T_n) states were calculated for *dimers* of **2–6** using geometries obtained from the X-ray analysis. Importantly, S_n and T_n energy levels for dimers were similar to those calculated for the respective monomers (SI, pages S42–50), however HOMO and LUMO in the dimeric structures were not localized in the same molecule (Figure 6A). Dimers with the highest absolute electron coupling values $|\boldsymbol{V}|_e$ (represented by blue vectors in Figure 5A) were only chosen, since they would account for the majority of excited state electron transitions. Accordingly, two dimers with high $|\boldsymbol{V}|_e$ values were selected for **2**, **3**, and **5**, and one dimer for **4**, $\mathbf{6}^{\alpha}$ and $\mathbf{6}^{\beta}$. To account for the most relevant *intermolecular* $S_1 \rightarrow T_n$ transition channels, the number of accessible T_n states for each of dimers (within 0.30 eV range) were multiplied by the respective $|\boldsymbol{V}|_e$ value. This led to a sum of $|\boldsymbol{V}|_e$–corrected accessible T_n states, which was designated as the L factor ($L = \sum_1^n(m \times |V|_{e(n)})$, where m = number of accessible $S_1 \rightarrow T_n$ transitions, n = number of dimers, $|\boldsymbol{V}|_{e(n)} = |\boldsymbol{V}|_e$ value of the corresponding dimer, See SI S51). We were delighted to see that the factor L correlated reasonably well with the phosphorescence QY (R^2 = 0.74, Figure 6B). Hence, combined TD-DFT data and CTI analysis provided a relatively good approximation of the measured phosphorescence QY values for solid-state emitters **2–6** despite the fact that not every possible dimer was considered in the calculations. Overall, the TD-DFT data suggest that the phosphorescence QY depends on both the energy gaps between the accessible $S_1 \rightarrow T_n$ transitions ($\Delta E_{S_1T_n}$ values) and CT between excited luminophores (represented by the absolute excited state electron electronic coupling values $|\boldsymbol{V}|_e$). Intermolecular interactions in the crystal lattice increase the number of accessible triplet states for $S_1 \rightarrow T_n$ transitions in phosphors **2–6**, resulting in similar phosphorescence QYs across the series. Presumably, multiple slow $S_1 \rightarrow T_n$ transitions in **3–6** compensate for the fast ISC channel associated with n-type orbital of the non-hindered sulfur atom in luminophore **2**.

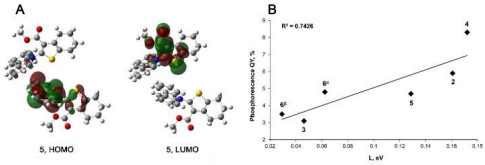

Figure 6. A: HOMO and LUMO representations for **5**; B: Correlation plot between the factor L and phosphorescence QYs; $L = \sum_1^n(m \times |V|_{e(n)})$, where m = number of accessible $S_1 \rightarrow T_n$ transitions, n = number of dimers, $|V|_{e(n)} = |V|_e$ value of the corresponding dimer.

Phosphorescent coating

Given that emitter **5** displayed ultra-long phosphorescence lifetime, it was employed in the design of a time-resolved anti-counterfeiting pattern. Accordingly, a contour of a cat, a letter "n" and an arrow was plotted using a previously published pyridinium luminophore,[31] whereas a symbol "π" and the cat eyes were coated with compound **5** (Figure 7). The latter was applied on a black paper surface as a solution in Et_2O, followed by solvent evaporation to afford crystalline coating. The whole pattern was visible under 365 nm excitation, whereas only the symbol "π" and the cat eyes remained visible after turning-off the excitation (Figure 7). The ultra-long lifetime of compound **5** allows for the visible identification of the coated patterns for at least two seconds after the cease of excitation. Importantly, emitter **5** did not lose its phosphorescent ability after the solvent-based coating, indicating that the phosphorescence properties do not depend on crystal size. Furthermore, the phosphorescence was not quenched by oxygen despite that the solvent-based coating and subsequent excitation was performed under ambient atmosphere. Finally, the patterns coated with **5** displayed unchanged phosphorescent behavior after exposure to oxygen and ambient light for more than a month.

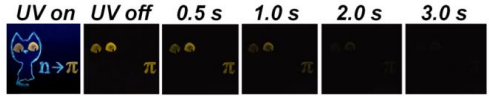

Figure 7. Anti-counterfeiting pattern created using **5** and an emitter with a short lifetime.

Conclusions

In conclusion, a straightforward molecular engineering strategy to decouple phosphorescence lifetime and quantum yields in purely organic luminophores is reported. The design strategy relies on the introduction of a steric bulk next to n-type orbital-containing sulfur atom of luminophore. Owing to the increased steric demands due to the alkyl groups, neighboring luminophore molecules adopt greater inter-emitter distances in a crystal lattice. The increase in the distance translates into prolonged phosphorescence lifetime while keeping phosphorescence QY virtually unchanged. The phosphorescence lifetime extension up to 35 times (from 21 ms to 723 ms) was readily achieved without sacrificing phosphorescence QYs. A good correlation (R^2=0.92) was observed between the intermolecular distance and the phosphorescence lifetime across a series of crystalline emitters possessing various steric bulk. The increase of the inter-emitter distance helps to hinder the dominating distance-dependent intermolecular $T_1 \rightarrow S_0$ relaxation channel while triggering multiple alternative through-space $T_1 \rightarrow S_0$ relaxation pathways that lead to considerably longer phosphorescence lifetimes. Important evidence favoring the presence of multiple inter-emitter $T_1 \rightarrow S_0$ relaxation pathways was acquired by a charge transfer integral (CTI) analysis of the crystal state dimers. Importantly, the calculated average absolute value of electronic coupling ($|V|$) for plausible CT relaxation pathways correlated extremely well with the phosphorescence lifetime (R^2=0.98). Furthermore, the combination of the CTI analysis and TD-DFT calculations of the accessible $S_1 \rightarrow T_n$ transitions energies ($\Delta E_{S_1T_n}$ values) for *dimers* provided a reasonably good model for the prediction of phosphorescence QYs. In sharp contrast, the phosphorescence QY could not be approximated by TD-DFT calculations of *monomeric* phosphorescent luminophores suggesting that intermolecular interactions in the crystal state increase the number of accessible triplet states for $S_1 \rightarrow T_n$ transitions. Presumably, multiple $S_1 \rightarrow T_n$ transitions compensate for the ISC channel associated with n-type orbital. The disclosed molecular engineering strategy offers a general approach to minimize the detrimental interplay between phosphorescence QY and lifetime, and also contributes to a mechanistic understanding of the solid state phosphorescence phenomenon. Considering the vast majority of phosphorescent materials possess a heteroatom lone pair, the developed approach may be especially useful in the design of purely organic phosphorescent materials with both high QY and ultra-long lifetimes.

ASSOCIATED CONTENT

Supporting Information. Associated content consists of synthesis of emitters, characterization, photophysical properties, DTF and CTI calculations, X-Ray analysis and the corresponding .cif files. This material is available free of charge via the Internet at http://pubs.acs.org.

AUTHOR INFORMATION

Corresponding Author

* Prof. Edgars Suna. E-Mail: edgars@osi.lv. Latvian Institute of Organic Synthesis, Aizkraukles 21, LV-1006, Riga, Latvia.

Author Contributions

The manuscript was written through contributions of all authors. / All authors have given approval to the final version of the manuscript. / ‡These authors contributed equally. (match statement to author names with a symbol)

Funding Sources

This work was funded by ERDF project No. 1.1.1.1/18/A/063.

ACKNOWLEDGMENT

We thank Dr S. Belyakov for X-ray crystallographic analysis.

REFERENCES

(1) (a) Kenry; Chen, C.; Liu, B. Enhancing the performance of pure organic room-temperature phosphorescent luminophores. *Nat. Commun.* **2019**, *10*, 2111. DOI: 10.1038/s41467-019-10033-2. (b) Hirata, S. Recent Advances in Materials with Room-Temperature Phosphorescence: Photophysics for Triplet Exciton Stabilization. *Adv. Opt. Mater.* **2017**, *5*, 1700116. DOI: 10.1002/adom.201700116.

(2) (a) Caporale, C.; Massi, M. Cyclometalated iridium(III) complexes for life science. *Coord. Chem. Rev.* **2018**, *363*, 71–91. DOI: 10.1016/j.ccr.2018.02.006. (b) Shi, H.; Wang, Y.; Lin, S.; Lou, J.; Zhang, Q. Recent development and application of cyclometalated iridium(III) complexes as chemical and biological probes. *Dalton Trans.* **2021**, *50*, 6410–6417. DOI: 10.1039/D1DT00592H. (c) Bin Mohd Yusoff, A. R.; Huckaba, A. J.; Nazeeruddin, M. K. Highly Efficient Phosphorescent Blue-Emitting [3+2+1] Coordinated Iridium (III) Complex for OLED Application. *Top. Curr. Chem.* **2017**, *375*. DOI: 10.1007/s41061-017-0126-7.

(3) (a) Mukherjee, S.; Thilagar, P. Recent advances in purely organic phosphorescent materials. *Chem. Commun.* **2015**, *51*, 10988–11003. DOI: 10.1039/C5CC03114A. (b) Zhao, W.; He, Z.; Lam, J. W. Y.; Peng, Q.; Ma, H.; Shuai, Z.; Bai, G.; Hao, J.; Tang, B. Z. Rational Molecular Design for Achieving Persistent and Efficient Pure Organic Room-Temperature Phosphorescence. *Chem.* **2016**, *1*, 592–602. DOI: 10.1016/j.chempr.2016.08.010.

(4) Zhou, J.; Li, J.; Zhang, K. Y.; Liu, S.; Zhao, Q. Phosphorescent iridium(III) complexes as lifetime-based biological sensors for photoluminescence lifetime imaging microscopy. *Coord. Chem. Rev.* **2022**, *453*, 214334. DOI: 10.1016/j.ccr.2021.214334

(5) (a) Niu, Z.; Ma, C.; Ye, W.; Wang, H.; Jia, W.; Shi, H.; Shi, H.; An, Z.; Huang, W. Colour-tunable ultralong organic phosphorescence upon temperature stimulus. *RSC Adv.* **2019**, *9*, 19075–19078. DOI: 10.1039/C9RA03537K. (b) Chen, J.; Rahman, N. U.; Mao, Z.; Zhao, J.; Yang, Z.; Liu, S.; Zhang, Y.; Chi, Z. Achievement of persistent and efficient organic room-temperature phosphorescence with temperature-response by adjusting the proportion of excited-state configurations in coupled molecules. *J. Mater. Chem. C* **2019**, *7*, 8250–8254. DOI: 10.1039/C9TC01870K. (c) Zhang, J.; Sharman, E.; Yang, L.; Jiang, J.; Zhang, G. Aggregation-Induced Enhancement of Molecular Phosphorescence Lifetime: A First-Principle Study. *J. Phys. Chem. C* **2018**, *122*, 25796–25803. DOI: 10.1021/acs.jpcc.8b07087.

(6) (a) Cai, S.; Shi, H.; Tian, D.; Ma, H.; Cheng, Z.; Wu, Q.; Gu, M.; Huang, L.; An, Z.; Peng, Q.; Huang, W. Enhancing Ultralong Organic Phosphorescence by Effective π-Type Halogen Bonding. *Adv. Funct. Mater.* **2018**, *28*, 1705045. DOI: 10.1002/adfm.201705045. (b) Huang, L.; Qian, C.; Ma, Z. Stimuli-Responsive Purely Organic Room-Temperature Phosphorescence Materials. *Chem. Eur. J.*, **2020**, *26*, 11914–11930. DOI: 10.1002/chem.202000526.

(7) (a) Xie, Z.; Zhang, X.; Wang, H.; Huang, C.; Sun, H.; Dong, M.; Ji, L.; An, Z.; Yu, T.; Huang, W. Wide-range lifetime-tunable and responsive ultralong organic phosphorescent multi-host/guest system. *Nat. Commun.* **2021**, *12*, 3522. DOI: 10.1038/s41467-021-23742-4. (b) Li, D.; Lu, F.; Wang, J.; Hu, W.; Cao, X.-M.; Ma, X.; Tian, H. Amorphous Metal-Free Room-Temperature Phosphorescent Small Molecules with Multicolor Photoluminescence via a Host–Guest and Dual-Emission Strategy. *J. Am. Chem. Soc.* **2018**, *140*, 1916–1923. DOI: 10.1021/jacs.7b12800. (c) Gan, N.; Shi, H.; An, Z.; Huang, W. Recent Advances in Polymer-Based Metal-Free Room-Temperature Phosphorescent Materials. *Adv. Funct. Mater.* **2018**, *28*, 1802657. DOI: 10.1002/adfm.201802657. (d) Hirata, S.; Totani, K.; Zhang, J.; Yamashita, T.; Kaji, H.; Marder, S. R.; Watanabe, T.; Adachi, C. Efficient Persistent Room Temperature Phosphorescence in Organic Amorphous Materials under Ambient Conditions. *Adv. Funct. Mater.* **2013**, *23*, 3386–3397. DOI: 10.1002/adfm.201203706.

(8) (a) Wu, H.; Gu, L.; Baryshnikov, G. V.; Wang, H.; Minaev, B. F.; Ågren, H.; Zhao, Y. Molecular Phosphorescence in Polymer Matrix with Reversible Sensitivity. *ACS Appl. Mater. Interfaces* **2020**, *12*, 20765–20774. DOI: 10.1021/acsami.0c04859. (b) Gao, H.; Ma, X. Recent progress on pure organic room temperature phosphorescent polymers. *Aggregate* **2021**, *2*, e38. DOI: 10.1002/agt2.38. (c) Wei, J.; Liang, B.; Duan, R.; Cheng, Z.; Li, C.; Zhou, T.; Yi, Y.; Wang, Y. Induction of Strong Long-Lived Room-Temperature Phosphorescence of N-Phenyl-2-naphthylamine Molecules by Confinement in a Crystalline Dibromobiphenyl Matrix. *Angew. Chem. Int. Ed.* **2016**, *55*, 15589–15593. DOI: 10.1002/anie.201607653.

(9) (a) Chen, C.; Huang, R.; Batsanov, A. S.; Pander, P.; Hsu, Y.-T.; Chi, Z.; Dias, F. B.; Bryce, M. R. Intramolecular Charge Transfer Controls Switching Between Room Temperature Phosphorescence and Thermally Activated Delayed Fluorescence. *Angew. Chem. Int. Ed.* **2018**, *57*, 16407–16411. DOI: 10.1002/anie.201809945. (b) Ma, C.; Ma, H.; Ling, K.; Zheng, R.; Gu, M.; Song, L.; An, Z.; Shi, H.; Huang, W. Insight into chirality on molecular stacking for tunable ultralong organic phosphorescence. *J. Mater. Chem. C* **2018**, *6*, 10179–10183. DOI: 10.1039/C8TC03297A. (c) Fan, Y.; Li, Q.; Li, Z. Organic luminogens bearing alkyl substituents: design flexibility, adjustable molecular packing, and optimized performance. *Mater. Chem. Front.* **2021**, *5*, 1525–1540. DOI: 10.1039/D0QM00851F. (d) Gu, L.; Shi, H.; Miao, C.; Wu, Q.; Cheng, Z.; Cai, S.; Gu, M.; Ma, C.; Yao, W.; Gao, Y.; An, Z.; Huang, W. Prolonging the lifetime of ultralong organic phosphorescence through dihydrogen bonding. *J. Mater. Chem. C* **2018**, *6*, 226–233. DOI: 10.1039/C7TC04452F. (e) Li, M.; Ling, K.; Shi, H.; Gan, N.; Song, L.; Cai, S.; Cheng, Z.; Gu, L.; Wang, X.; Ma, C.; Gu, M.; Wu, Q.; Bian, L.; Liu, M.; An, Z.; Ma, H.; Huang, W. Prolonging Ultralong Organic Phosphorescence Lifetime to 2.5 s through Confining Rotation in Molecular Rotor. *Adv. Opt. Mater.* **2019**, *7*, 1800820. DOI: 10.1002/adom.201800820. (f) Li, Q.; Li, Z. Molecular Packing: Another Key Point for the Performance of Organic and Polymeric Optoelectronic Materials. *Acc. Chem. Res.* **2020**, 53, 962–973. DOI: 10.1021/acs.accounts.0c00060.

(10) (a) Lai, L.; Fang, B.; Fan, M.; Cheng, W.; Yin, M. *J.* Modulating Room-Temperature Phosphorescence through the Synergistic Effect of Heavy-Atom Effect and Halogen Bonding. *Phys. Chem. C* **2021**, *125*, 16350–16357. DOI: 10.1021/acs.jpcc.1c04989. (b) Li, B.; Gong, Y.; Wang, L.; Lin, H.; Li, Q.; Guo, F.; Li, Z.; Peng, Q.; Shuai, Z.; Zhao, L.; Zhang, Y. Highly Efficient Organic Room-Temperature Phosphorescent Luminophores through Tuning Triplet States and Spin-Orbit Coupling with Incorporation of a Secondary Group. *J. Phys. Chem. Lett.* **2019**, *10*, 7141–7147. DOI: 10.1021/acs.jpclett.9b02885 (c) Shi, H.; An, Z.; Li, P.-Z.; Yin, J.; Xing, G.; He, T.; Chen, H.; Wang, J.; Sun, H.; Huang, W.; Zhao, Y. Enhancing Organic Phosphorescence by Manipulating Heavy-Atom Interaction. *Crys. Growth Des.* **2016**, *16*, 808–813. DOI: 10.1021/acs.cgd.5b01400. (d) Nitti, A.; Botta, C.; Forni, A.; Cariati, E.; Lucenti, E.; Pasini, D. Crystallization-induced room-temperature phosphorescence in fumaramides. *CrystEngComm* **2020**, *22*, 7782–7785. DOI: https://doi.org/10.1039/DoCE01253J.

(11) (a) Yang, J.; Zhen, X.; Wang, B.; Gao, X.; Ren, Z.; Wang, J.; Xie, Y.; Li, J.; Peng, Q.; Pu, K.; Li, Z. The influence of the molecular packing on the room temperature phosphorescence of purely organic luminogens. *Nat. Commun.* **2018**, *9*, 840. DOI: 10.1038/s41467-018-03236-6. (b) Zhou, C.; Zhang, S.; Gao, Y.; Liu, H.; Shan, T.; Liang, X.; Yang, B.; Ma, Y. ernary Emission of Fluorescence and Dual Phosphorescence at Room Temperature: A Single-Molecule White Light Emitter Based on Pure Organic Aza-Aromatic Material. *Adv. Funct. Mater.* **2018**, *28*, 1802407. DOI: 10.1002/adfm.201802407. (c) Jia, W.; Wang, Q.; Shi, H.; An, Z.; Huang, W. Manipulating the Ultralong Organic Phosphorescence of Small Molecular Crystals. *Chem. Eur. J.* **2020**, *26*, 4437–4448. DOI: 10.1002/chem.201904500. (d) Tian, S.; Ma, H.; Wang, X.; Lv, A.; Shi, H.; Geng, Y.; Li, J.; Liang, F.; Su, Z. M.; An, Z.; Huang, W. Utilizing d-pπ Bonds for Ultralong Organic Phosphorescence. *Angew. Chem. Int. Ed.* **2019**, *58*, 6645–6649. DOI: 10.1002/anie.201901546.

(12) Yang, Z.; Mao, Z.; Zhang, X.; Ou, D.; Mu, Y.; Zhang, Y.; Zhao, C.; Liu, S.; Chi, Z.; Xu, J.; Wu, Y. C.; Lu, P. Y.; Lien, A.; Bryce, M. R. Intermolecular Electronic Coupling of Organic Units for Efficient Persistent Room-Temperature Phosphorescence. *Angew. Chem. Int. Ed.* **2016**, 55, 2181–2185. DOI: 10.1002/anie.201509224.

(13) (a) Li, X. N.; Yang, M.; Chen, X. L.; Jia, J. H.; Zhao, W. W.; Wu, X. Y.; Wang, S. S.; Meng, L. Y.; Lu, C. Z. Synergistic Intra- and Intermolecular Noncovalent Interactions for Ultralong Organic Phosphorescence. *Small* **2019**, *15*, 1903270. DOI: 10.1002/smll.201903270. (b) Gong, Y.; Chen, G.; Peng, Q.; Yuan, W. Z.; Xie, Y.; Li, S.; Zhang, Y.; Tang, B. Z. Achieving Persistent Room Temperature Phosphorescence and Remarkable Mechanochromism from Pure Organic Luminogens. *Adv. Mater.* **2015**, *27*, 6195–6201. DOI: 10.1002/adma.201502442.

(14) Ma, H.; Peng, Q.; An, Z.; Huang, W.; Shuai, Z. *J. Am. Chem. Soc.* **2018**, *141*, 1010–1015.; Zhao, W.; Cheung, T. S.; Jiang, N.; Huang, W.; Lam, J. W.; Zhang, X.; He, Z.; Tang, B. Z. Boosting the efficiency of organic persistent room-temperature phosphorescence by intramolecular triplet-triplet energy transfer. *Nat. Commun.* **2019**, *10*, 1595. DOI: 10.1038/s41467-019-09561-8.

(15) (a) Xiong, Y.; Zhao, Z.; Zhao, W.; Ma, H.; Peng, Q.; He, Z.; Zhang, X.; Chen, Y.; He, X.; Lam, J. W.; Tang, B. Z. Designing Efficient and Ultralong Pure Organic Room-Temperature Phosphorescent Materials by Structural Isomerism. *Angew. Chem. Int. Ed.* **2018**, 57, 7997–8001. DOI: 10.1002/anie.201800834. (b) Zhang, T.; Gao, H.; Lv, A.; Wang, Z.; Gong, Y.; Ding, D.; Ma, H.; Zhang, Y.; Yuan, W. Z. Hydrogen bonding boosted the persistent room temperature phosphorescence of pure organic compounds for multiple applications. *J. Mater. Chem. C* **2019**, *7*, 9095–9101. DOI: 10.1039/C9TC02879J.

(16) Hexane matrix was used to avoid the introduction of lone electron pairs near the luminophore through the solvent.

(17) The involvement of thermally delayed fluorescence in the crystal state emission of **2** was ruled out by variable temperature experiments that demonstrated a direct proportionality between the intensity of fluorescence and phosphorescence and temperature in the range from 178 to 293 K (see SI, S16).

(18) (a) Chen, X.; Liu, Z. F.; Jin, W. J. The Effect of Electron Donation and Intermolecular Interactions on Ultralong Phosphorescence Lifetime of 4-Carnoyl Phenylboronic Acid. *J. Phys. Chem. A* **2020**, *124*, 2746–2754. DOI: 10.1021/acs.jpca.9b11943. (b) Nidhankar Goudappagouda, A. D.; Mohana Kumari, D. S.; Chaubey, S. K.; Nayak, R.; Gonnade, R. G.; Kumar, G. V. P.; Krishnan, R.; Babu, S. S. Self-Assembled Helical Arrays for the Stabilization of the Triplet State. *Angew. Chem. Int. Ed.* **2020**, *59*, 13079. DOI: 10.1002/anie.202005105.

(19) Liu, Z. F.; Chen, X.; Wu, W. X.; Zhang, G. Q.; Li, X.; Li, Z. Z.; Jin, W. J. 1,3,5-Trifluoro-2,4,6-triiodobenzene: A neglected NIR phosphor with prolonged lifetime by σ-hole and π-hole capture. *Spectrochim. Acta. A Mol. Biomol. Spectrosc.* **2020**, *224*, 117428. DOI: 10.1016/j.saa.2019.117428.

(20) (a) Leduskrasts, K.; Kinens, A.; Suna, E. Cation–π interactions secure aggregation induced emission of planar organic luminophores. *Chem. Commun.* **2019**, 55, 12663–12666. DOI: 10.1039/C9CC06829E. (b) Wen, Y.; Liu, H.; Zhang, S.; Gao, Y.; Yan, Y.; Yang, B. One-dimensional π–π stacking induces highly efficient pure organic room-temperature phosphorescence and ternary-emission single-molecule white light. *J. Mater. Chem. C* **2019**, *7*, 12502–12508. DOI: 10.1039/C9TC04580E.

(21) Kirner, S.; Sekita, M.; Guldi, M. D. 25th Anniversary Article: 25 Years of Fullerene Research in Electron Transfer Chemistry. *Adv. Mater.* **2014**, *26*, 1482–1493. DOI: 10.1002/adma.201304928.

(22) (a) Dai, Y.; Liu, H.; Geng, T.; Ke, F.; Niu, S.; Wang, K.; Qi, Y.; Zou, B.; Yang, B.; Mao, W. L.; Lin, Y. Pressure-induced excimer formation and fluorescence enhancement of an anthracene derivative. *J. Mater. Chem. C* **2021**, *9*, 934–938. DOI: 10.1039/D0TC04677A. (b) Wang, J.; Dang, Q.; Gong, Y.; Liao, Q.; Song, G.; Li, Q.; Li, Z. Precise Regulation of Distance between Associated Pyrene Units and Control of Emission Energy and Kinetics in Solid State. *CCS Chemistry* **2021**, *3*, 274–286. DOI: 10.31635/ccschem.020.202000556.

(23) The photoluminescent properties of **3–6** were also studied in MeCN solution at ca. 10^{-5} M concentration (see SI, pages S14–15), at room temperature and under ambient atmosphere.

(24) (a) Pedretti, A.; Mazzolari, A.; Gervasoni, S.; Fumagalli, L.; Vistoli, G. The VEGA suite of programs: an versatile platform for cheminformatics and drug design projects. *Bioinformatics* **2020**, *37*, 1174–1175. DOI: 10.1093/bioinformatics/btaa774. (b) Pedretti, A.; Villa, L.; Vistoli, G. VEGA--an open platform to develop chemo-bio-informatics applications, using plug-in architecture and script programming. *J. Comput. Aided* **2004**, *18*, 167–173. DOI: 10.1023/b:jcam.0000035186.90683.f2. (c) Pedretti, A.; Villa, L.; Vistoli, G. VEGA: a versatile program to convert, handle and visualize molecular structure on Windows-based PCs. *J. Mol. Graph.* **2002**, *21*, 47–49. DOI: 10.1016/s1093-3263(02)00123-7. (d) Pedretti, A.; Villa, L.; Vistoli, G. Atom-type description language: A universal language to recognize atom types implemented in the VEGA program. *Theor. Chim. Acta* **2003**, *109*, 229–232. DOI: 10.1007/s00214-002-0402-6.

(25) The calculations were performed using Gaussian 09 software. The use of CAM-B3LYP/6-311++g(2df,p) basis set afforded similar results.

(26) Schäfer, C.; Ruggenthaler, M.; Appel, H.; Rubio, A. Modification of excitation and charge transfer in cavity quantum-electrodynamical chemistry. *PNAS* **2019**, *116*, 4883–4892. DOI: 10.1073/pnas.1814178116.

(27) Brown, J. S. Catnip (version 1.9), **2018**. Available from https://github.com/JoshuaSBrown/QC_Tools.

(28) Shuai, Z.; Li, W.; Ren, J.; Jiang, Y.; Geng, H. Applying Marcus theory to describe the carrier transports in organic semiconductors: Limitations and beyond. *J. Chem. Phys.* **2020**, *153*, 080902. DOI: 10.1063/5.0018312.

(29) (a) Pan, S.; Chen, Z.; Zheng, X.; Wu, D.; Chen, G.; Xu, J.; Feng, H.; Qian, Z. Ultralong Room-Temperature Phosphorescence from Supramolecular Behavior via Intermolecular Electronic Coupling in Pure Organic Crystals. *J. Phys. Chem. Lett.* **2018**, *9*, 3939–3945. DOI: 10.1021/acs.jpclett.8b01697. (b) Wang, T.; Hu, Z.; Nie, X.; Huang, L.; Hui, M.; Sun, X.; Zhang, G. Thermochromic aggregation-induced dual phosphorescence via temperature-dependent sp^3-linked donor-acceptor electronic coupling. *Nat. Commun.* **2021**, *12*, DOI 10.1038/s41467-021-21676-5. (c) Tian, Y.; Gong, Y.; Liao, Q.; Wang, Y.; Ren, J.; Fang, M.; Yang, J.; Li, Z. Adjusting Organic Room-Temperature Phosphorescence with Orderly Stimulus-Responsive Molecular Motion in Crystals. *Cell Rep. Phys. Sci.* **2020**, *1*, 100052. DOI: 10.1016/j.xcrp.2020.100052.

(30) Bissesar, S.; Raamsdonk, D. M.; Gibbons, D. J.; Williams, R. M. Spin Orbit Coupling in Orthogonal Charge Transfer States: (TD-)DFT of Pyrene—Dimethylaniline. *Molecules* **2022**, *27*, 891. DOI: 10.3390/molecules27030891.

(31) Leduskrasts, K.; Suna, E. Aggregation induced emission in one easy step: pyridinium AIEgens and counter ion effect. *RSC Adv.* **2020**, *10*, 38107–38113. DOI: 10.1039/D0RA07137D.

Kaspars Leduskrasts dzimis 1989. gadā Siguldā. Ķīmijas maģistra grādu ieguva Latvijas Universitātē 2014. gadā. Kopš 2011. gada strādā Latvijas Organiskās sintēzes institūta Organiskās sintēzes perspektīvo tehnoloģiju laboratorijā, ko vada profesors Edgars Sūna. Zinātniskās intereses aptver luminiscences jomu ar dziļāku ievirzi starpmolekulāro mijiedarbību un molekulārjā dizainā.

ISBN 978-9934-18-847-3